Spherical flame propagation behavior of pulverized coal particles and ammonia in a turbulent environment

（微粉炭とアンモニアの乱流混焼場における球状火炎伝播特性）

HADI bin Khalid

Spherical flame propagation behavior of pulverized coal particles and ammonia in a turbulent environment

By

HADI bin Khalid

Submitted to the Division of Mechanical and Space Engineering, Graduate School of Engineering, Hokkaido University, Japan, in Partial Fulfillment of the Requirement for the Degree of Doctor of Philosophy in Mechanical and Space Engineering

February 2019

Acknowledgments

Part of this work was supported by JST Sakigake (PRESTO) Grant Number JPMJPR1542, and the space utilization working group of HASTIC. The authors are indebted to Dr. Suda of IHI Co., Prof. Kitagawa of Kyushu Univ., Prof. Hayakawa of Tohoku Univ. for their helpful advices and the Central Research Institute of Electric Power Industry for providing coal particle samples. The ammonia combustion study was the Collaborative Research Project of the Institute of Fluid Science, Tohoku University.

I like to express my most sincere gratitude to my advisor, Prof. Nozomu Hashimoto. I have learned so many things including the scientific knowledge and the research skills from him. He professionally guides me very details in various skills in the research work. He also personally guides me along my study in the doctoral course. On top of that, I like to express my appreciation to Prof. Osamu Fujita. Prof. Osamu Fujita was accepting me as a doctoral course student in his laboratory. He guided me in the research activities and gave me a lot of support. Both professors are very kind and a great scientist.

I would like to thank Prof. Harunori Nagata, Prof. Osamu Fujita, Prof. Nobuyuki Oshima and Prof. Nozomu Hashimoto for their services on my doctoral committee and their support. I appreciated Prof. Masao Watanabe, Prof. Takashi Nakamura, Prof. Takemi Chikahisa, Prof. Hideyuki Ogawa, Prof. Tsuyoshi Totani, Prof. Yuichi Murai, Prof. Yutaka Tabe, Prof. Hiroshi Terashima and Prof. Gen Shibata on judgment committee.

I like to thank Prof. Hideaki Kobayashi and Prof. Akihiro Hayakawa from Tohoku University for the collaborative research work on ammonia combustion. They were kindly sharing their knowledge and support us on research, and the related activities as well. I like to thank Prof. Toshiaki Kitagawa and Prof. Hiroaki Watanabe from Kyushu University for their helpful advice. Furthermore, I wish to thank Prof. Kaoru Maruta and Prof. Hisashi

Nakamura from Kyushu University for their kind support.

I like to thank my master-course advisor, Prof. Intan Zaurah Mat Darus, and bachelor-course study, Prof. Mohd Zarhamdy Md Zain from University Teknologi Malaysia (UTM) for their helpful advice. They kindly supported me a lot in the research work in UTM. Also, I like to thank all the professors and lecturers in UTM, especially in the Faculty of Mechanical Engineering, UTM.

I appreciate Dr SungHwan Youn, Dr Hui Yan, Dr Yongho Chung, Dr Ajit Kumar Dubey, Mr. Kenichi Sato, Mr. Yusuke Konno, Mr. Masashi Nagachi, Mr. Guo Feng and Mr. Yushin Naito for their help and support, especially in the scientific manner. I like to appreciate my research group members, Mr. Ryo Ichimura, Mr. Genya Hashimoto and Mr. Xia Yu. I want to thank all members of the Laboratory of Space Utilization from the year of 2015 to 2019 for their great support. I like to thank the secretary, Ms. Miho Taga for her kind help and support along I study in this laboratory. Also, I like to thank Hokkaido University staff for their helpful support.

I like to appreciate the Ministry of Education Malaysia and the Malaysian government for providing me with the scholarship to pursue my study in Japan for PhD. course. I like to thank my friends and all the people who are supporting me until these days. I am sorry that it is difficult to state all the names here.

I like to appreciate my wife, Intan Suraya Binti Ahmad Thahir, and my son, Izz Firas bin Hadi. Finally, with great humility and gratitude, I thank my parents, for their endless love and concern.

Thank you very much!

Summary of the present study

The present study aims to clarify the flame propagation behavior of pulverized coal particle clouds in coal-ammonia mixing combustion. It is expected that ammonia as a hydrogen-energy carrier would improve the ignition capability of coal particles in the coal-ammonia mixing combustion. The intention of the study is the combustion in a turbulent environment. The three categories of the experiment have been performed; pulverized coal combustion, ammonia combustion, and pulverized coal-ammonia (mixing) combustion.

A unique experimental apparatus was developed to suit all categories of combustion in a turbulent and quiescent environment. The experiments on spherical flames propagations were performed by using a spherical-inner shape closed vessel. The turbulent flow field in the vessel was generated by counter-rotation of two identical fans. The turbulence intensity was changed by changing the fan rotational speed. A linear relationship between fan rotational speed, N and turbulence intensity, u' was obtained from particle image velocimetry (PIV) measurements. The turbulence was considered homogeneous, and there was no regular bulk motion in the center of the combustion vessel. A dispersion system was employed to disperse the pulverized coal particles into combustion field. The pulverized coal was dispersed homogeneously in the combustion field by 300 kPa dispersion gas (ambient gas). It was confirmed that the dispersion flow was not influencing the flame propagation behavior.

With the application of the present experimental apparatus, the pulverized coal clouds not sustained flame propagation by using the air as the ambient gas. Therefore, diluted oxygen (40 vol% O_2 and 60 vol% N_2) was used as the ambient gas to achieve flame propagation. For a qualitative comparison, the ammonia-O_2N_2 and mixing combustion also used similar ambient gas. In addition, for validation of the methods in this present study, the

experiment on the ammonia-air mixtures was performed and the results were compared to the previous research findings that available in the literature.

Common bituminous coal (C5) with fuel ratio of 1.56, and three types of low ignitable coal consist of TW, KK and UL with fuel ratio of 2.5, 3.17 and 5.3, respectively were tested. Fuel ratio is the ratio of fixed carbon to the volatile matter. Low ignitable coals have higher fuel ratio than the common bituminous coal. In general, higher fuel ratio is difficult to ignite. In the C5 coal combustion for various coal concentrations and turbulence intensities, the turbulence intensity has a significant effect on flame propagation velocity, compared to the effect of coal concentration. This is due to the effect of turbulence heat transfer. Turbulence heat transfer increased the volatile matter release rate, thus increased the flame propagation velocity. Flame propagation capability of low ignitable coals for various coal concentrations and various turbulence intensities also clarified.

Moreover, Experiment under 1g and μg environments clarified the effects of gravity, turbulence intensity, and fuel ratio on the spherical turbulent flame propagation behavior of a pulverized coal particle cloud. The coal particle cloud is more flammable in μg than in the 1g environment. Natural convection, which exists in the 1g environment, has a significant effect on the flame propagation behavior of C5 and TW coal particle clouds in the quiescent environment. In a turbulent, no significant difference of the flame propagation velocity in μg and 1g environment.

Experiments on ammonia-air and ammonia-O_2N_2 premixed combustion were performed for various equivalence ratios and turbulence intensities. Flame propagation behavior of ammonia-air in the quiescent environment was obtained and showed good agreement to the previous study in the literature. Flame propagation probability limit for the ammonia-air mixture in various turbulence intensities was clarified. The ammonia-air mixture in lean condition tended to sustain flame propagation even in higher turbulence

intensity, up to 1.29 m/s. In the quiescent environment, the limit of equivalence ratio of ammonia-air to sustain the flame propagation is between; 0.7 to 1.2, which is similar to the previous study. Meanwhile, for ammonia-O_2N_2, the limit of equivalence ratio is between; 0.4 to 2.0. Flame propagation behavior of ammonia-O_2N_2 mixture was compared to the ammonia-O_2N_2 flame propagation behavior in the mixing combustion with coal particles.

Mixing combustion of coal-ammonia-O_2N_2 mixtures was experimentally studied for the C5, TW, KK and UL coal for various turbulence intensities. The coal concentration was set to 0.6 kg/m^3, and the equivalence ratio of ammonia-O_2N_2 is 0.6. In the C5 coal combustion, the lowest coal concentration = 0.6 kg/m^3 was sustained flame propagation in all tested turbulence intensities. For the coal concentration = 0.6 kg/m^3, without ammonia addition, the KK and UL coal were not sustaining flame propagation, while TW coal sustaining flame propagation only in the high turbulence intensities. With ammonia addition, the flame propagation velocity of C5 coal in mixing combustion about five times faster than that in coal combustion. In addition, ammonia flame increased the ignition capability of low ignitable coals. Ammonia flame increased the volatile matter release rate of the coal particles, thus flame propagation velocity increases. Therefore, in the mixing combustion, TW, KK and UL coal sustained flame propagation in all turbulence intensities tested in the present study.

Based on the thermal input, with ammonia addition (equivalence ratio = 0.6) and coal concentration of 0.6 kg/m^3, coal particles can be saved around 20% (weight %). The findings of the present study can contribute to the fuel cost reduction and the improvement of energy security by being able to utilize the low ignitable pulverized coal particles. Moreover, in the coal-fired boiler, expected that the co-firing of coal-ammonia help to increase the burner stability, considering the flame propagation velocity is one of the important parameters for the flame stability.

***Keywords*:** Pulverized coal, coal-ammonia combustion, turbulence intensity, low ignitable coal, spherical turbulent flame propagation, mixing combustion, microgravity combustion

Thesis Supervisor : Nozomu HASHIMOTO

Title : Associate Professor

Table of Contents

Nomenclature

L_f	longitudinal integral length scale
u'	turbulence intensity
G	coal concentration
N	fan rotational speed
C_p	specific heat under constant pressure
C_v	specific heat under constant volume
D	mass diffusivity
g	acceleration of gravity
K	flame stretch rate
L_b	burned gas Markstein length
r	flame radius
R	gas constant
S_L	laminar burning velocity
S_n	flame velocity
S_u	unstretched burning velocity
t	time
T_b	temperature in burned mixture
T_u	temperature in unburned mixture

Greek Symbols

α	thermal diffusivity
γ	specific heat ratio
δ_f	flame thickness
δ_r	reaction zone

$\delta\imath$	preheating zone thickness
v	kinematic viscosity
ρ	density
ρ_b	density in burned mixture
ρ_u	density in unburned mixture
$\emptyset$	equivalence ratio

Dimensionless Numbers

Le	Lewis number ($=\alpha/D$)
Ma	Markstein number ($=L_b/\ \delta\imath$)

Subscript

b	burned mixture
f	flame
u	unburned mixture

Chapter 1 Introduction

This chapter describes the introduction of the present study, the research background, the aim of the study, research objectives, significance of the study, and the novelty of the present research.

1.1 Introduction

Among the various fossil fuels, coal continues to serve as an essential energy source because there remains an abundant supply of accessible deposits worldwide. One of the primary uses of coal is in the electrical power generation industry. Pulverized coal, which is utilized in many thermal-power stations, is a particularly notable example of the application of coal-power production; therefore, a fundamental understanding of the combustion characteristics of pulverized coal is necessary to improve fuel usage efficiency.

In a pulverized coal combustion process, the pulverized coal is in the fineness particles form, and injected through burners into the furnace with combustion air. The fine coal particles heat up rapidly, undergo pyrolysis which the volatile matter released, and thus ignition takes place. Figure 1.1 shows the schematic of the pulverized coal combustion mechanism. In many thermal-power plants, coal-fired boilers combust pulverized coal

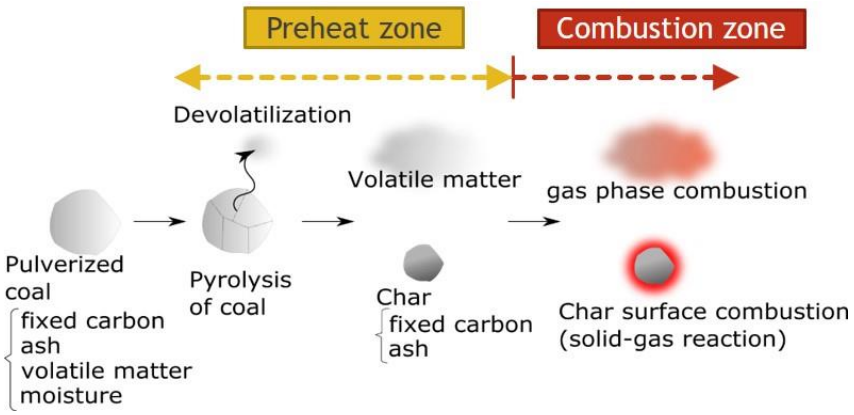

Figure 1. 1 Schematic of pulverized coal combustion mechanism.

particles in a turbulent environment. In the furnace of the boilers, the complex phenomena regarding the turbulent flow, heat transfer, and chemical reaction are occurred [1]. The flame propagation behavior is one of the most important properties for the flame stability of the burner [2]. Therefore, the flame propagation velocity is one of the important parameters that determines the flame stability. The volatile matter release rate and the amount of volatile matter generated strongly affect flame stability [3].

Nowadays, ammonia (NH_3) is getting more attention as one of the new energy carriers. Ammonia as a hydrogen-energy carrier because of its high hydrogen content. On top of that, ammonia is relatively simple in transportation and storage compared to the hydrogen (H_2) which more complicated and high cost. Also, ammonia as a carbon-free fuel which can reduce the CO_2 emission.

The common bituminous coal was widely used in combustion compared to the low ignitable coal with high fuel ratio. Utilization of the low ignitable coal would improve energy security. Kurose et al. [4] investigated the high fuel ratio coals for fuel ratio between 1.46 to 7.10 by using coal combustion test furnace. In the present study, the tested coals with fuel ratio between 1.56 to 5.3. The present study intended to investigate the flame propagation behavior of the mixing combustion of ammonia and pulverized coal particle clouds for the common bituminous coal and low ignitable coal. With the expectation that the ammonia as an energy carrier would improve the ignition capability of the pulverized coal particles, the increasing of the flame propagation velocity would help to increase the flame stability of the burner.

1.2 Research Background

In the future, large transactions of new energy carrier such as ammonia (NH_3) were expected. The infrastructure for ammonia distribution and ammonia production has already been established. The main motivation to utilize ammonia is due to the production, storage and transport infrastructure. This is because the financial and regulatory barriers are lower than for liquid hydrogen. Utilization of the ammonia as a new energy carrier in a coal-fired power plant seems beneficial to the industry and consumer. Figure 1.2 shows the schematic flow of ammonia from production stages to the utilization options. Utilization of ammonia as a new energy carrier in the existing coal-fired thermal power plant is very promising compared to applications in fuel cells or high-efficiency gas turbine. This is because ammonia can be burned directly in the burner. A huge amount for utilization of ammonia is possible if the new energy carrier can be introduced for the co-firing to existing large-scale coal-fired boilers or furnaces.

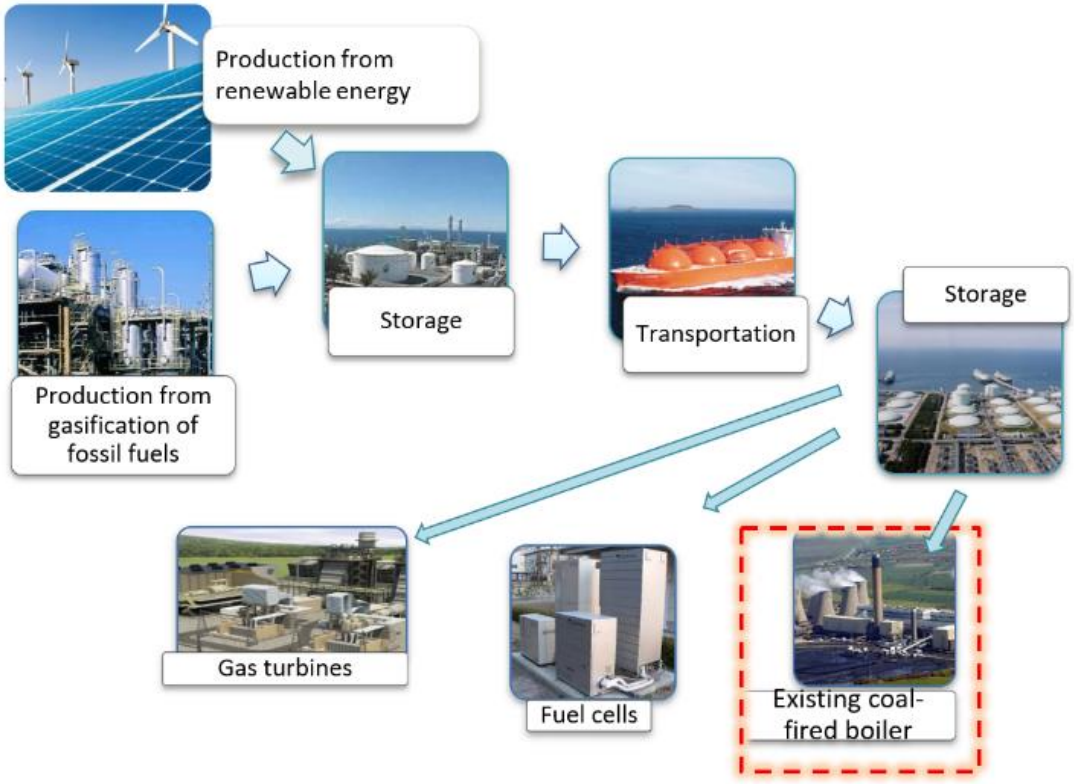

Figure 1. 2 A production, storage, transportation and utilization of ammonia.

1.3 Research aims

The present study aims to clarify the flame propagation behavior of pulverized coal particle clouds in coal-ammonia mixing combustion. Common bituminous coal and low ignitable coal were used in the mixing combustion. The study observed the ignition capability improvement of pulverized coal particle clouds by co-firing with ammonia as an energy carrier. Figure 1.3 shows the concept of ignition improvement of coal particles by mixing combustion of pulverized coal particles and ammonia. Compare to solid fuel, gaseous fuel combustion is faster. Expected that the ammonia flame will increased the ignition capability of coal particles. Thus, increased the flame propagation velocity of coal flame in the coal-ammonia mixing combustion.

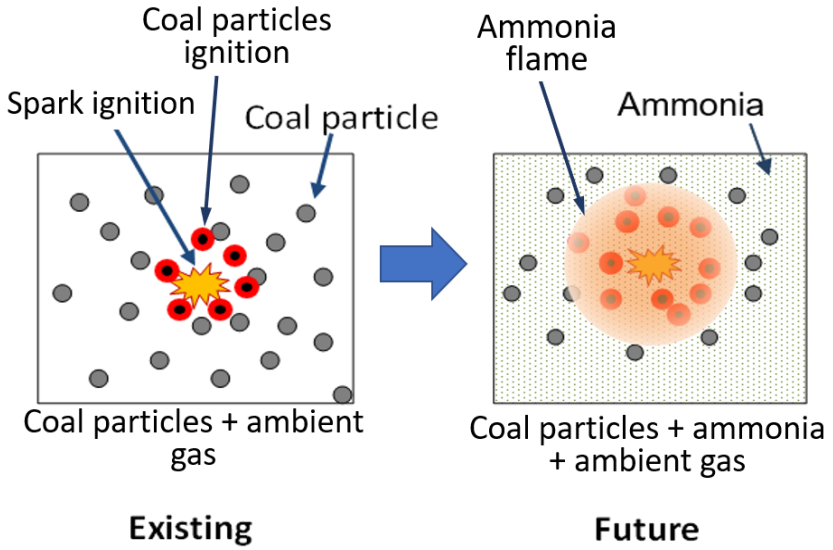

Figure 1. 3 The concept of ignition improvement of coal particles.

Figure 1.4 shows the schematic of a coal-fired power plant which the addition of the ammonia tank and the additional necessary equipment on the existing coal-fired power plant system. Pulverized coal particles combusted in a turbulent environment in the burner zone. Therefore, the turbulence intensity was considered as an essential parameter in the present study.

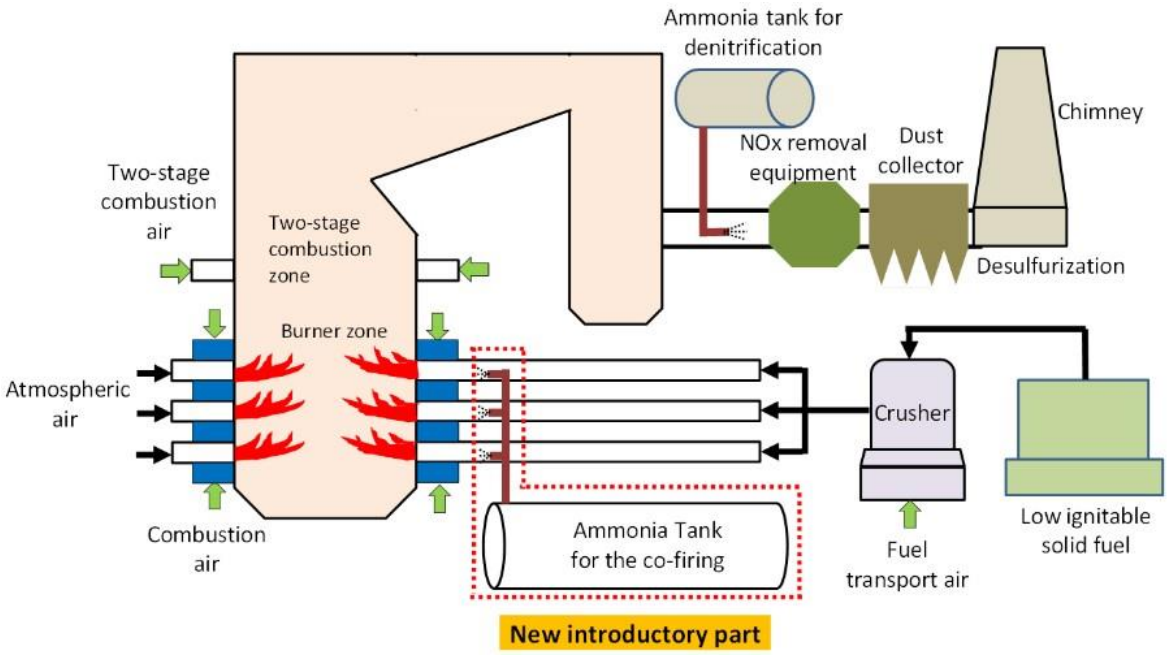

Figure 1. 4 Schematic of pulverized coal-fired power plant with ammonia co-firing.

1.4 Objectives of the Study

1. To clarify the effect of turbulence intensity on flame propagation behavior of coal particle clouds.
2. To clarify the effect of coal fuel ratio on flame propagation behavior of pulverized coal particle clouds.
3. To reveal the effect of the addition of ammonia on the ignition characteristics and flame propagation velocity of common bituminous and low ignitable coal particle clouds.

1.5 Significance of the Study

1. CO_2 emission reduction by substituting part of pulverized coal particles by ammonia.
2. Fuel cost reduction by being able to utilize low ignitable pulverized coal particles.

3. Improvement of energy security by being able to utilize low ignitable pulverized coal particles.

1.6 Novelty of research

1. Ignition and combustion of low ignitable pulverized coal particles by the co-combustion of ammonia.
2. Flame propagation behavior of pulverized coal clouds in a turbulent environment.
3. Flame propagation behavior of ammonia in a turbulent environment.

Chapter 2 Literature review

Chapter 2 describe the previous related study of pulverized coal clouds combustion in normal gravity and microgravity, spherical gaseous fuel combustion, ammonia combustion and turbulence flow field in combustion vessel.

2.1 Coal combustion

2.1.1 Flame propagation velocity of quiescent pulverized coal clouds

According to pulverized coal particle clouds study, in a quiescent environment, coal particles concentration has a significant effect on the flame propagation velocity. Figure 2.1 shows the effect of coal concentration on flame propagation velocity. In the quiescent environment, between coal concentration, *G* of 0.66 and 1.56 kg/m³, the higher coal concentration increased the flame propagation velocity [5].

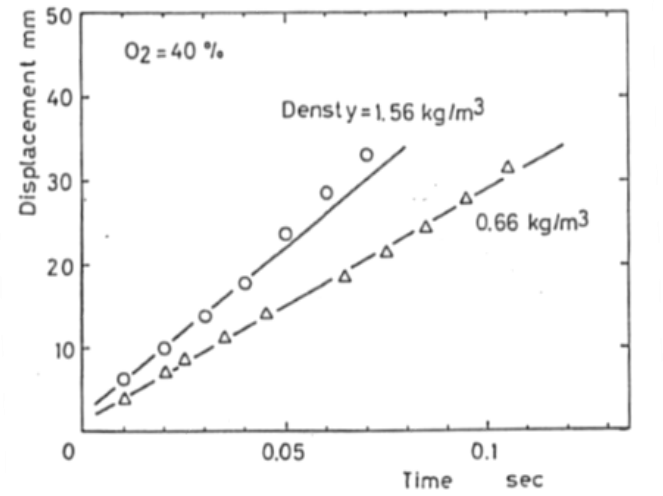

Figure 2. 1 Displacement of flame front for various coal concentrations [5].

The spherical coal cloud combustion study by T.Suda, et al.[2], investigates flame propagation of pulverized coal clouds for several types of coal (as shown in Table 2.1) in microgravity to ensure the quiescent environment. Figure 2.2 shows the unique

Table 2. 1 Physical and chemical analysis of coal [2]

Analysis	Coal A	Coal B	Coal C
Proximate [wt%]			
Moisture	5.5	3.5	2.8
Ash	10.5	11.7	12.1
Volatile	46.0	36.2	32.9
Fixed Carbon	38.0	48.6	52.2
Ultimate [wt%, dry]			
Carbon	65.9	68.2	71.1
Hydrogen	5.8	5.0	4.9
Nitrogen	1.0	1.4	1.6
Sulfur	0.2	1.0	0.6
Oxygen	16.1	12.1	9.3
Heating value [kJ/kg]	27,700	27,900	28,900

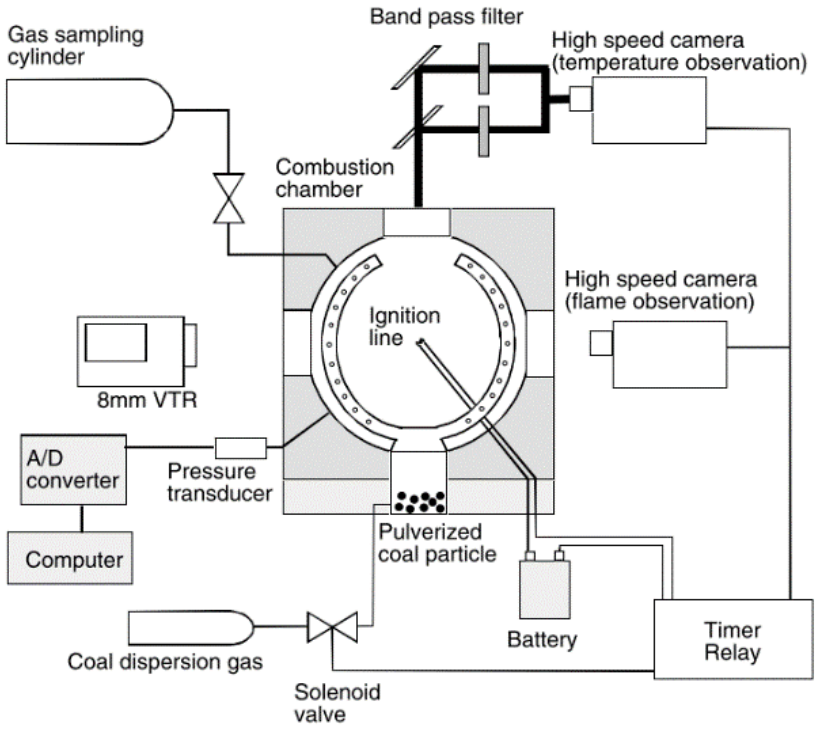

Figure 2. 2 Schematic of experimental apparatus with curling horn [2].

experimental setup used for the microgravity experiment in drop tower facilities Japan microgravity center (JAMIC). Coal particle dispersion system consists of curling horn with a significant number of small holes. The pulverized coal particles dispersed into the combustion field by using a dispersion gas. The mixture ignited at the quiescent

environment in microgravity condition. The spherical flame shape was obtained from the experiment in the quiescent environment as shown in Fig. 2.3. Figure 2.4 shows the coal concentration has a significant effect on the flame propagation velocity in a quiescent environment. The maximum flame propagation velocities were around coal concentration, G=1.3 kg/m³. It is a common understanding that coal concentration has a significant effect on flame propagation velocity in the quiescent environment and laminar flow [6-8].

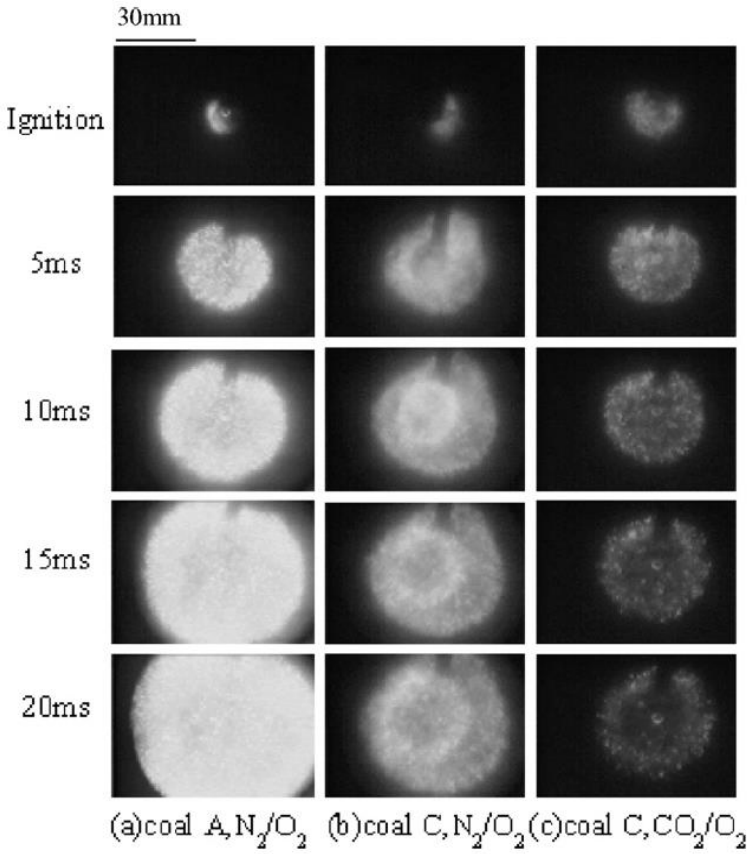

Figure 2. 3 Flame propagation in coal dust clouds particle diameter: 53-63 [2].

The luminous flame front of pulverized coal clouds was easy to determined by direct observation using the high-speed camera. Flame propagation speed obtained by measuring the diameter of the flame front [2,9,10]. For lower volatile matter coal, flame propagates slower than higher volatile matter coal and the brightness of the flame also decreased [2].

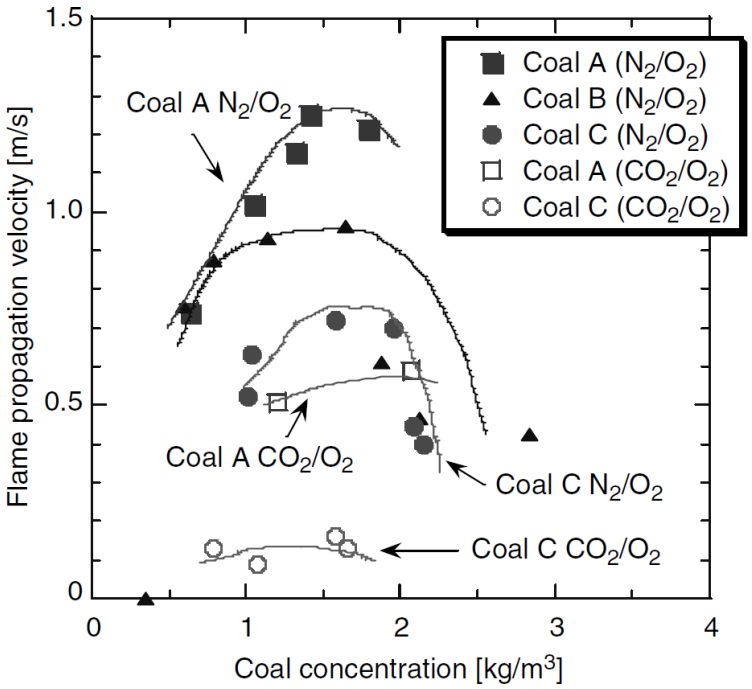

Figure 2. 4 Effect of coal concentration on flame propagation velocity particle diameter: 53-63 μm, O_2 : 40% [2].

2.2 Spherical flame of gaseous fuels

2.2.1 Ammonia-air premixed combustion in a quiescent environment

Flame propagation limit of the ammonia-air mixture investigated by Hayakawa et al. [11] showed a similar result to the previous study. For *Pi* = 0.1 MPa , the flame does not propagate at equivalence ratio, Ø of 0.7 to 1.3 [11], as shown in Fig. 2.5. According to Law C.K.[12], the lean and rich flammability limits for ammonia flame are between Ø = 0.63 to 1.4. Schlieren photography was employed for flame imaging, however for ammonia-air the flame front in atmospheric pressure was relatively not so clear compared to other gaseous fuel. This is due to the flame thickness for ammonia-air was relatively thicker than other gaseous fuel because the unstretched laminar burning velocity of ammonia-air premixed flames are relatively slower than other gaseous fuel (i.e : methane-air premixed flames) [11].

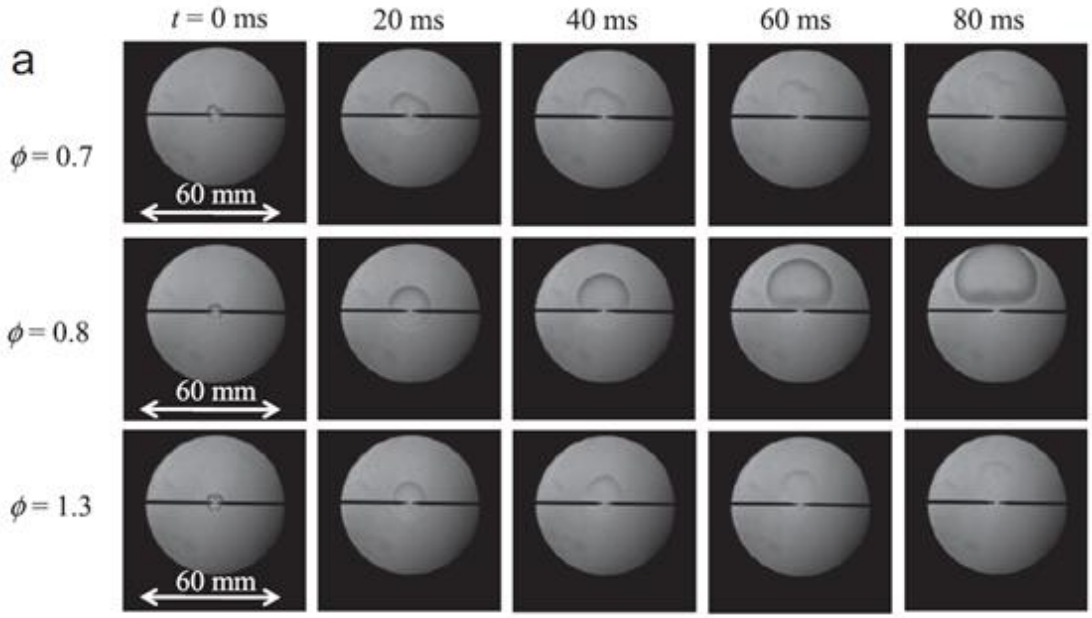

Figure 2. 6 Schlieren flame images of ammonia-air premixed flames at various equivalence ratios, Ø, with elapsed time from the ignition, t, at Pi=0.1 MPa [11].

Furthermore, the buoyancy effect influences the flame propagation of ammonia-air because of its low burning velocity compared to other gaseous fuel. Figure 2.6 shows the unstretched laminar burning velocity of the ammonia-air mixture. Burned gas Markstein length is less than zero in the lean condition, as shown in Fig. 2.7. The Lewis number of

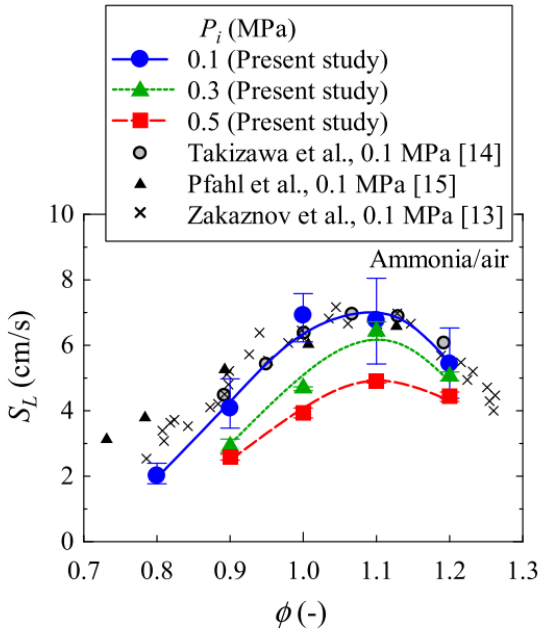

Figure 2. 5 Relationship between unstretched laminar burning velocity, S_L and equivalence ratio, Ø [11].

ammonia-air flames of a lean mixture is less than unity. Therefore, the burned gas Markstein length at lean mixtures are negative because the temperature and burning velocity of stretched flames increase due to the thermo diffusive effects [11].

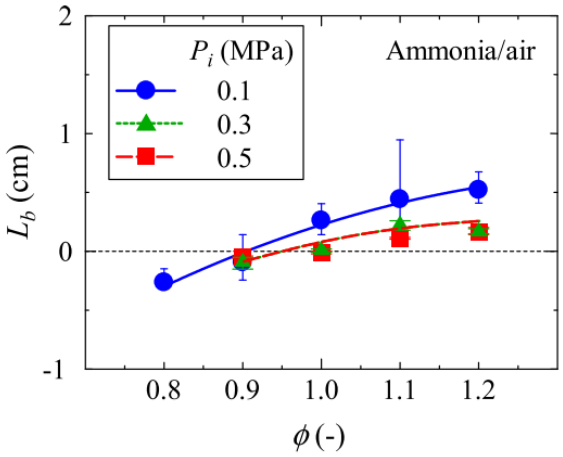

Figure 2. 7 Relationships between burned gas Markstein length, L_b and equivalence ratio, $\emptyset$ [11].

2.2.2 Spherical turbulent flame

Goulier et al. [13] investigate the effect of turbulence on the flame propagation speed of hydrogen-air in a closed vessel. The turbulence flow generated by eight fans. Figure 2.8 shows the Schlieren photography setup and the flame images for turbulence intensity, u' = 0 and 1.5 m/s for hydrogen-air mixtures with cellular flame.

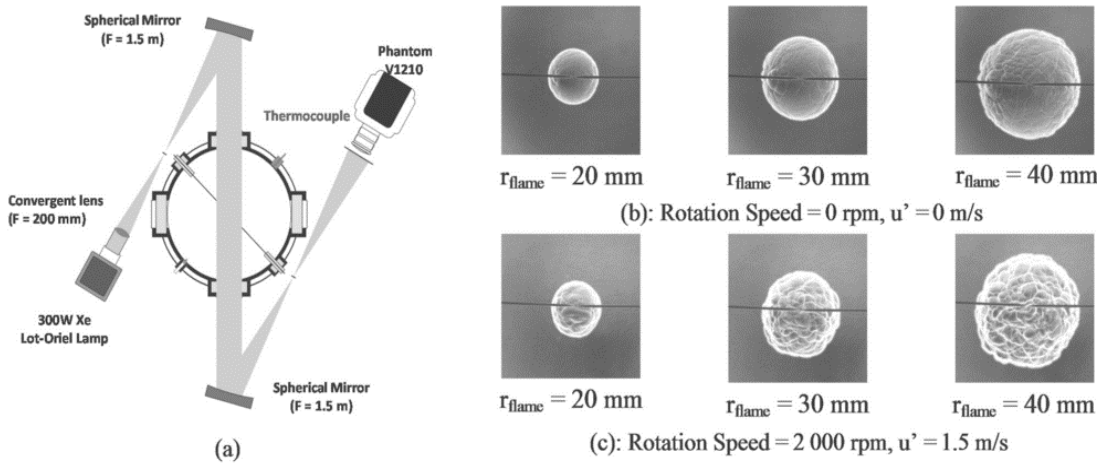

Figure 2. 8 Schematic of Schlieren imaging and examples of images acquired for a mixture containing 24% H_2 + 76% air initially at 1 atm and 296 K. (a) optical setup; (b) the mixture was initially at rest (turbulence intensity, u_0 = 0 m/s); (c) the mixture was initially turbulent (turbulence intensity, u_0= 1.5 m/s) [13].

Bradley et al. [14] reported the experimental studies of premixed, turbulent, gaseous explosion flames in a fan-stirred bomb. The gaseous fuels are propane and methane. Figures 2.9 shows flame contour for initial pressure of 0.1 and 0.5 MPa for various turbulence intensities. In a turbulent environment, for the spherical turbulent flame propagation, such irregular flame shape was observed as shown in Fig. 2.9. From the point of ignition, flames grow reasonably uniform, with a little crossing of contours, a consequence of either

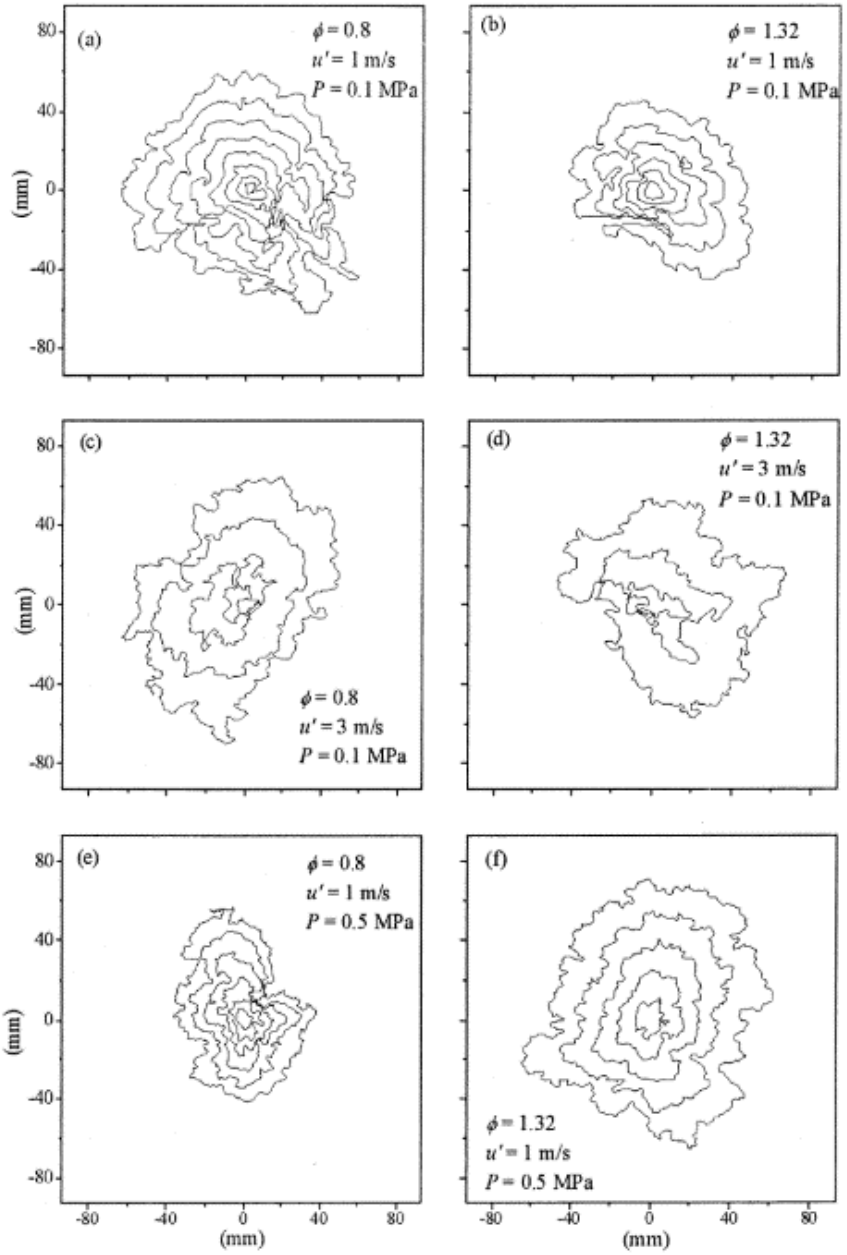

Figure 2. 9 Flame contour for representative propane-air mixture. The spark gap position was at coordinate (0,0) [14].

convection of the whole flame or interaction with a large turbulent eddy that drives the flame front backwards [14].

2.3 Turbulence flow field generated by fans rotation

Smallbone et al. [15] reported the laminar and turbulent burning velocity of premixed hydrogen-air flame measured in fans stirred closed vessel. The turbulence flow field generated by counter-rotation of two identical fans, on the top and bottom of the vessel, as shown in Fig. 2.10. This approach was adopted to develop the experimental apparatus in the present study, which use the counter-rotation of two fans.

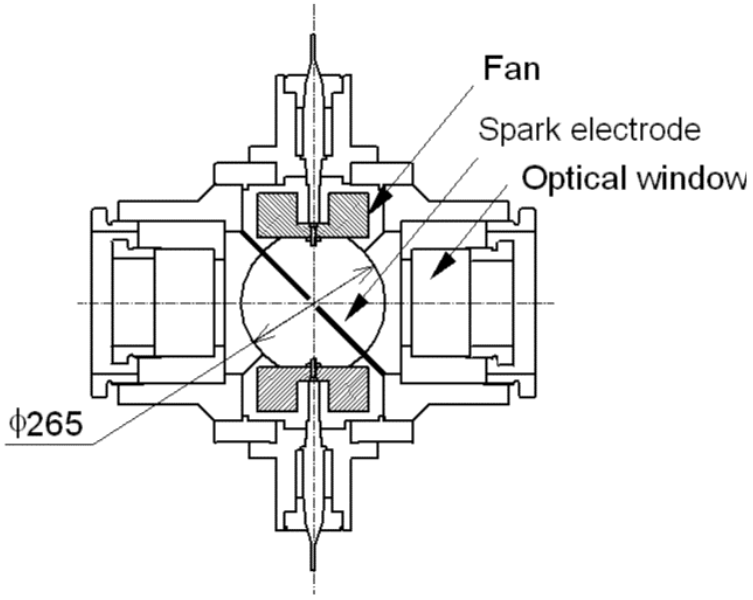

Figure 2. 10 Schematic of combustion vessel with two fans [15].

Particle image velocimetry (PIV) measurement was employed to develop the turbulence intensity and fan speed correlation. A linear relationship between turbulence intensity and fan speed was obtained from the PIV measurement, as shown in Fig. 2.11. In the center of the combustion vessel, the turbulence was considered homogeneous with no

regular bulk motions [15]. Goulier et al. [13] described the PIV measurements showed that homogeneous and isotropic turbulence created in the vessel by using several fans.

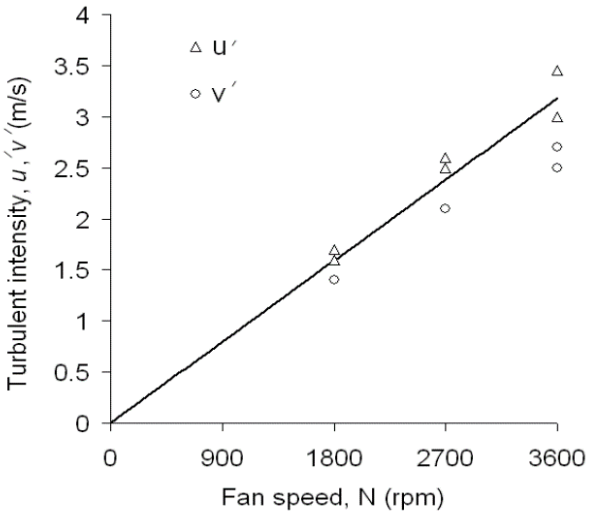

Figure 2. 11 Fan rotational speed versus turbulence intensity [9].

Chapter 3 Methods

This chapter describes the experimental apparatus, the experimental procedure and the methods of data collection. The newly developed experimental apparatus meets the requirement for coal and ammonia combustion in a quiescent and turbulent environment. The experiments also performed in the normal gravity and microgravity environment. The selected materials for the chamber and accessories were compatible with the ammonia combustion.

3.1 Experimental apparatus and procedures

3.1.1 Coal-O_2N_2 (coal) combustion

Experiments were carried out using a constant volume spherical inner shape combustion chamber as shown in Fig. 3.1. The inner spherical diameter is 200 mm. The distance between the floor and ceiling is 280 mm. The total volume of the chamber was

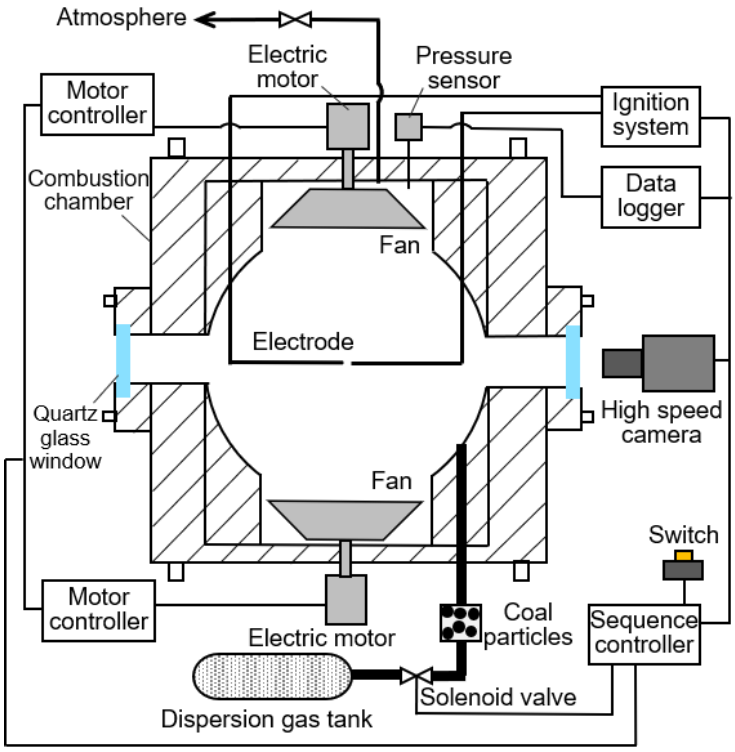

Figure 3. 1 Schematic of experimental apparatus for coal combustion.

approximately 6.2×10^{-3} m^3 or 6.2 liters. A spark igniter composed of two stainless steel electrodes with a diameter of 1.8 mm mounted inside the chamber with a spark gap at the center of combustion field. The spark gap which is the distance between the two sharp tip electrodes was set to 2 mm, where the gap within 1 to 3 mm is suitable to generate accurate spark energy [16]. A capacitor discharge ignition (CDI) circuit was adopted for the spark ignition, as shown in Fig. 3.2. 469 VDC charged four units of capacitors with a total 50 µF. To ensure the ignition of pulverized coal particles, the total spark energy of 5.5 J discharged to the ignition coil that connected to electrodes. The turbulent flow field was generated in the chamber by counter-rotation of two identical seven-bladed fans located vertically and symmetrically. The diameter of the fans is 150 mm. The fan shaft connected to DC motor (Graphite Brushes, 150W) that equipped with the encoder. A motor controller (ESCON 50/5) attached to each DC motor to control the fan rotational speed (rpm). The fan rotation was set by input the desired rpm value using the motor controller software (ESCON Studio). The fan rotation system with feedback signal by encoder ensured the consistent fan rotational speed.

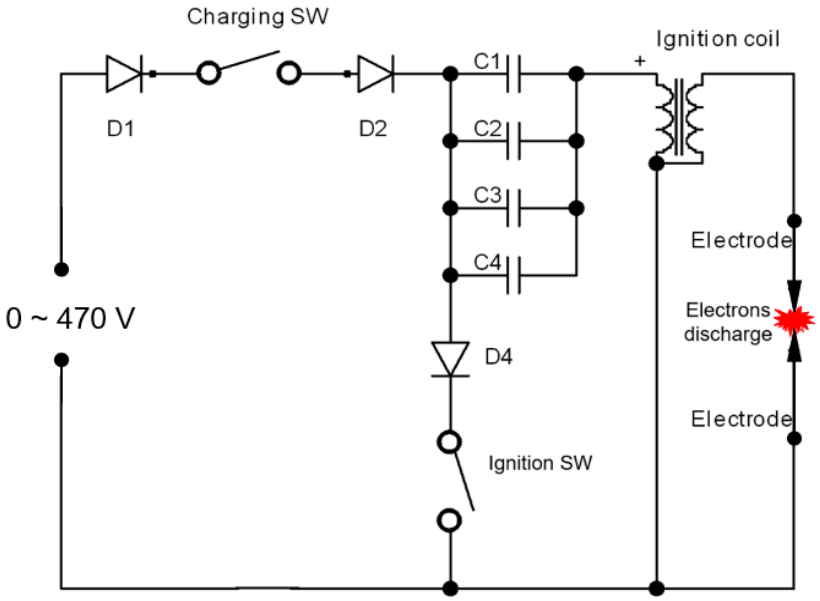

Figure 3. 2 Schematic of CDI circuit embedded in the spark ignition system.

Flame propagation of pulverized coal particles cloud was observed by direct imaging at a sample rate of 1800 fps using a high-speed camera (Phantom Miro-C with UV lens) through 50 mm diameter quartz glass window. Pressure history inside the combustion chamber was measured using the pressure sensor (Valcom VPRTF-A4, -0.1~0.2 MPa) and recorded by Hioki 8870 data logger. Another pressure sensor (Valcom VPRTF-A4, -0.1~0.1 MPa) and digital panel meter (F37N-S Valcom) were for monitoring the pressure of gas mixtures in the dispersion tank.

Common bituminous pulverized coal particles (C5) with an average diameter of 48 μm on a mass basis used as the fuel. Table 3.1 shows the properties of the C5 coal. Diluted oxygen (40 vol% O_2 and 60 vol% N_2) was used as the ambient gas to achieve flame propagation. The coal concentration, *G* in the combustion field was set to 0.3, 0.6, 1.3, 2.0 and 2.3 kg/m³. According to work by Suda et al. [2], the highest velocity of flame propagation in a quiescent pulverized coal particle cloud in microgravity (μg) environment

Table 3. 1 Physical and chemical analysis of coals.

	Common bituminous coal	**Low-volatile coal**		
	C5	TW	KK	UL
Analysis				
Proximate [wt%]				
Moisture[b]	0.7	2.3	0.3	3.0
Ash[a]	14.2	19.9	12.9	21.2
Volatile matter[a]	33.5	22.9	20.9	12.5
Fixed carbon[a]	52.3	57.2	66.2	66.3
Fuel ratio	1.56	2.5	3.17	5.3
Ultimate [wt%, dry]				
Carbon	70.5	69.2	76.7	71.8
Hydrogen	4.64	3.64	4.09	2.48
Nitrogen	1.66	1.54	1.31	1.52
Oxygen	8.59	5.4	3.6	2.8
Sulfur	0.46	0.41	1.46	0.34
Heating value [MJ/kg]	27.8	27.2	30.1	27.2

[a] Dry basis.

[b] As received.

was obtained when the coal concentration was around 1.3 kg/m³. However, in the present study in normal gravity (1g) environment, flame propagation could only be observed for a G = 1.3 kg/m³ in a quiescent environment (without fan rotation).

The experiments started with emptied the combustion chamber and the dispersion tank to a -100 kPa via a vacuum pump. After emptying the tank, the gas used to disperse the coal particles, also comprising 40 vol% O_2 and 60 vol% N_2, was filled in a dispersion tank at a total pressure of 300 kPa (gauge pressure of 200 kPa). Out of -100 kPa pressure inside the chamber, the ambient gas was mixed in the combustion chamber for a volume 84% only, to allow the pressure of volume 16% to reach 0.1 MPa (atmospheric pressure) after the addition of the dispersion gas with the coal particles. Before emptying the chamber, coal particles loaded into four filter cups and tubes corresponding to the symmetrical configuration of four inlets. Figure 3.3 shows the schematic of coal particles dispersed from the symmetrical configuration of four inlets. This configuration was located at the middle of the vertical axis of the combustion chamber. Therefore, on the vertical axis, the dispersion was in the middle. Thus, the dispersion direction is towards the center of the spherical combustion field. The dispersion gas for all four filter elements is from the same dispersion tank.

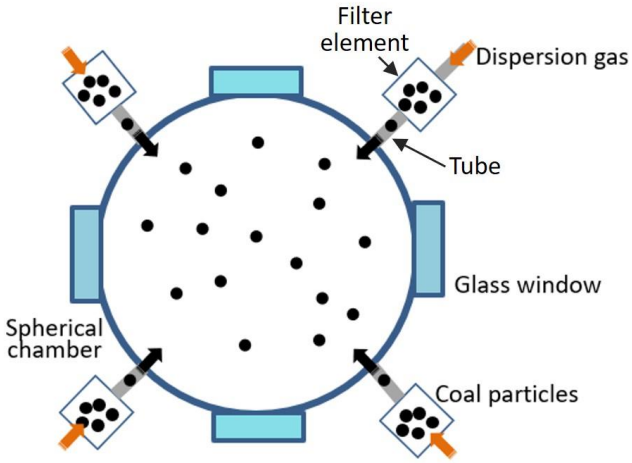

Figure 3. 3 Schematic of coal particles dispersed from four inlet.

The coal particles were dispersed into the chamber by a sweeping flow from the dispersion tank for 0.7 s. At 0.3 s after the end of the dispersion, the mixture was ignited at the center of chamber at 0.1 MPa (atmospheric pressure). For the experiments in a turbulent environment, rotation of the fans was started approximately 3 minutes prior to the dispersion and kept running at a constant (prespecified) speed during flame propagation. The fans rotation speed was confirmed by measuring the rotation of fan's shaft physically using a digital tachometer. The mass of coal particles remaining in the filter cups and tubes after the dispersion was measured to confirm the mass of coal particles dispersed into the chamber. After each experiment, the chamber was opened by detaching the lid, and the inner chamber was cleaned for the next experiment.

The maximum errors for the O_2 concentration, the pressure inside the chamber, and the coal concentration are 1.2%, 5%, and 4%, respectively. According to the results of the present study, the errors can be neglected for the conclusion. The present technique was validated by combusting premixed quiescent ammonia-air at 0.1 MPa. For an equivalence ratio of 1.0, the laminar burning velocity from the present study is 6.85 cm/s, which is almost the same as that reported by Hayakawa et al.: 6.91 cm/s [17]. The minimum of three experimental data sets for each condition of pulverized coal particle clouds was used for the analysis.

Relaxation time characterizes the time required for a particle to adjust its velocity to a new condition of flow. The particle relaxation time, t_0 estimated by Eqn. (1) ;

$$t_0 = \frac{\rho_p d_p^2}{18\mu_g} \quad (1)$$

where ρ_p is the particle density, d_p is the particle diameter and μ_g is the gas dynamic viscosity. In the present study, the ambient gas is diluted oxygen (40 vol% O_2 and 60 vol%

N_2). By taking the bulk coal particle density as 833 kg/m³ and the average particle diameter as 48 µm on a mass basis, the particle relaxation time estimated as 5.7 ms. It showed that the coal particles follows the turbulent flow during the ignition and flame propagation.

Ammonia-air and ammonia-O_2N_2 mixtures combustion were used to investigate the effect of dispersion flow on the flame propagation behavior. The separate experiments on quiescent mixtures, and the mixtures with dispersion flow that same procedure as coal combustion were performed. Figure 3.4 shows the flame radius as a function of elapsed time for the quiescent mixture, and ammonia-air mixture with dispersion flow. The result showed that almost no different of flame radius as a function of time for both conditions.

Ammonia-air has relatively lower flame propagation velocity and almost the same as coal-O_2N_2 at the flame radius of 10.45 mm, while ammonia-O_2N_2 has relatively higher flame propagation velocity, as shown in Fig. 3.5. Flame propagation velocities were compared at a flame radius of 10.45 mm, as described later in Section 4.1. Both ammonia-air and ammonia-O_2N_2 mixtures showed the dispersion flow does not influence the flame propagation behavior. Therefore, in the present study, the effect of dispersion flow on flame propagation was negligible.

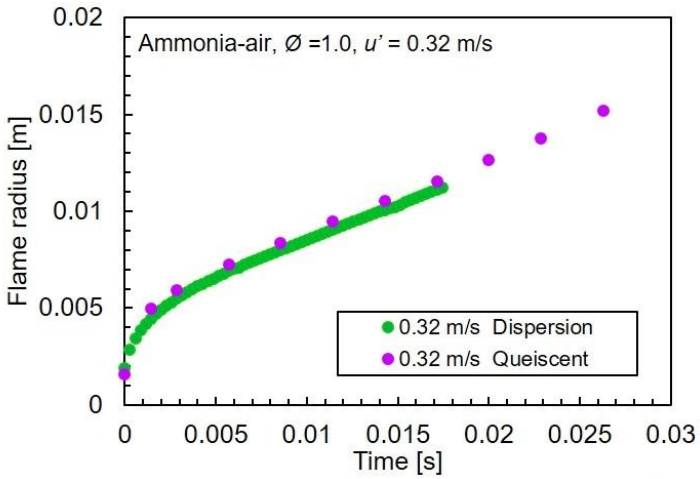

Figure 3. 4 Flame radius as a function of elapsed time for quiescent mixture, and mixture with dispersion flow.

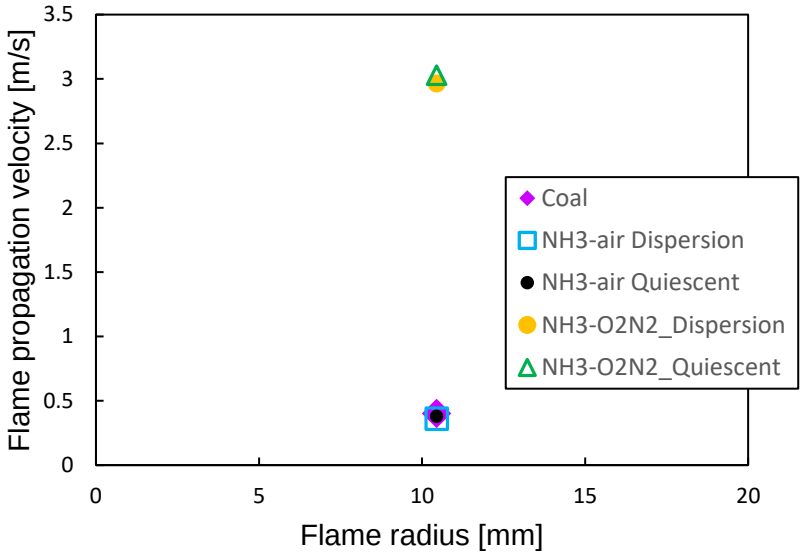

Figure 3. 5 Flame propagation velocity in quiescent mixture, and mixture with dispersion flow.

Table 3.2 shows the estimation of the equivalence ratios for various coal concentration, *G* for C5 coal. The calculated equivalence ratios were based on ultimate analysis as shown in Table 3.1. For the coal particles, the carbon, hydrogen, oxygen, nitrogen and sulfur were considered as the fuels to calculate the equivalence ratios.

Table 3. 2 Equivalence ratios for various coal concentrations, *G* of C5 coal.

Coal concentration, *G* [kg/m³]	Equivalence ratio, Ø
0.6	1.47
1.3	3.18
2.0	4.89
2.3	5.62

3.1.2 Coal-O_2N_2 (coal) combustion in microgravity

Pulverized coal cloud combustion experiment in microgravity (μg) was performed by using the same experimental apparatus as in normal gravity experiment. However, with modification on direct imaging configuration by using a reflective mirror due to a limited spatial volume. In microgravity experiments without fan rotation, there is no relative

velocity of the gas and coal particles. Two types of pulverized coal were used as the fuel in microgravity experiment; C5 and TW coal with different fuel ratio as properties of each are shown in Table 3.1 (in Section 3.1.1). Fuel ratio is the ratio of fixed carbon to the volatile matter. In general, higher fuel ratio is difficult to ignite. Coal concentration (G) inside the combustion chamber was fixed at 2.0 kg/m^3. Only the G = 2.0 kg/m^3 showed flame propagation for all type of coal in the tested turbulence intensity. The same coal concentration was employed to make the comparison of 1g and μg results.

In general, a similar procedure and similar ambient gas as coal combustion in normal gravity experiment was used in the microgravity experiment. A sequencer was employed to ensure precise operation timing. A programmable controller (Keyence KV-1000) was used as the sequencer. The sequence and ON/OFF time of the experimental devices were programmed into the sequencer. The sequence controller switch (SCS) is the virtual switch in the sequencer programming. The operations of the experiment begin with turn ON the SCS.

In the microgravity experiments, the coal particles were first loaded in four filter cups and tubes within equal amounts on a weight basis. Then, the ambient gas was mixed in the chamber and dispersion tank as described above in Section 3.1.1. Figure 3.6 shows the experimental apparatus as an inner capsule in μg experiment. Before the whole capsule placed in the top of the drop tower, on the ground, the inner capsule placed inside of the outer capsule, as shown in Fig. 3.7. For experiments with the turbulent conditions, the turbulence-inducing fans were manually switched ON before putting the capsule at the top of drop tower and the fans continued rotating at a constant prespecified speed during the experiment. After the capsule was released, the microgravity switch was triggered, which turns ON the SCS. All operations then began running in sequence. The pressure inside the

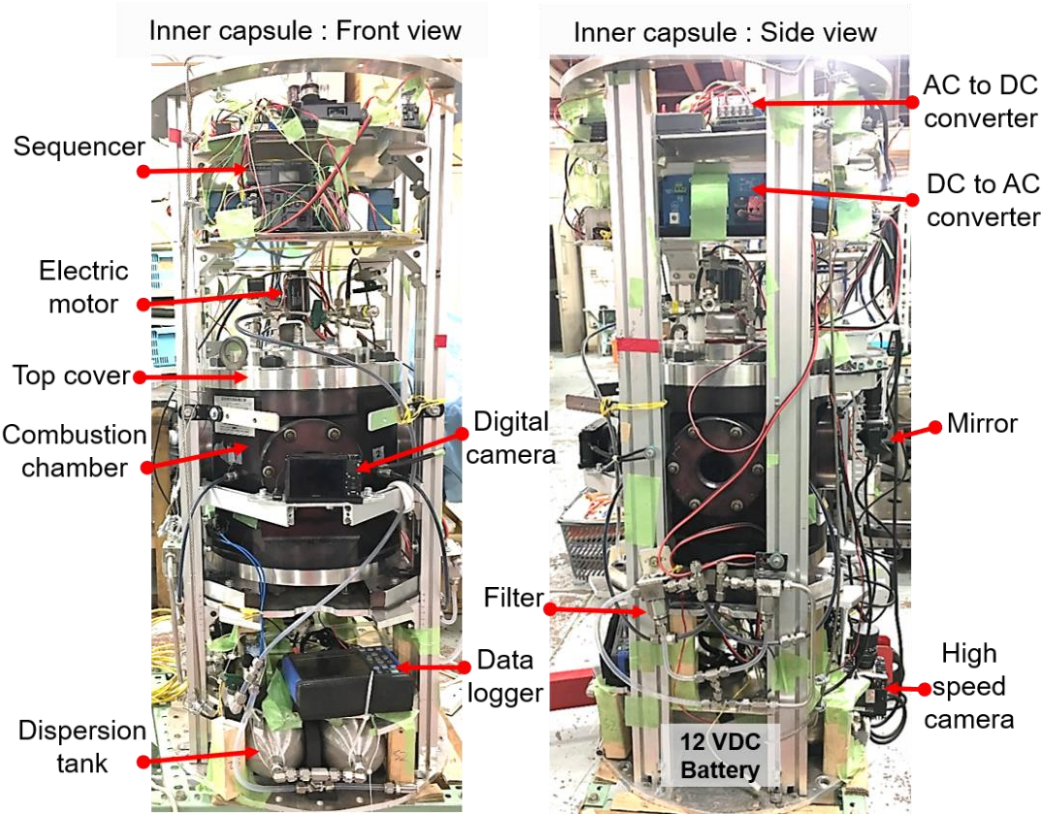

Figure 3. 6 Experimental apparatus (inner capsule) for normal gravity experiment.

chamber was recorded via the data logger and the solenoid valve was switched on to begin coal particle dispersion for 0.7 s. After 0.3 s the ending of the dispersion, the camera started imaging and the coal particle cloud was ignited at the center of chamber at atmospheric pressure. According to a total microgravity time approximately 2.5 s, the flame propagation time allowance was set to 1 s. The sequence of operation in microgravity experiment shown in Fig. 3.8. After each experiment, any coal particles remaining in the tube or filter were measured. For the experiments under normal gravity conditions, to start the experiment operations, the SCS was manually triggered. The coal concentration inside the combustion chamber was within ± 4% of the target value, for all tests.

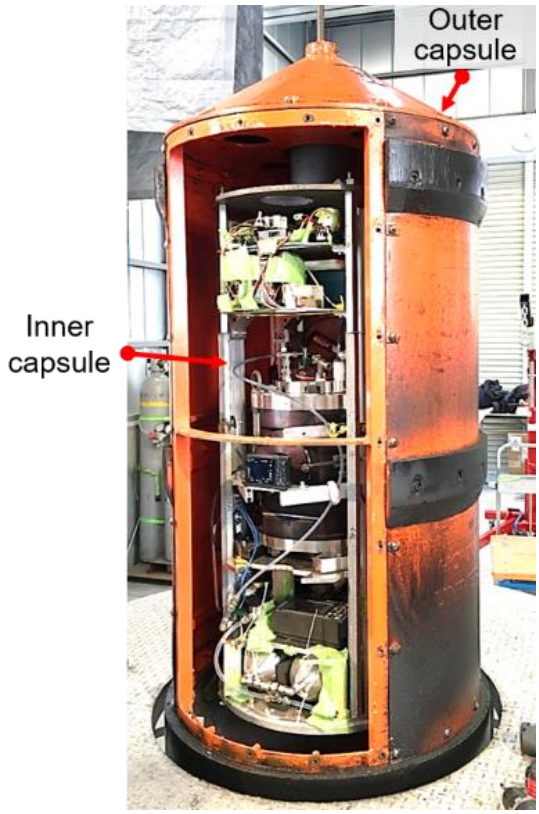

Figure 3. 8 Inner capsule placed inside the outer capsule for microgravity experiment in drop tower facility.

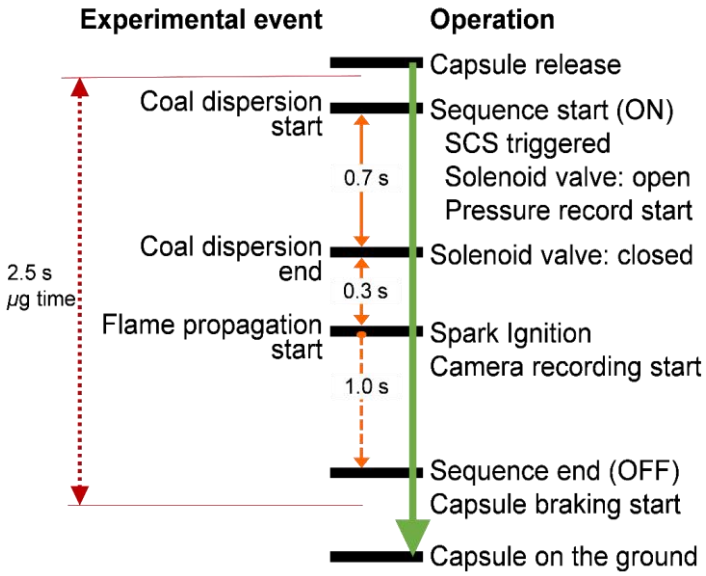

Figure 3. 7 Sequence of operation in the microgravity experiment.

3.1.3 Ammonia combustion

Ammonia-air and ammonia-O_2N_2 premixed combustion experiment were performed for various equivalence ratios and turbulence intensities. The experiments were performed by using the same experimental apparatus for coal combustion. However, the dispersion system was not used because the gas mixture was prepared in the chamber for the premixed ammonia combustion. The Schlieren photography and OH radical imaging were employed to capture the flame images, as shown in Fig. 3.9 and Fig. 3.10. The ignition energy was set to 2.8 J, same to [11]. Before the ignition, the mixtures were carefully mixed inside the chamber with the fan rotation for about 10 minutes, and the fans kept rotating at the pre-specified for the turbulent condition. For the quiescent condition, the fan rotation stops 3 minutes prior to spark ignition to ensure the quiescent environment inside the chamber.

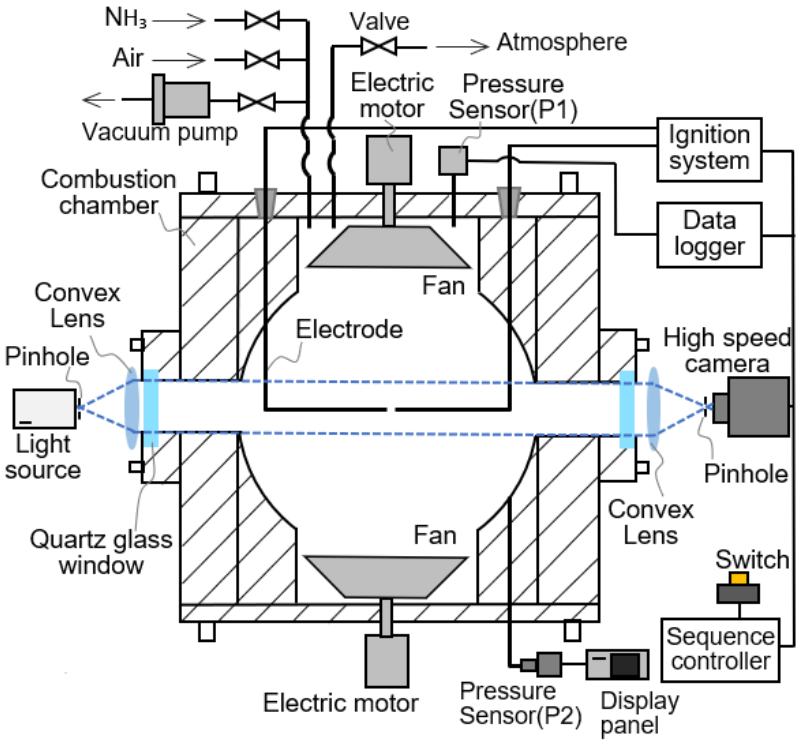

Figure 3. 9 Schematic of experimental apparatus for ammonia combustion.

Table 3.3 shows the properties of ammonia-air mixtures [17] and Table 3.4 for ammonia-O_2N_2. The $\emptyset$, ρ_u, ρ_b, λ, c_p, α, ν and Le are equivalence ratio, unburned mixture density, burned gas density, thermal conductivity, specific heat at constant pressure, thermal diffusivity, kinematic viscosity and Lewis number, respectively. The λ, c_p, α, ν and Le were calculated by using the website of the David Dandy research group at Colorado State University [18].

Table 3. 3 Properties of ammonia-air mixtures.

ϕ [-]	ρ_u [kg/m^3]	ρ_b [kg/m^3]	λ [10^{-3}W/m/K]	c_p [J/kg/K]	α [10^{-5}m^2/s]	ν [10^{-5}m^2/s]	Le [-]
0.6	1.115	0.202	27.08	1099	2.210	1.564	0.95
0.7	1.105	0.183	27.19	1114	2.210	1.562	0.95
0.8	1.095	0.168	27.29	1128	2.209	1.561	0.94
0.9	1.087	0.156	27.39	1141	2.208	1.559	0.93
1.0	1.078	0.147	27.48	1155	2.208	1.558	--
1.1	1.070	0.147	27.56	1168	2.207	1.557	1.10
1.2	1.062	0.148	27.64	1180	2.205	1.556	1.10
1.3	1.055	0.150	27.71	1192	2.204	1.554	1.09

Table 3. 4 Properties of ammonia-O_2N_2 mixtures.

ϕ [-]	ρ_u [kg/m^3]	ρ_b [kg/m^3]	λ [10^{-3}W/m/K]	c_p [J/kg/K]	α [10^{-5}m^2/s]	ν [10^{-5}m^2/s]	Le [-]
0.2	1.1612	0.27957	26.913	1048.4	2.2107	1.5691	0.971
0.3	1.1398	0.21432	27.142	1077.3	2.2102	1.5662	0.953
0.4	1.1204	0.178	27.34	1104.7	2.209	1.5635	0.936
0.5	1.1025	0.15506	27.513	1130.6	2.2072	1.561	0.921
0.6	1.0861	0.1394	27.666	1155.2	2.2051	1.5585	0.906
0.7	1.071	0.12813	27.802	1178.5	2.2027	1.5562	0.892
0.8	1.057	0.11972	27.922	1200.7	2.2002	1.554	0.88
0.9	1.044	0.1134	28.03	1221.8	2.1975	1.5519	0.868
1.0	1.0319	0.10893	28.128	1241.9	2.1948	1.5499	--
1.1	1.0206	0.10646	28.216	1261.1	2.1921	1.548	1.138
1.2	1.0101	0.10575	28.296	1279.5	2.1895	1.5462	1.135
1.3	1.0002	0.10609	28.369	1297	2.1868	1.5444	1.133
1.4	0.99092	0.107	28.435	1313.8	2.1842	1.5428	1.13
1.5	0.98219	0.10827	28.496	1329.9	2.1816	1.5412	1.127
1.6	0.97397	0.10978	28.552	1345.3	2.1791	1.5396	1.125
1.7	0.96621	0.11147	28.604	1360.1	2.1767	1.5381	1.122
1.8	0.95887	0.11331	28.652	1374.3	2.1743	1.5367	1.119
1.9	0.95191	0.11528	28.697	1387.9	2.172	1.5353	1.116
2.0	0.94532	0.11736	28.738	1401.1	2.1698	1.534	1.114
2.1	0.93906	0.11953	28.776	1413.7	2.1676	1.5328	1.111
2.2	0.93311	0.1218	28.812	1425.9	2.1655	1.5315	1.108

3.1.4 Coal-NH_3-O_2N_2 (Mixing combustion)

Experiments on coal-NH_3-O_2N_2 or coal-ammonia (mixing combustion) were performed for the coal concentration, G = 0.6 kg/m³ and NH_3-O_2N_2 at equivalence ratio, $Ø$ = 0.6. In the C5 coal combustion, the lowest coal concentration = 0.6 kg/m³ was sustained flame propagation in all tested turbulence intensities. Considering the volatile matter gas released from coal particles, the lean condition of the ammonia-O_2N_2 mixture was selected. The mixture inside the chamber was set to -25 kPa to allow the dispersion gas mixture that carries the coal particles to achieve the atmospheric pressure (0.1 MPa) after dispersion. The mixture was ignited at atmospheric pressure, the same as the coal combustion. The flame propagation behavior was recorded by direct imaging and OH radical imaging simultaneously from the same window, as shown in Fig. 3.10. A half mirror was employed for the simultaneously of direct imaging for coal flame and OH radical imaging for ammonia flame. The image intensifier equipped with 300 nm bandwidth filter and UV lens was used

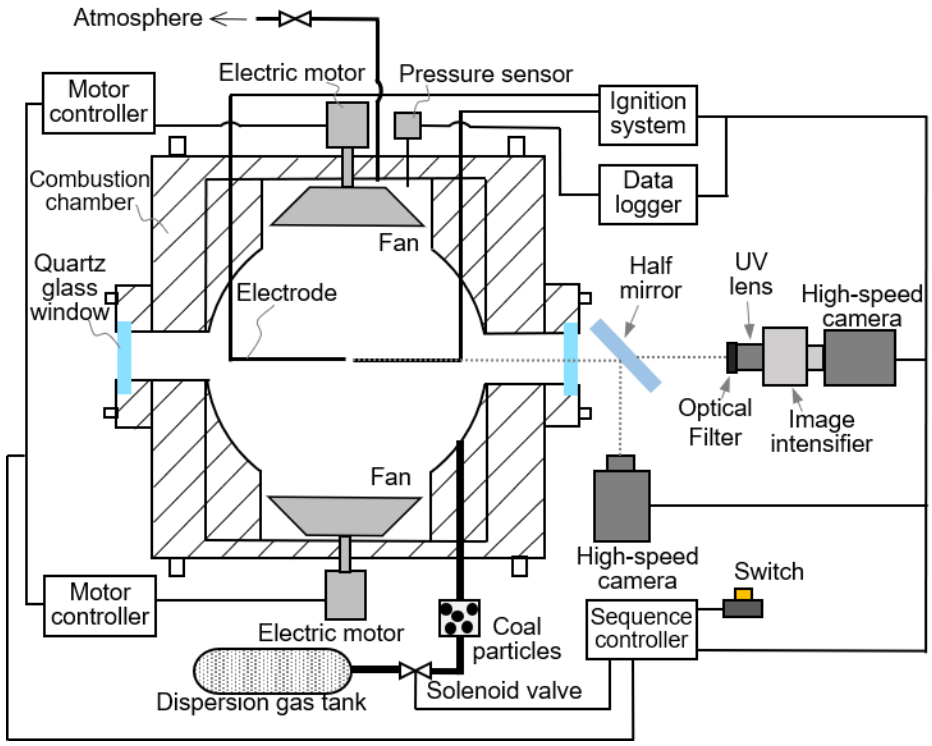

Figure 3. 10 Schematic of experimental apparatus for mixing combustion.

for OH radical imaging in the precise time to gives the readable OH radical images for analysis.

Table 3.5 shows the thermal input from coal for coal concentration, G = 0.6 kg/m³ and NH_3-O_2N_2 mixture for equivalence ratio, $\emptyset$ = 0.6. It shows the coal (by weight) needed in the combustion field to maintain the total thermal input after substituting by thermal input from ammonia in mixing combustion. It also shows the amount (by weight %) of coal can be subtracted in the mixing combustion. For the mixing combustion, the error of coal concentration is ± 3%.

Table 3. 5 Thermal input from coal and ammonia.

Substance	Low Heating Value (LHV) [MJ/kg]	Coal for G = 0.6 kg/m³ [kg]	Thermal input from coal for G=0.6 kg/m³ [MJ]	Thermal input from ammonia for $\emptyset$=0.6 [MJ]	Needed thermal input from coal [MJ]	Coal needed [kg]	Coal subtracted [kg]	Coal subtracted [%]	Coal, G error [weight %]
Coal (C5)	27.8	0.003714	0.103249	0.021221	0.0820279	0.002951	0.0007634	20.5535	±3
Coal (TW)	27.2	0.003714	0.101021	0.021221	0.0797995	0.002934	0.0007802	21.0069	±3
Coal (KK)	30.1	0.003714	0.111791	0.021221	0.0905701	0.003009	0.0007050	18.9829	±3
Coal (UL)	27.2	0.003714	0.101021	0.021221	0.0797995	0.002934	0.0007802	21.0069	±3
Ammonia	18.6	-	-	0.021221	-	-	-	-	-

Table 3.6 shows the equivalence ratios for various coal types. For the coal particles, the carbon, hydrogen, oxygen, nitrogen and sulfur were considered as the fuels to calculate the equivalence ratios. The calculated equivalence ratios were based on the ultimate dry analysis shown earlier in Table 3.1.

Table 3. 6 Equivalence ratios, $\emptyset$ for various coal types.

Coal type	Coal concentration by LHV [kg/m³]	(Fuel/Gas) stoichiometric [-]	Fuel/Gas [-]	Equivalence ratio, $\emptyset$
C5	0.6	0.658711	0.767175	1.16
TW	0.6	0.604335	0.714153	1.18
KK	0.6	0.589508	0.787923	1.34
UL	0.6	0.536055	0.702395	1.31

3.2 Turbulence intensity and fan speed correlation

A correlation between fan rotational speed, N and turbulence intensity, u' determined from particle image velocimetry (PIV) measurements. By using the experimental apparatus in the present study, the PIV measurement was carried out by Seika Digital Image Co., Ltd in the Laboratory of Space Utilization, Hokkaido University. The PIV measurement equipment consists of a CCD camera of 1600 x 1200 pixels resolution, a double-pulsed Nd:YAG laser of 532 nm wavelength with delay 10 μs, a timing controller, and seeding generator. To trace the turbulent flow, the oil mist of 1 μm in size was used as particle tracing seed. Figure 3.11 shows the combustion chamber with the experimental apparatus and equipment of PIV measurements.

Various scale eddies exist in a turbulent flow field; therefore, two measurements were necessary which are the small and large measurement field. Analysis window was set to 32 x32 pixels with 50% overlap for both measurement field. Small measurement field of 8 mm window with 7 μm pixel size in flow for high resolution, whereas 60 mm window

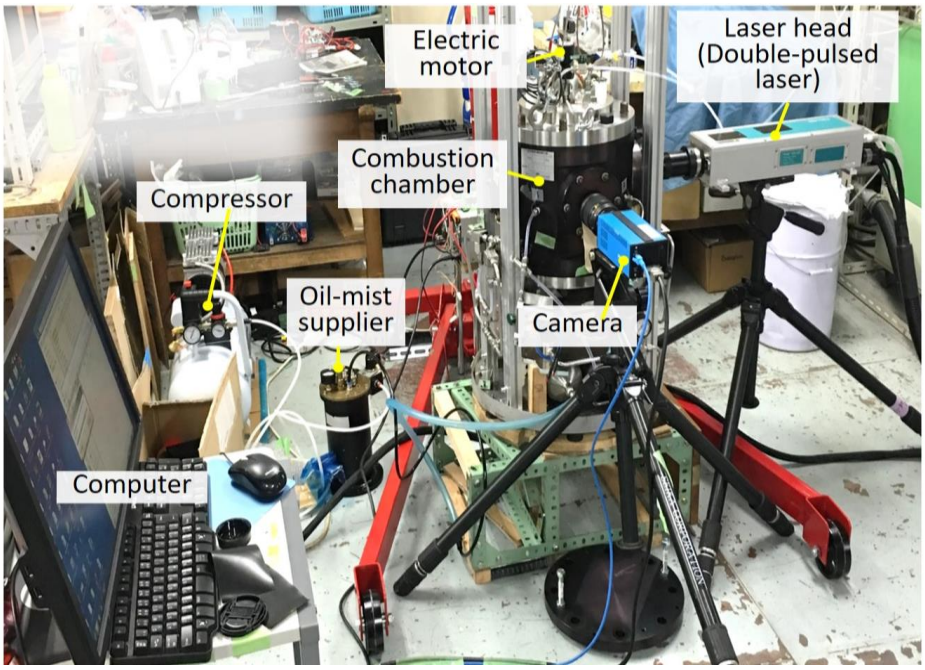

Figure 3. 11 Equipment of PIV measurement.

size with 54 μm pixel size in the flow of large field measurement. A MicroNikkor105mm f/2.8G and Nikkor28mm f/1.8 lens were employed to image the turbulent flow for the small and large measurement field, respectively.

Figure 3.12 shows the relationship between the fan rotational speed and the turbulence intensity. It is shown that the turbulence intensity is proportional to the fan speed. The turbulence was considered homogeneous with no regular bulk motion in the center of the combustion vessel [15]. The integral length scale of turbulence was determined by utilizing the data obtained from the PIV measurement.

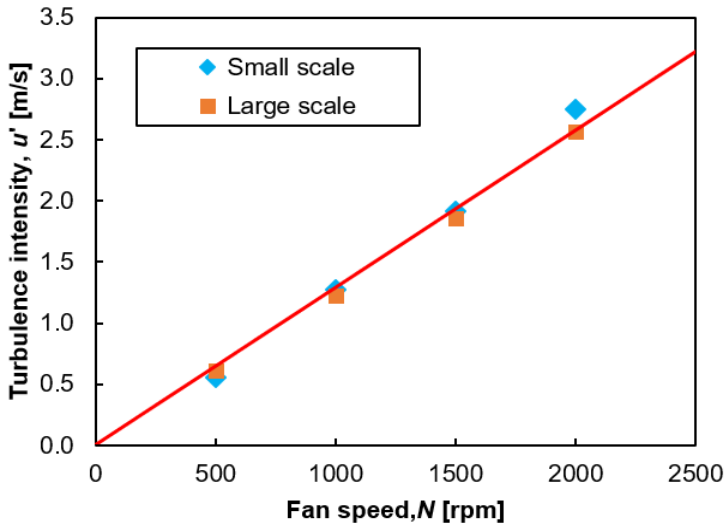

Figure 3. 12 Turbulence intensity, *u*' as a function of fan speed, *N*.

The result of large measurement field was adopted to estimate the longitudinal integral length scale. In the present study, distribution of turbulence intensity analysis area of 47 x 34 mm was adopted. The longitudinal velocity correlation coefficients, $R_{11}(x)$ were calculated using the fluctuation component of velocity obtained from the PIV measurement. Hence, $R_{11}(x)$ was approximated by an exponential function as shown in (2).

$$R_{11}(x) \approx exp(-px^q) \qquad (2)$$

where x is the separation distance along the horizontal axis of the turbulence intensity analysis area, as shown in Fig. 3.13. The constant $p = 7.80 \times 10^{-3}$ and $q = 1.54$ were determined from least-square fitting. Figure 3.13 shows that the solid curve is approximated curve of $R_{11}(x)$ by Eqn. (2). The longitudinal integral length scale, L_f is defined as the integration of $R_{11}(x)$ with respect to x from zero to infinity. Therefore, the integration can be determined using Gamma function, Γ, as expressed in Eqn. (3).

$$L_f = \int_0^\infty R_{11}(x)dx$$
$$= p^{-1/q} \cdot \Gamma\left(1 + \frac{1}{q}\right) \quad (3)$$

The longitudinal integral length scale, L_f of 20.9 mm was calculated regardless of the turbulence intensity. The approach follows that of Smallbone et al. [15] and Hayakawa et al. [19]. The calculated L_f in the present study was close to the value in the previous studies [14,19].

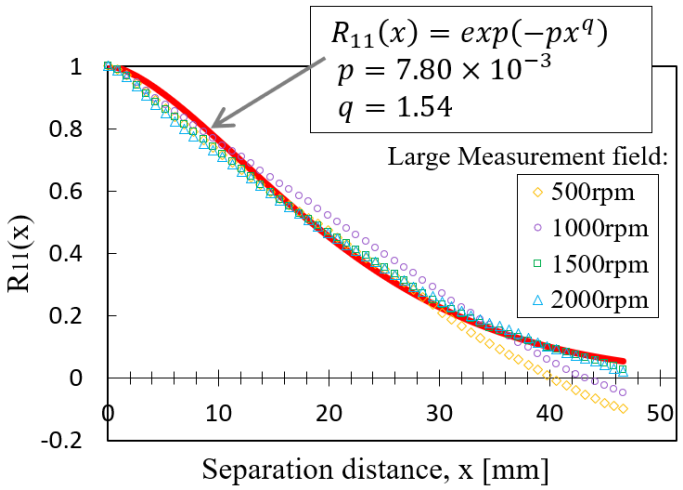

Figure 3. 13 Variation of longitudinal velocity correlation coefficient, $R_{11}(x)$, with distance, x.

Chapter 4 Result and discussion

This chapter describes the results and discussion for coal combustion, ammonia combustion, and the coal-NH_3-O_2N_2 or coal-ammonia (mixing) combustion.

4.1 Coal-O_2N_2 combustion (in microgravity)

4.1.1 Flame propagation behavior

The separate experimental series were performed for the results described in this section. The flame propagation behavior for the C5 and TW coal in microgravity (μg) condition for G = 2.0 kg/m³ for u' of 0, 0.32, 0.65 and 0.97 m/s were clarified. The significantly different flame propagation behavior for u' = 0 m/s were observed under 1g and μg conditions. Under μg, flame propagation was sustained even after the elapsed time of 200 ms, whereas the flame went extinct under 1g condition, as shown in Fig. 4.1. The coal particle clouds were observed as more flammable under μg than under 1g environment.

The different phenomenon is due to the effect of natural convection. Under μg environment, the flame propagates spherically from the center of the combustion chamber. The heat from the burned region is transferred to unburned region outwardly. The volatile matter is released from unburned coal particles when the unburned coal particles are heated up. After that, the released volatile matter was burned continuously. Therefore, the flame propagation is sustained by the series of continuous processes, namely, the heating of unburned particles, the evolution of volatile matter from unburned particles, and the combustion reaction of volatile matter in the gas phase.

While under 1g environment, the natural convection induced flow deformed the whole flame shape. Thus, the ratio of the area of flame front to the volume of the burned region under 1g environment is higher than the similar ratio under μg. The high ratio of the area of flame front to the volume of the burned region under 1g reduced the flame

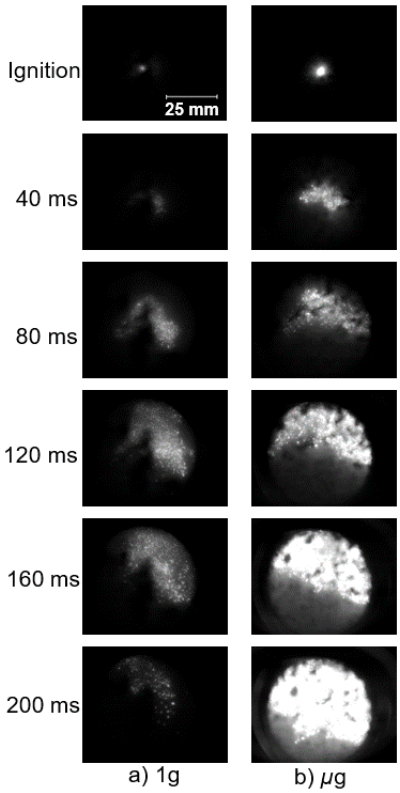

Figure 4. 1 Flame propagation behavior of TW coal particle cloud at u'= 0 m/s in a) 1g, and b) μg.

temperature. Moreover, the flame front is stretched by the deformation of the overall shape of the unburned region, due to the natural convection induced flow in the combustion field. The stretch of the flame front also caused the flame temperature to decrease. Consequently, the flame under 1g environment quenched after the significant effect of deformation caused by the natural convection.

The flame radius of C5 and TW at u' = 0.32 m/s increases as elapsed time increases, both in 1g and μg, as shown in Fig. 4.2. However, compared to C5 and TW coal in 1g, the flame radius increasing with acceleration for C5 coal in μg. The flame propagation velocity was obtained from the relationship of a flame radius and elapsed time. As shown in Fig. 4.3, flame propagation velocity increases as the flame radius increases. However, the flame propagation velocity of C5 coal under μg increased more rapidly. Whereas the flame propagation velocity of C5 coal increased gradually, and the flame propagation velocity of

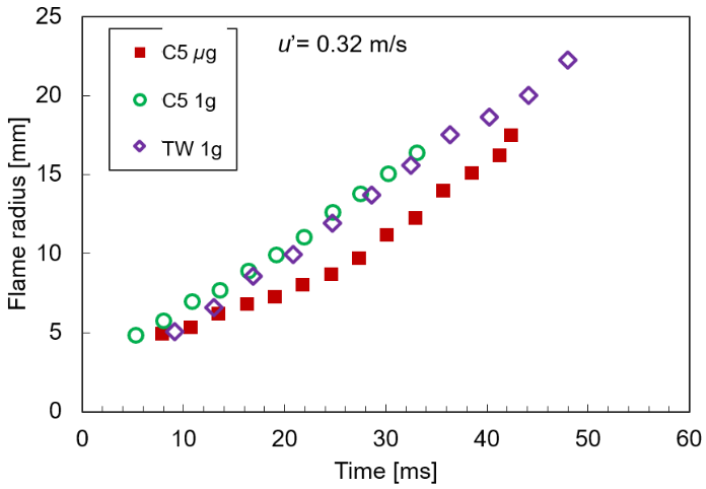

Figure 4. 2 Flame radius as a function of elapsed time for C5 and TW coal at u'=0.32 m/s in 1g and μg.

TW coal increased even more slowly in 1g. It demonstrates that the heat loss in μg is lower than in 1g. It also illustrates the effect of fuel ratio on the flame propagation velocity. The flame propagation velocity of C5 coal with relatively lowest fuel ratio is higher than the TW coal. This showed the amount of volatile matter of coal particles indicated the volatile matter gas density in the coal cloud. Thus, the volatile matter gas combustion determines the flame propagation velocity of the coal cloud. Within the observation range, all the flame propagation velocity showed increasing trend without any constant value. In the present study, the fully developed velocity values were not obtained. Flame propagation velocities

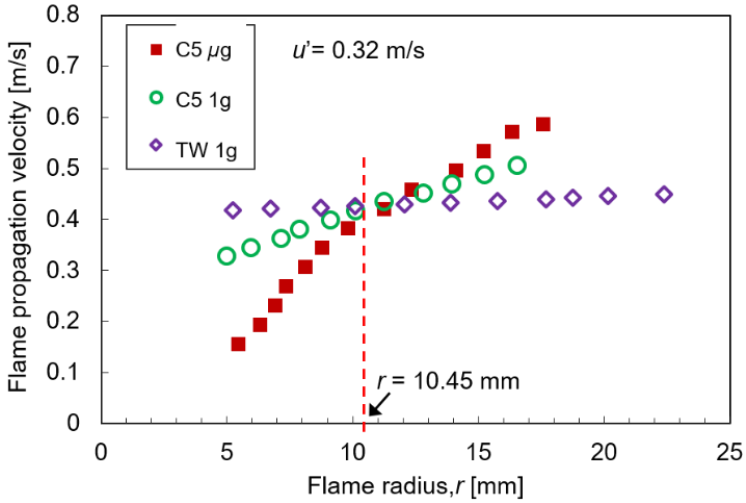

Figure 4. 3 Relationship between flame propagation velocity and flame radius for C5 and TW coal at u'=0.32 m/s in 1g and μg.

at a flame radius of 10.45 mm were plotted to determine the flame propagation velocity as a function of turbulence intensity, as shown in Fig. 4.4. The flame radius of 10.45 mm was chosen because it is equivalent to the flame diameter of 20.9 mm, which is the same length as the longitudinal integral length scale, L_f, calculated in the analysis of the turbulent field inside the chamber, as described in Section 3.2. Overall, flame propagation velocity was shown to increase with increasing turbulence intensity. The flame propagation velocity for some cases were not showed in Fig. 4.13 even the flame propagation capability was obtained in Table 4.1. This is because the flame radius was not obtained, part of the flame images was covered by coal particles that sticking on the quartz glass window due to high coal concentration of 2.0 kg/m³.

Table 4.1 summarized the capability for C5 and TW coal particle clouds to sustain flame propagation for coal concentration of 2.0 kg/m³ in 1g and μg conditions. Coal cloud flame is a luminous flame. The "flame propagation" define as the coal particle cloud propagates from the spark ignition period with continuous expansion scale of luminous flame in the whole combustion field. In opposite, the "flame extinction" define as just a spark ignition phenomenon was observed, or no continuous expansion scale of luminous

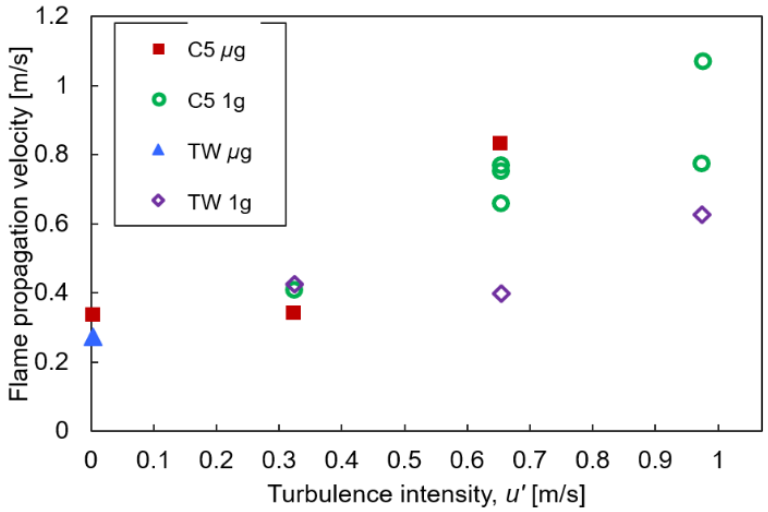

Figure 4. 4 Flame propagation velocity for C5 and TW coal for various turbulence intensities, u' in 1g and μg.

Table 4. 1 Flame propagation capabilities in 1g and μg.

Coal brand	**C5**		**TW**	
Turbulence intensity, *u*' [m/s]	**1g**	**μg**	**1g**	**μg**
0	x	O	x	O
0.32	O	O	O	O
0.65	O	O	O	O
0.97	O	no exp.	O	no exp.

O: Flame propagation; x: Flame extinction; no exp.: No experiment conducted

flame. At *u*'= 0 m/s, the flame was propagated for C5 and TW coal under μg, but not in the 1g environment. Furthermore, the flame was propagated under 1g with turbulent conditions for C5 and TW coal with a fuel ratio of 1.56 and 2.5, respectively. Thus, turbulence was shown to have a positive effect on the flame propagation of coal particle clouds. Experiments for all conditions cannot be performed due to a limited number of μg experiment.

4.1.2 Concluding remarks

The experiments under 1g and μg environments clarified the effects of gravity, turbulence intensity, and fuel ratio on the spherical turbulent flame propagation behavior of a pulverized coal particle clouds in a turbulent flow field. In μg, the coal particle cloud is more flammable than in the 1g environment. Natural convection, which exists in the 1g environment, has a significant effect on the flame propagation behavior of common bituminous coal (C5) and low ignitable coal (TW) particle cloud at *u*' = 0 m/s. Natural convection causes the deformation of the burned region which leads the ratio of the area of the flame front to the volume of the burned region to increase and also leads the flame front to be stretched. The absence of natural convection in the μg environment makes the flame propagation to be sustained. In a turbulent, no significant different of the flame propagation velocity in μg and 1g environment. Turbulence intensity has a positive effect on flame

propagation velocity for C5 and TW coal. The results in this section were from separated experimental series from the results in Section 4.2. However, for the C5 coal in 1g, it shows good agreement to the results in Section 4.2.

4.2 Coal-O_2N_2 combustion (in normal gravity)

Section 4.1 described that, for the spherical turbulent flame propagation of pulverized coal particle cloud, no significant difference of the flame propagation velocity in μg and 1g environment. Therefore, the series of the experiment was performed in normal gravity (1g) to investigate the effect of turbulence intensity and coal concentration on the flame propagation behavior of coal particle clouds.

4.2.1 Flame propagation behavior

The luminous flames of coal particle clouds with clearly flame front were observed. Figure 4.5 shows sequential flame images of the spherical turbulent pulverized coal clouds flame propagation for coal concentration, G = 1.3 kg/m^3 for turbulence intensities, u' of 0.32, 0.65, 0.97 and 1.29 m/s. The luminous flame images were shown from the spark ignition until 20 ms. As the flame propagated from the center, the irregular shapes of the flame front were observed. However, for the whole flame in all cases, the flame propagated almost spherically. Particularly for the lower turbulence intensity, the irregular shape of the flame front maybe due to the heat loss to the electrodes, in the horizontal direction. In addition, the various scales of turbulent eddies wrinkled the flame front is expected to contribute to the irregular shape of the whole flame. Also, there is a possibility that the turbulent eddies drive the flame front backwards. Flame fronts with irregular shapes also observed for gaseous hydrocarbon fuel's flame in a turbulent environment [14]. The flame diameter was

determined by measuring the distance between the farthest flame fronts to represent the scale of the flame. As shown in Fig. 4.5, at the same elapsed time, the flame scales increases as the turbulence intensity increases.

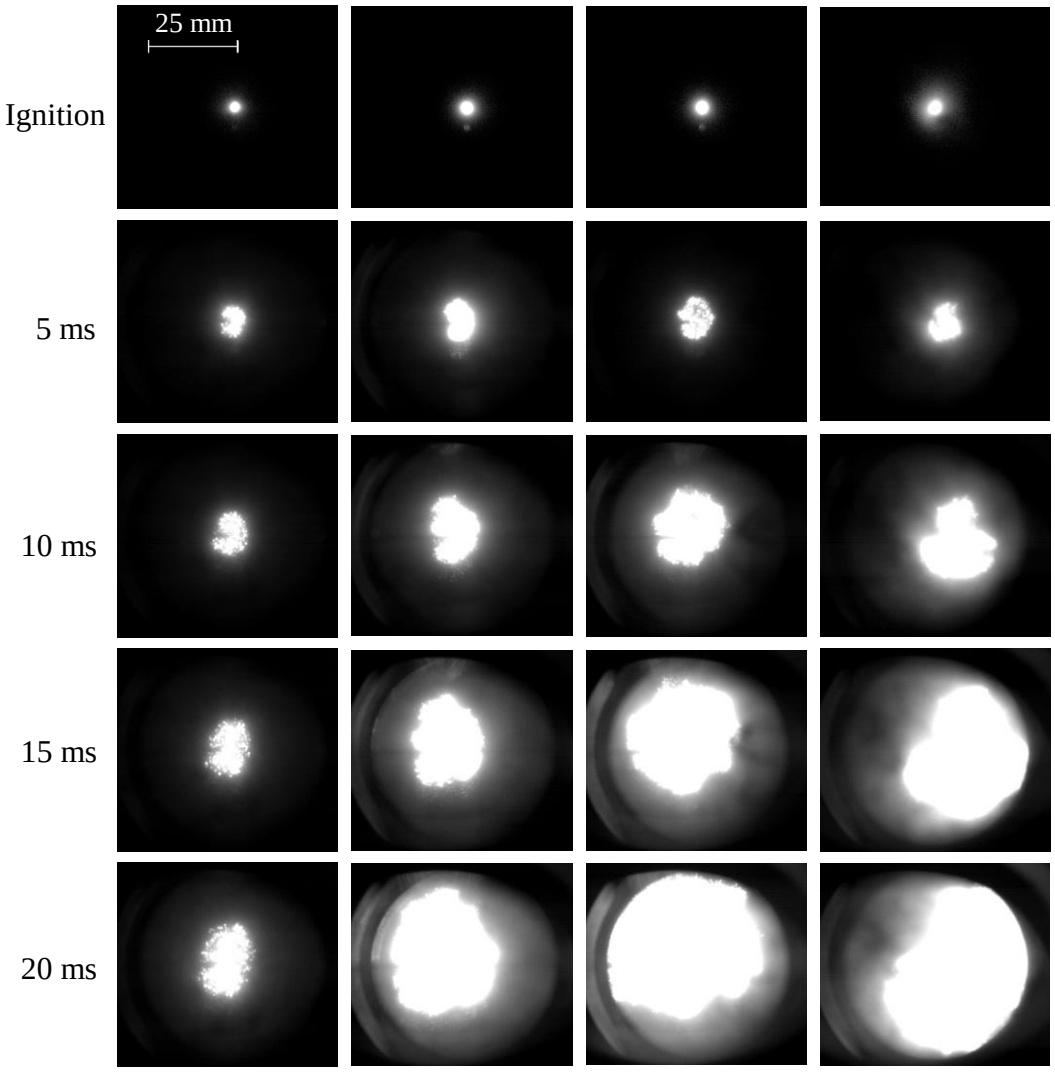

Figure 4. 5 Flame propagation at atmospheric pressure in 40% O_2 and 60% N_2 ambient gas mixture for G = 1.3 kg/m³.

In the present study, the effect of spark ignition on coal clouds flame was examined. Figure 4.6 shows the sequential spark images at the center of the combustion field from the ignition (electron discharged) started until 5 ms, with and without a coal particle cloud. Ignition in the air (without coal cloud), at the first few milliseconds, a small ball-shaped spark kernel was observed as shown in Fig. 4.6 (a). The spark kernel disappeared by 5 ms.

In opposite, with coal cloud, a larger spark kernel was observed at the ignition, which is probably caused by the spark through the coal particles, as shown in Fig. 4.6 (b). Since the small spark kernel in Fig. 4.6 (a) disappeared by 5 ms, then the larger kernel observed in Fig. 4.6 (b) at 5 ms identified as a flame kernel. Therefore, the first 5 ms determined as the ignition affected period in the present study [20].

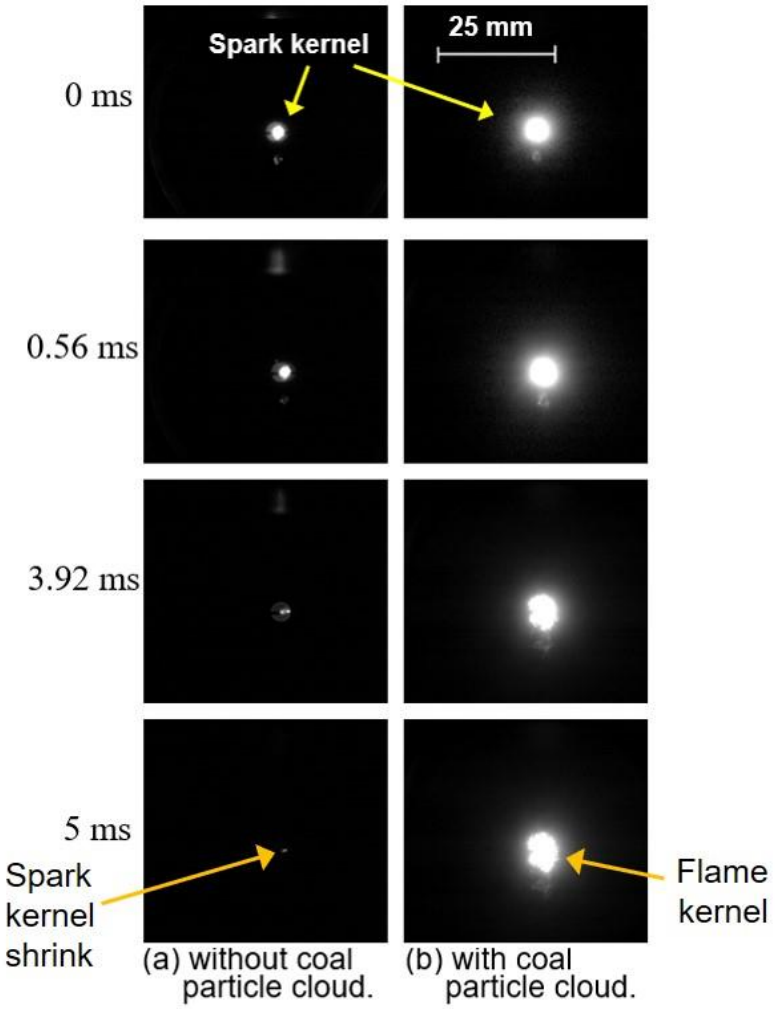

Figure 4. 6 Spark images (a) without a coal particle cloud (in air), and (b) with a coal particle cloud (u' = 0.32 m/s, G = 2.0 kg/m3).

Figure 4.7 illustrates the pressure history inside the chamber at the turbulence intensity of u'= 0.32 m/s, G = 1.3 kg/m³. The pressure is within ± 5% of the atmospheric pressure after the dispersion of coal particles and remains almost constant from the onset of ignition until 60 ms during the flame propagation. The similar pressure histories were

observed for all cases. Therefore, the pressure inside the chamber was assumed to be constant during flame propagation within the limit of observation range.

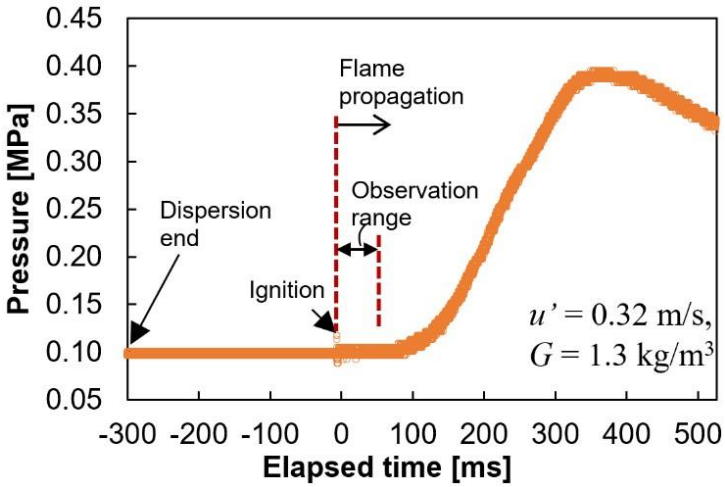

Figure 4. 7 Pressure history during flame propagation.

4.2.2 Flame propagation velocity

It is shown in Fig. 4.8, the relationship between flame radius and elapsed time from 5 ms after the onset of spark ignition for various turbulent intensities for G = 1.3 kg/m³. After 5 ms, the flame propagation was assumed to be not affected by the ignition energy. The ignition affected period was not considered in the calculation of flame propagation

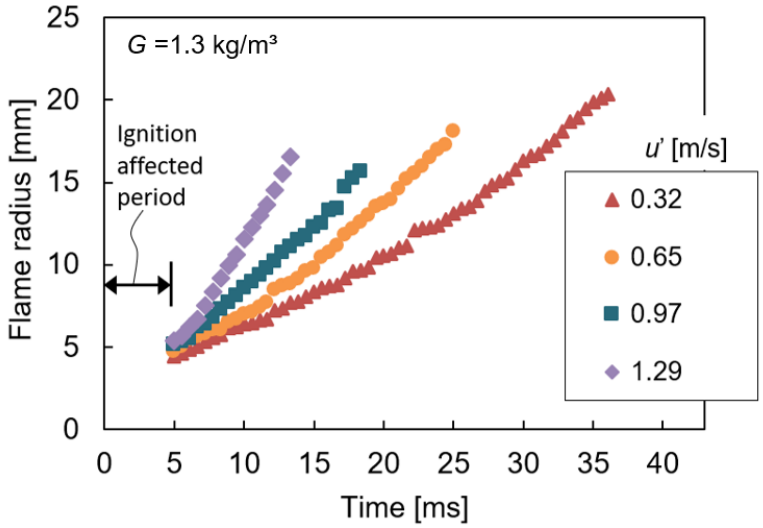

Figure 4. 8 Flame radius as a function of elapsed time.

velocity. As shown in Fig. 4.8, the flame radius increment rate increases as the turbulence intensity increases for all of the turbulence intensities. Similar trends observed for all cases in the present study. The flame radius was measured until the flame front reaches the edge of the window. The maximum radius for each case may differ due to flame shapes that wrinkled by turbulent eddies.

Figure 4.9 shows the relationship between flame propagation velocities and flame radius. Only flame propagation velocities at 5 ms after ignition and onwards were shown in Fig. 4.9. It showed the flame propagation velocity increases as the flame radius increases for all cases. The flame propagation velocity increased because of a widening of the range of eddies that wrinkled the flame front increases as the flame radius increases. Thus, the flame surface area increases, then the heat and mass transfer rates increase causing the volatile matter release rate increases as well. Consequently, the flame propagation velocity increases because the fuel in the gas phase was increased. Similar trends can be seen in the gaseous fuel combustion [11].

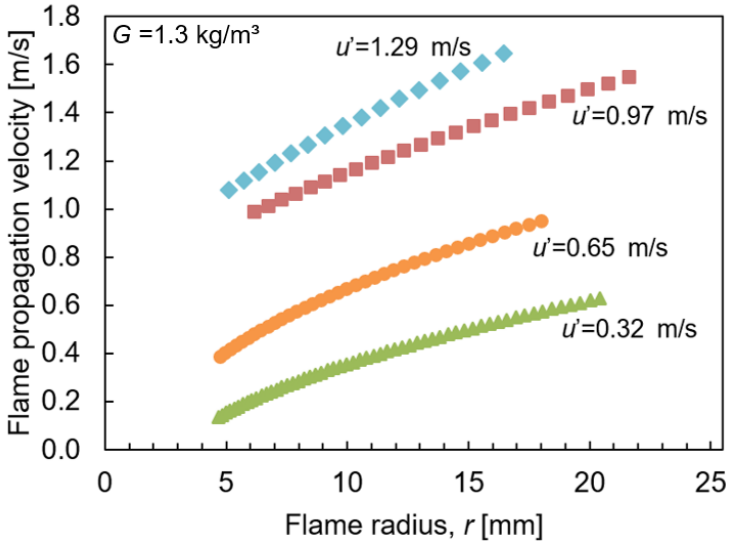

Figure 4. 9 Relationship between flame propagation velocity and flame radius for various *u*'.

Figure 4.10 shows the effect of turbulence intensity on the flame propagation velocity. The flame propagation velocity increases as turbulence intensity increases, similar

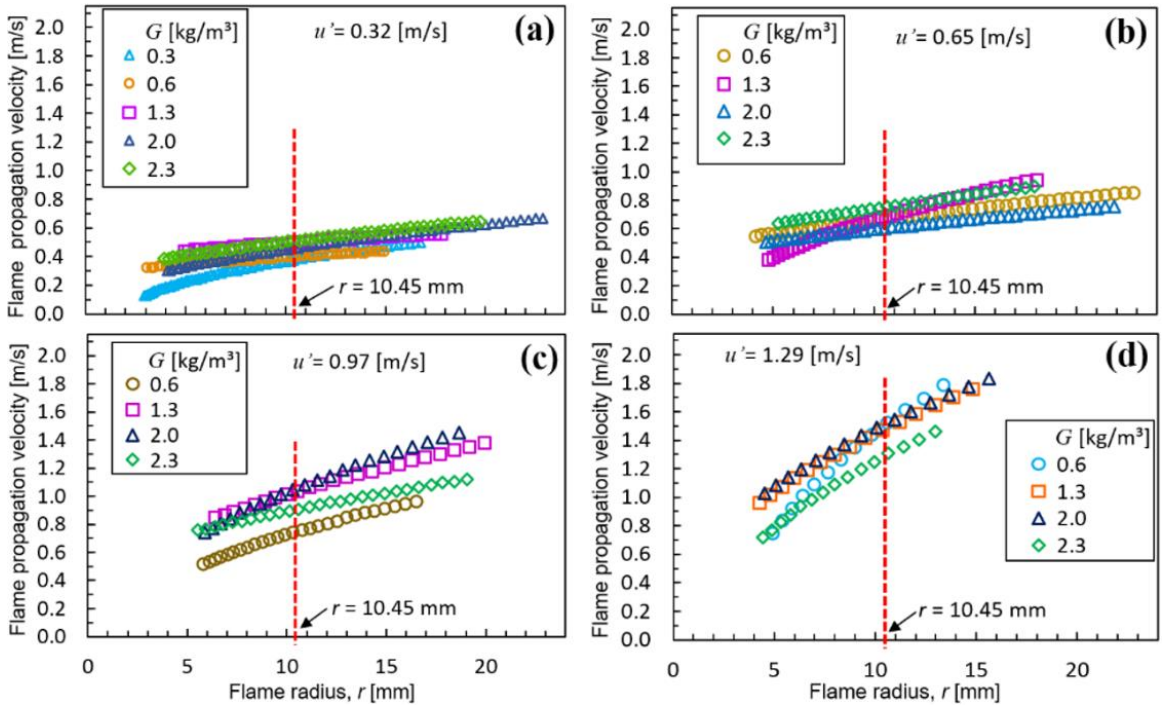

Figure 4. 10 Relationship between flame propagation velocity and flame radius for (a) u'= 0.32 m/s, (b) u'= 0.65 m/s , (c) u'= 0.97 m/s, and (d) u'=1.29 m/s [20].

trends were observed for all cases in the present study. For all cases, the flame propagation velocity as a function of flame radius showed an increasing trend and did not reach any constant value within the observable range of the flame radii. The fully developed velocity values were not obtained in the present study. Therefore, the approach by Mandilas et al. [21] and Kitagawa et al. [22] was adopted. The flame radius of 10.45 mm as shown in Fig. 4.10 was chosen because it is equivalent to the flame diameter of 20.9 mm, which is the same length as the longitudinal integral length scale, L_f, calculated in the analysis of the turbulent field inside the chamber, as described in Section 3.2.

Figure 4.11 shows the relationship between flame propagation velocity and turbulence intensities at the flame radius of 10.45 mm for various coal concentrations. Flame propagation for G = 0.3 kg/m³ only for u'= 0.32 m/s. Except for the lowest coal concentration of G = 0.3 kg/m³, in general, the flame propagation velocity increases as the turbulence intensity increases regardless of the coal concentration. Kitagawa et al.[22]

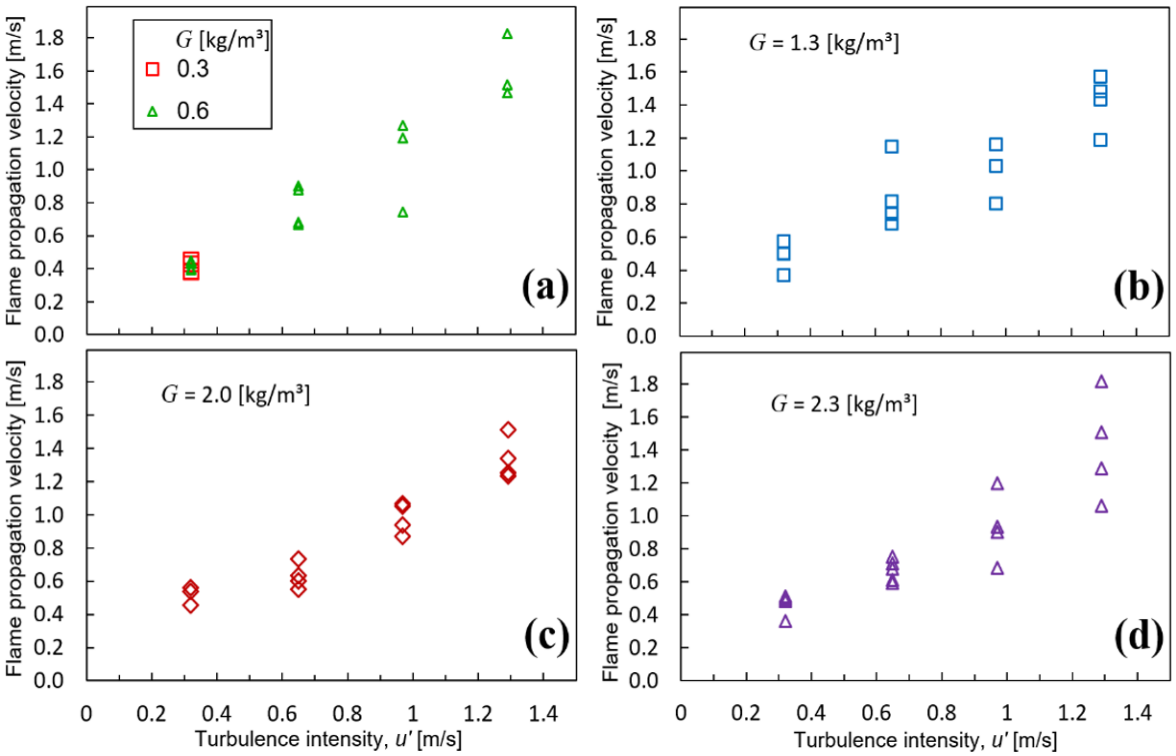

Figure 4. 11 Flame propagation velocity at various turbulence intensities, *u'* for (a) *G* = 0.3 and 0.6 kg/m³, (b) *G* =1.3 kg/m³, (c) *G* = 2.0 kg/m³, and (d) *G* = 2.3 kg/m³ [20].

suggested the flame propagation velocity increases as the turbulence intensity increases for gaseous fuel. They suggested that increases in the flame front area caused increases in the flame propagation velocity by flame wrinkling due to turbulence. The same explanation can be applied to the results of the present study.

However, the coal concentration not showing an obvious effect on the flame propagation velocity. The tendency is different from flame propagation in a quiescent environment. For the flame propagation in a quiescent environment, the trends of flame propagation velocity as a function of coal concentration showed such a maximum value, as mentioned in Chapter 2. The tendency in a quiescent environment maybe can be explained as follows. In a quiescent environment, the flame propagation velocity mainly controlled by the heat conduction between the gas and the particles and the radiation between the particles, as described by Suda et al. [2]. Thus, the distance between the coal particles significantly

affects the flame propagation behavior. Therefore, the coal concentration, which determines the distance between the coal particles, has a significant effect on the flame propagation velocity in a quiescent environment. However, in a turbulent environment, turbulent eddies acting on the flame front including wrinkled the flame front. The flame propagation velocity considered to be dominated mainly by turbulent heat transfer. Consequently, the flame propagation velocity increase as the turbulence intensity increases due to increases of turbulent eddies on the flame front. The flame propagation velocity of a turbulent coal cloud is up to approximately 5 times faster than that of the quiescent environment. Accordingly, the effect of turbulence intensity on the flame propagation velocity is dominant, and the effect of the coal concentration is minimal. This is a unique feature of flame propagation in a turbulent field, which different from flame propagation in the quiescent environment.

Significant effects of the coal concentration on the flame propagation velocity were observed in pulverized coal particle combustion in laminar flow [3]. Moreover, in a spherical flame propagation of gaseous fuel, it was observed that the equivalence ratio strongly affects the flame propagation velocity [22]. However, in a turbulent coal particle cloud, the flame propagation velocity is not much different for various coal concentrations at a given turbulence intensity. According to Xu et al. [23], in a pulverized coal particle turbulent jet flame, eddies in the particle-loading turbulent jet strongly affect the ignition process, shortening the ignition delay time. However, there was no obvious effect of coal concentration on the ignition distance [23]. This tendency corresponds well with the results of our study.

The scatter plot observed for high turbulence intensities as shown in Fig. 4.11. This is due to the relatively lower flame propagation velocity of pulverized coal particle clouds; therefore, the flame shape is highly deformed in high turbulence intensities. A similar

tendency has been observed for gaseous flame propagation [13,14]. The additional reason is that the effects of eddies on flame propagation increases with increasing turbulence intensity. Various scales of turbulent eddies exist in a turbulent flow field and the wrinkling effects of each eddy are different. Therefore, the nonuniformity of the wrinkling effects of the eddies on each case is increase with the increasing turbulence intensity.

4.2.3 Concluding remarks

The effect of turbulence intensity and coal particle concentration on the flame propagation of pulverized coal particle clouds at atmospheric pressure were clarified. The results showed the flame propagation velocity of a pulverized coal particle cloud increases with increasing flame radius in a turbulent field. This caused by a widening of the range of eddies that serve to increase the flame front area as the flame radius increases, as expected in gaseous fuel combustion. Furthermore, the flame propagation velocity of a pulverized coal particle cloud increases as the turbulence intensity increases. This tendency may be due to the increase in the turbulent heat transfer rate at the flame front as the turbulence intensity increases. Compared to the turbulence intensity, the coal concentration has a weak effect on the flame propagation velocity.

4.3 Ammonia combustion

4.3.1 NH_3-air (Ammonia-air) combustion in turbulent

Figure 4.12 shows the sequence of a flame images for Ø = 0.9 and 1.0 at *u*'= 0.32 and 0.65 m/s. At the same elapsed time, the flame scale increases as turbulence intensity increases. This is due to the increase in number and size of turbulence eddies acting on the flame front. Kitagawa et al. [22] suggested that the wrinkling of the flame front caused the increase of the flame propagation velocity due to turbulence, thus increased the flame front area. Therefore, flame propagation velocity increases as the turbulence intensity increases.

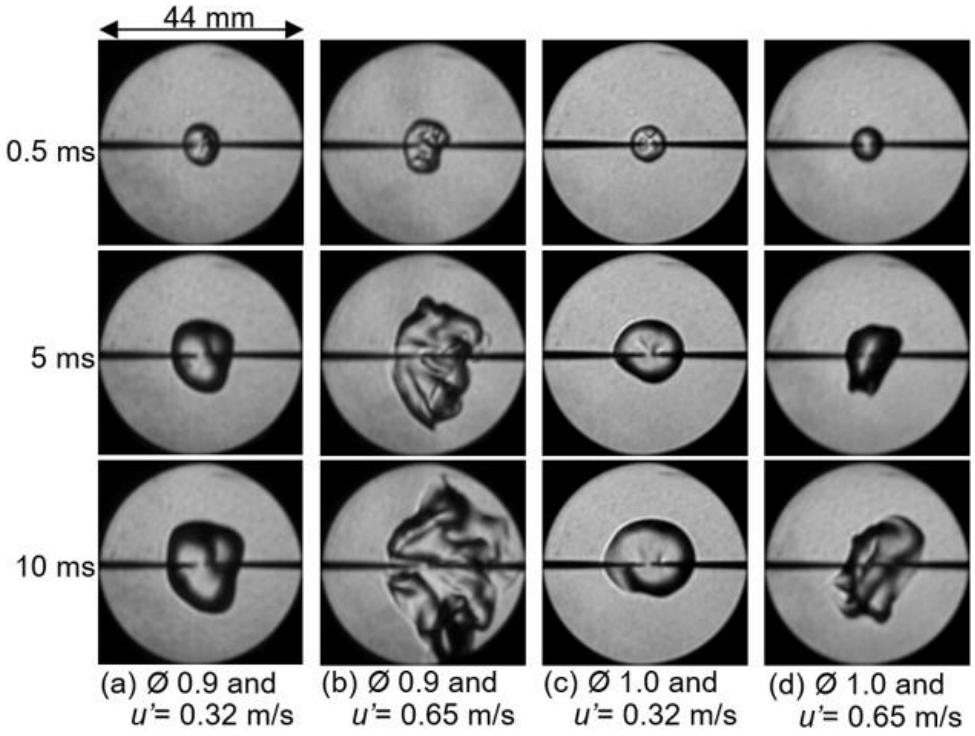

Figure 4. 12 Sequence of flame images for Ø = 0.9 and 1.0 in u'= 0.32 and 0.65 m/s.

Figure 4.13 shows the flame radius as a function of time. The flame radii increment rate was slightly higher as the flame radii increases, for all cases. This is because as the flames scale increases, the range of eddies that increased the flames front area is widened. The flame radius determined by converting the flame area from Schlieren flame images to

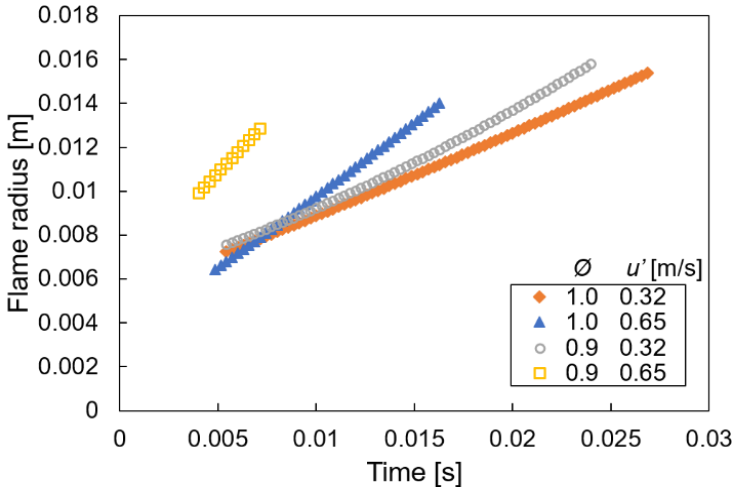

Figure 4. 13 Flame radius as a function of time for *Ø* = 0.9 and 1.0 at *u*'= 0.32 and 0.65 m/s.

the equivalent area of a circle, the same approach as [19,22,24]. Flame propagation velocity was determined from the relationship between the flame radius and elapsed time.

Figure 4.14 shows the relationship between flame propagation velocity and equivalence ratio for *u*'= 0.32 and 0.65 m/s. Similar practice as mentioned earlier, flame propagation velocities at the flame radius of 10.45 mm were displayed in Fig. 4.14. For ammonia-air with relatively thick flame thickness, flame images in some conditions were difficult to analysis due to the unclear of the flame front. Only the conditions with a clear flame front were analyzed and showed in Fig. 4.14. In higher turbulence intensity, the

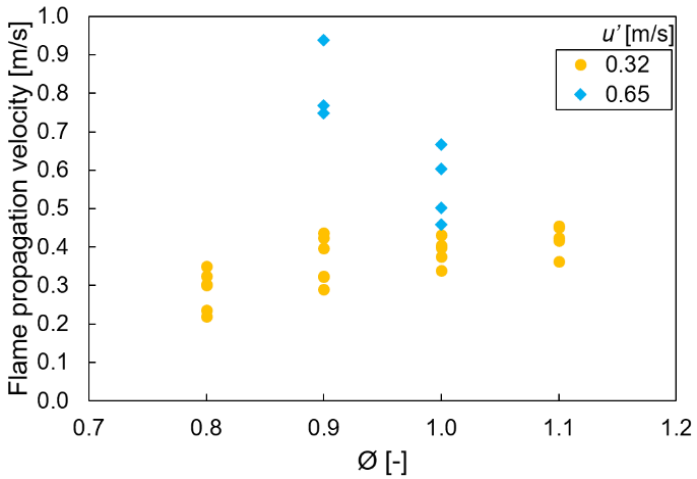

Figure 4. 14 Relationship between flame propagation velocity and equivalence ratio, *Ø*, for *u*'= 0.32 and 0.65 m/s.

ammonia-air mixture has a relatively higher burning velocity in the lean condition due to the *Le* effect. In the lean condition, *Le* is less than unity as shown in Table 3.3 (Section 3.1.3). At the *Le* less than unity, the flame front area can be increased due to the thermo-diffusive effect. Consequently, the flame propagation velocity increases. The higher burning velocity also due to the negative value of burned gas Markstein length, L_b as showed by Hayakawa et al. [11] (Section 2.2.1). Figure 4.15 [25] shows the relationship between Markstein number, *Ma* (=L_b/ δ_l), and equivalence ratio, *Ø* from the present study of ammonia-air combustion in the quiescent environment. In the lean mixtures, the *Ma* < 0, as shown in Fig. 4.15, which close to the result of Hayakawa et al. [11].

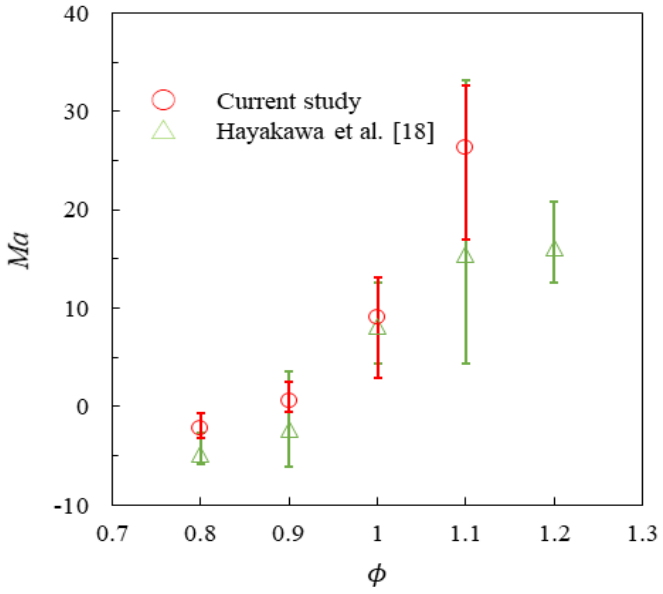

Figure 4. 15 Relationship between Markstein number, *Ma*, and equivalence ratio, *Ø* for ammonia-air mixtures [25].

Figure 4.16 [25] shows the relationship between unstretched laminar burning velocities, S_l and equivalence ratio, *Ø*, from the present study. The results from the previous studies of Hayakawa et al. [11], Takizawa et al. , Pfahl et al. and Zakarnov et al. also showed in the same figures. The unstretched laminar burning velocity was the maximum near the *Ø* = 1.1. The results from the present study showed a good agreement with the previous study.

However, in the present study under the conditions of Ø= 0.7 and 1.2, the unstretched laminar burning velocity cannot be obtained because the flame front from Schlieren flame images was unclear due to the effect of buoyancy. Figure 4.17 shows the effect of buoyancy on ammonia-air flames in a quiescent environment.

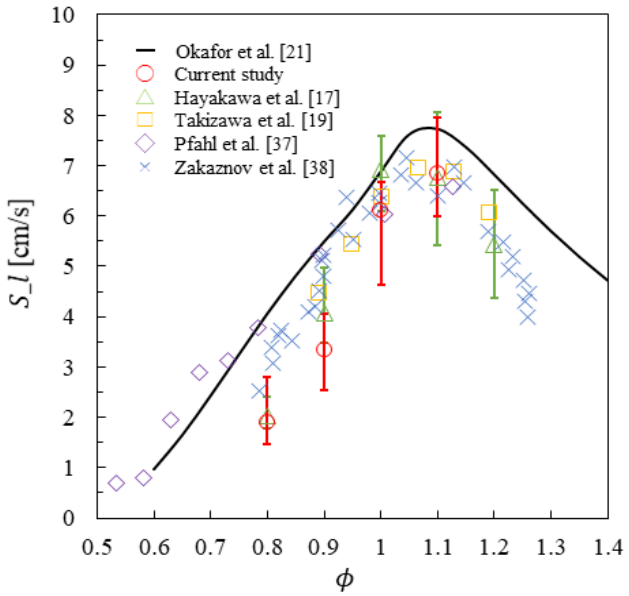

Figure 4. 16 Relationship between unstretched laminar burning velocities, Sı and equivalence ratio, Ø [25].

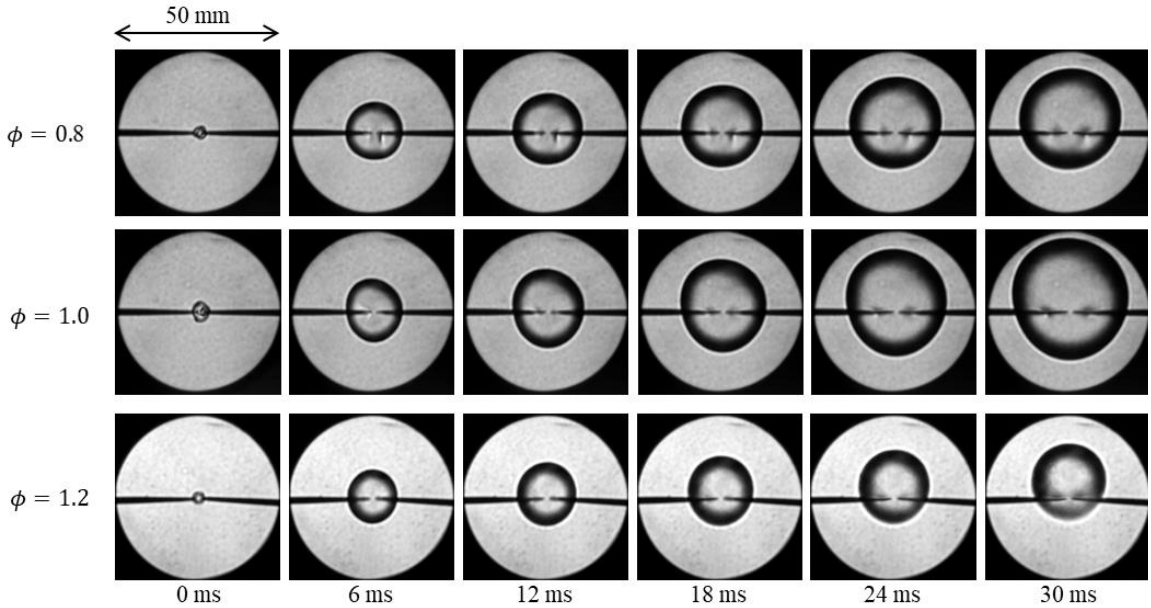

Figure 4. 17 Effect of buoyancy on ammonia-air flames in a quiescent environment [25].

Figure 4.18 shows the normalized turbulent flame propagation velocity to laminar flame propagation velocity, S_T/S_L for various equivalence ratio at u'= 0.32 and 0.65 m/s. The turbulent flame propagation velocity for $Ø$ = 0.9 at u' = 0.65 m/s is significantly higher than other cases. Due to the high flame propagation velocity, the capability of the ammonia-air mixture to sustain the flame propagation in turbulent flow field for $Ø$ = 0.9 is the highest among all equivalence ratios examined in the present study. As shown in Fig. 4.18, for $Ø \leq$ 1.0, S_T/S_L increases as the equivalence ratio decreases both for u'= 0.32 and 0.65 m/s.

Figure 4.19 shows the flame propagation probability map of the ammonia-air flames for various equivalence ratios and turbulence intensities. It also shows the limit for flame propagation for the lean and rich equivalence ratio in various turbulence intensities. It showed the ammonia-air for $Ø$ = 0.9 with relatively high burning velocity as described above tended to sustain flame propagation even in higher turbulence intensity, up to 1.29 m/s, as shown in Fig. 4.19.

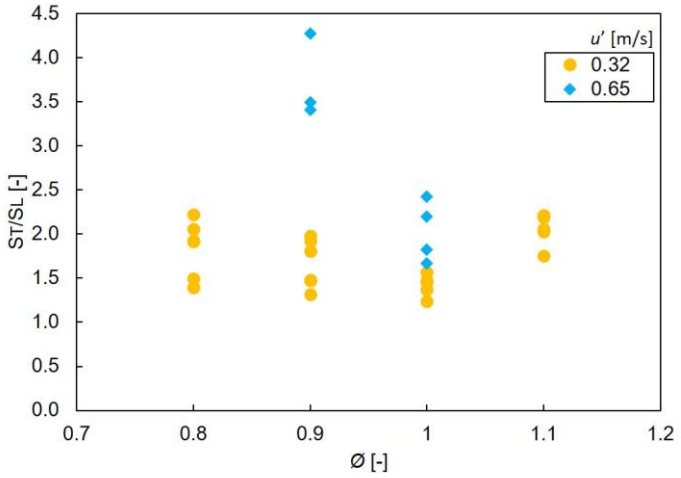

Figure 4. 18 Normalized of turbulent flame propagation velocity for various equivalence ratios at u'= 0.32 and 0.65 m/s.

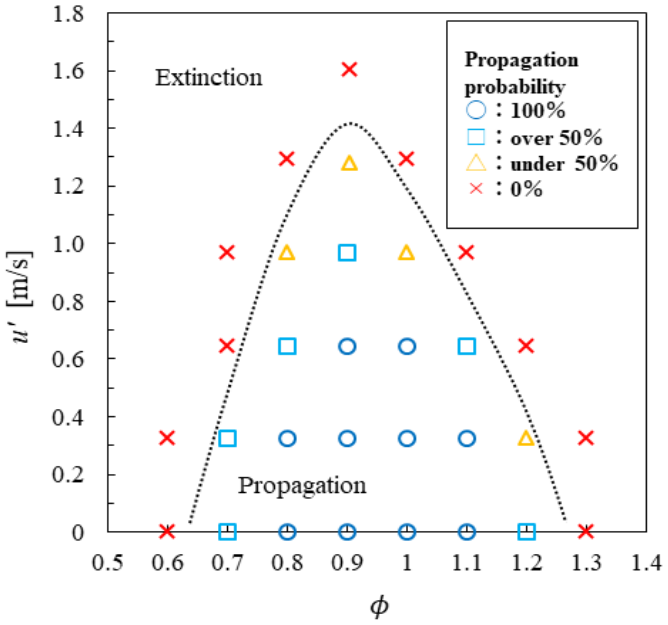

Figure 4. 19 Flame propagation probability map of the ammonia-air flames for various turbulence intensities, *u*' [25].

4.3.2 Concluding remarks

In the present study, flame propagation limit is between equivalence ratio of 0.7 to 1.2 for *u*' = 0 m/s, which is a good agreement to the previous study [11]. In a turbulent environment, the flame propagation velocity increases as the turbulence intensity increases, similar to the other gaseous fuel. The flame propagation velocity of ammonia-air in a lean condition relatively higher in high turbulence intensity due to effects of turbulent eddies, Lewis number, *Le* and burned gas Markstein length, L_b. The maximum burning velocity, for laminar is in the rich mixture condition, but in turbulent is in the lean mixture condition. Results also show the normalized turbulent flame propagation velocity, for $Ø \leq 1.0$, S_T/S_L increases as the equivalence ratio, *Ø* decreases.

4.3.3 NH_3-O_2N_2 (ammonia-O_2N_2) combustion in turbulent

Experiments on ammonia-O_2N_2 combustion were performed to compare the qualitative results to the coal-O_2N_2 (coal) combustion and coal-NH_3-O_2N_2 (mixing) combustion. Table 4.2 shows the limit of equivalence ratio for ammonia-O_2N_2 to sustain flame propagation in a quiescent environment. According to the results, the equivalence ratios for ammonia-O_2N_2 are between 0.4 to 2.0 sustained a flame propagation.

Table 4. 2 Flame propagation limit for ammonia-O_2N_2 for various equivalence ratio, *Ø*.

	Equivalence ratio, Ø																			
u' [m/s]	0.2	0.3	0.4	0.5	0.6	0.7	0.8	0.9	1.0	1.1	1.2	1.3	1.4	1.5	1.6	1.7	1.8	1.9	2.0	2.1	2.2
0	×	×	○	○	○	○	○	○	○	○	○	○	○	○	○	○	○	○	○	×	×

○ : Flame propagation, × : No flame propagation

The ammonia-O_2N_2 experiments in turbulent were performed for the selected conditions to check the overall trends for various equivalence ratios and turbulence intensities. Figure 4.20 shows the flame propagation velocity of ammonia-O_2N_2 for various turbulence intensities and equivalence ratios at the flame radius of 10.45 mm. In general, the results showed that not much different of the flame propagation velocity for u' = 0, 0.32 and 0.65 m/s. This is due to the relatively high flame propagation velocity for ammonia-O_2N_2. For ammonia-O_2N_2 mixtures, expected that the effect of turbulent eddies on wrinkling the flame front might be significant only at the higher turbulence intensity than the tested values. Ammonia-O_2N_2 combustion at an equivalence ratio of 0.6 was compared to the mixing combustion. The trends of the flame radius and flame propagation velocity at an equivalence ratio of 0.6 compared to the trends of the flame radius and flame propagation velocity of coal-ammonia (mixing) combustion, as shown in figures in the following section (Section 4.4).

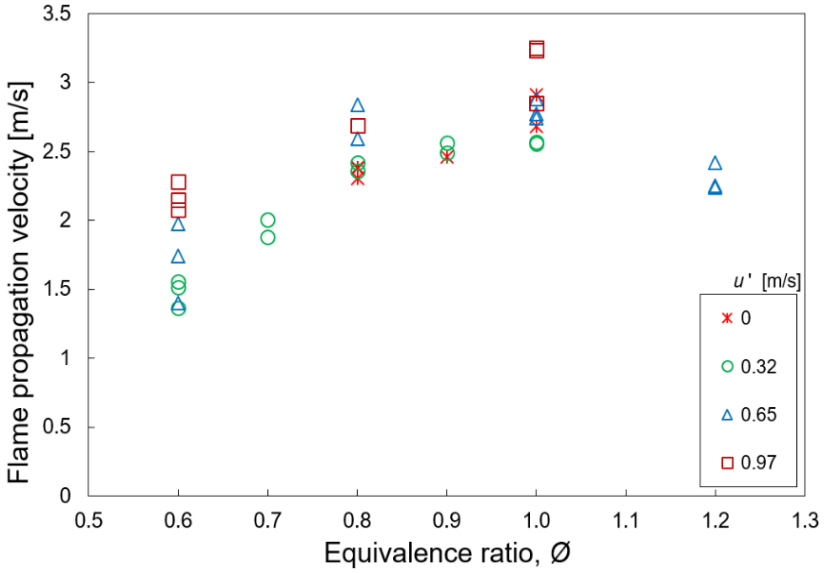

Figure 4. 20 Flame propagation velocity as a function of equivalence ratio for ammonia-O_2N_2.

4.4 Coal-NH_3-O_2N_2 (coal-ammonia mixing combustion)

4.4.1 Flame propagation capability in coal-O_2N_2 (coal) combustion

Experiments on low ignitable coals were performed to examine the capability of the TW, KK and UL coal to sustain flame propagation in coal-O_2N_2 mixture (coal combustion). The results are compared to TW, KK and UL coal in mixing combustion, in the following section. Table 4.3 shows the capability of various coal types to sustain a flame propagation in the coal combustion for various coal concentration, G and turbulence intensities, u'. In coal combustion, except the very low coal concentration of G = 0.3 kg/m³, C5 coal sustained flame propagation in all tested condition. The results of C5 coal combustion is the same results in Section 4.1. TW coal sustained flame propagation for G = 2.0 and 2.3 kg/m³, and low G in high u' only. KK coal sustained flame propagation for G = 2.0, and 1.3 kg/m³ in

Table 4. 3 Capability of various type of coal to sustain flame propagation in coal-O_2N_2 mixture.

			Turbulence intensity, u' [m/s]			
Coal type	Fuel ratio	Coal concentration, G [kg/m³]	0.32	0.65	0.97	1.29
C5	1.56	0.3	O	×	×	×
		0.6	O	O	O	O
		1.3	O	O	O	O
		2.0	O	O	O	O
		2.3	O	O	O	O
TW	2.5	0.6	×	×	O	O
		1.3	×	×	O	O
		2.0	O	O	O	O
		2.3	O	O	O	O
KK	3.17	0.6	×	×	×	×
		1.3	×	×	×	O
		2.0	O	O	O	O
		2.3	×	×	×	×
UL	5.3	0.6	×	×	×	×
		1.3	×	×	×	×
		2.0	×	×	×	×
		2.3	×	×	×	×

O Flame propagation
× No flame propagation

high *u*' only. Furthermore, UL coal not sustained flame propagation for all tested conditions. The tendency is based on the different fuel ratio of the coal particles. It also demonstrates that the TW and KK coal sustained a flame propagation in high turbulent intensities due to the turbulence heat transfer. Turbulent heat transfer increased the flame propagation velocity, as described in coal combustion (Section 4.2).

4.4.2 Flame propagation of coal and ammonia in mixing combustion

Experiments on coal-NH_3-O_2N_2 or coal-ammonia mixing combustion of common bituminous coal (C5) and low ignitable coal (TW, KK, and UL) were performed for G = 0.6 kg/m³ and equivalence ratio, $\emptyset$ of NH_3-O_2N_2 is 0.6 for u' = 0.32, 0.65 and 0.97 m/s. In the C5 coal combustion, the lowest coal concentration = 0.6 kg/m³ was sustained flame propagation in all tested turbulence intensities. Therefore, the G = 0.6 kg/m³ was set for the mixing combustion to examine the flame propagation behavior of low G in mixing combustion. Considering the volatile matter gas released from coal particles, the lean condition of ammonia-O_2N_2 mixture $\emptyset$ = 0.6 was selected. In the mixing combustion, diluted oxygen (40 vol% O_2 and 60 vol% N_2) was used as the ambient gas, similar to the coal combustion (Section 4.1 and 4.2).

In the present study, direct imaging represents the coal flame and OH radical imaging for ammonia flame. Figure 4.21 shows the simultaneous images of (a) direct flame imaging for coal flame, and (b) OH radical imaging for ammonia flame in mixing combustion of C5 coal for u' = 0.32 m/s. To measure the flame diameter, the color of OH radical images was reduced to make the flame front more visible. Figure 4.21 b(i) shows an example of the OH radical image after the color changed. The raw images were turned to binary images to show the measured flame front. As shown with the red color arrow in Fig.

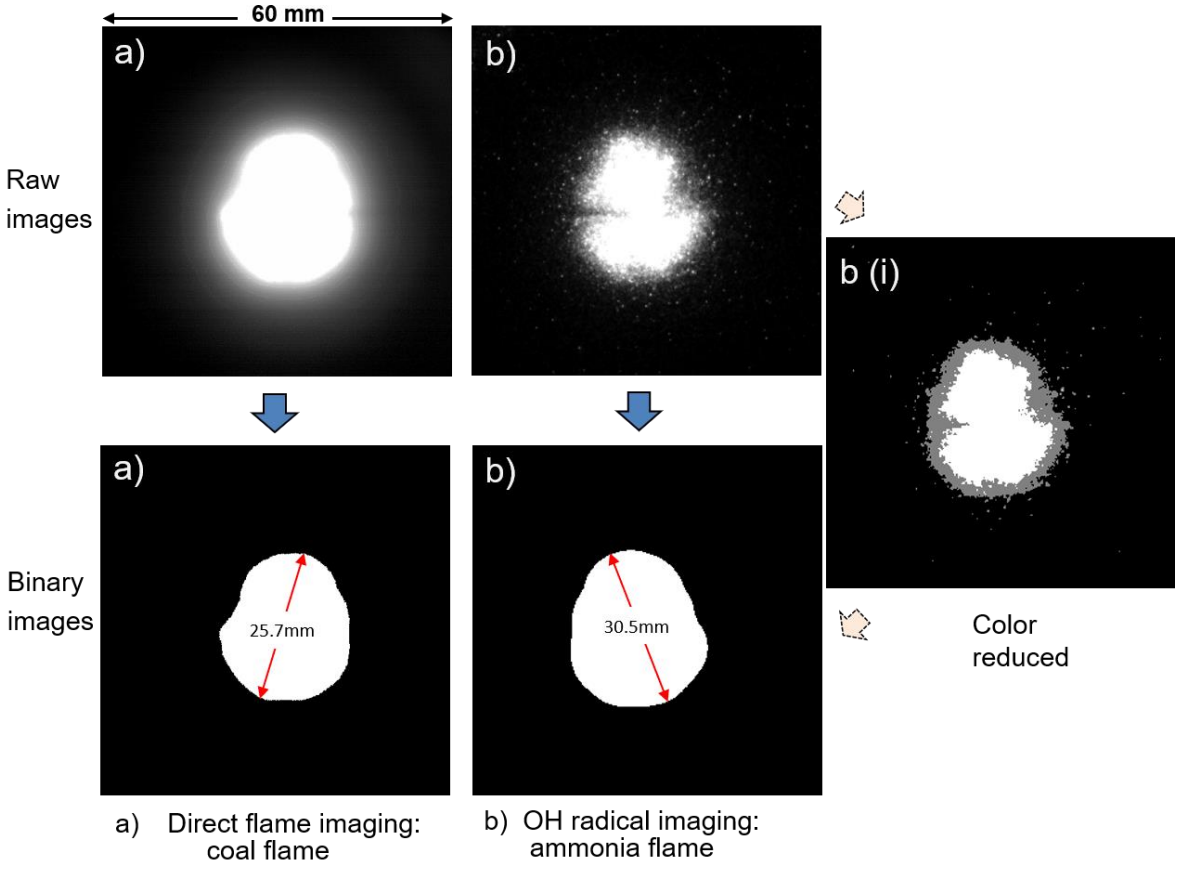

Figure 4. 21 Raw flame images turned to the binary images.

4.21, the flame radius was measured between the farthest of the flame front, a similar approach as coal combustion. According to the radius time histories, the ignition affected period did not influence the flame radius after 2 ms from the ignition. It was shorter than that 5 ms in coal combustion. This is expected due to the relatively high flame propagation velocity of mixing combustion. Therefore, flame radii were measured from 2 ms after the spark ignition until the maximum scale of flame that reaches the edge of the window.

Figure 4.22 shows the flame image from direct imaging and OH radical imaging for comparison of C5 coal combustion. Figure 4.22 shows (a) C5 coal flame in coal combustion, (b) C5 coal flame in mixing combustion, (c) ammonia flame in mixing combustion, and (d) ammonia flame in ammonia-O_2N_2 combustion. At the same elapsed time, the relatively

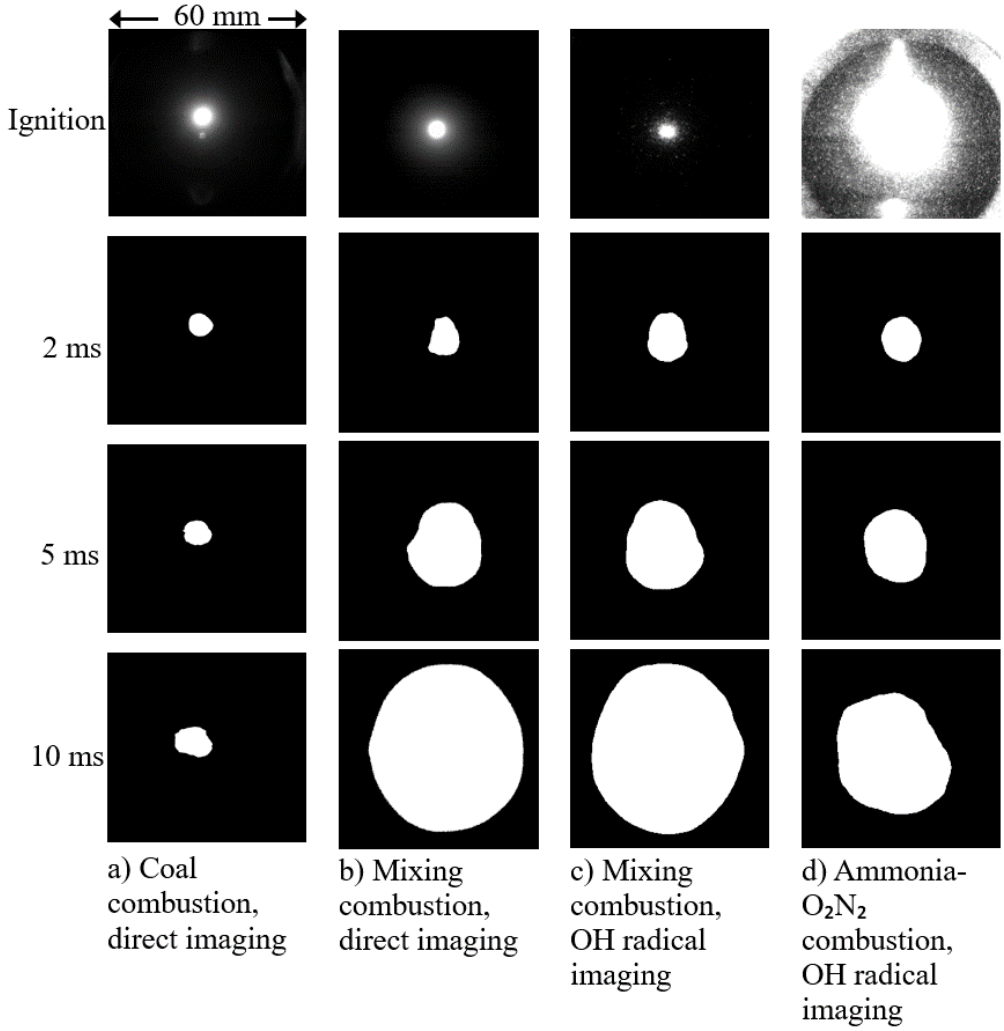

Figure 4. 22 The C5 coal flame and ammonia flame for *u*' = 0.32 m/s.

small scale of flame images can be observed for coal flame in coal combustion compared to coal flame in mixing combustion. Also, the small scale of ammonia flame in ammonia-O_2N_2 combustion compared to ammonia flame in mixing combustion. It showed the flame propagation in mixing combustion is relatively higher compared to those in the coal combustion and the ammonia-O_2N_2 combustion.

Figure 4.23 shows the flame image from direct imaging and OH radical imaging for comparison of UL coal combustion. Figure 4.23 shows (a) no flame propagation for UL in coal combustion, (b) UL coal flame in mixing combustion, (c) ammonia flame in mixing combustion, and (d) ammonia flame in ammonia-O_2N_2 combustion. In the coal combustion,

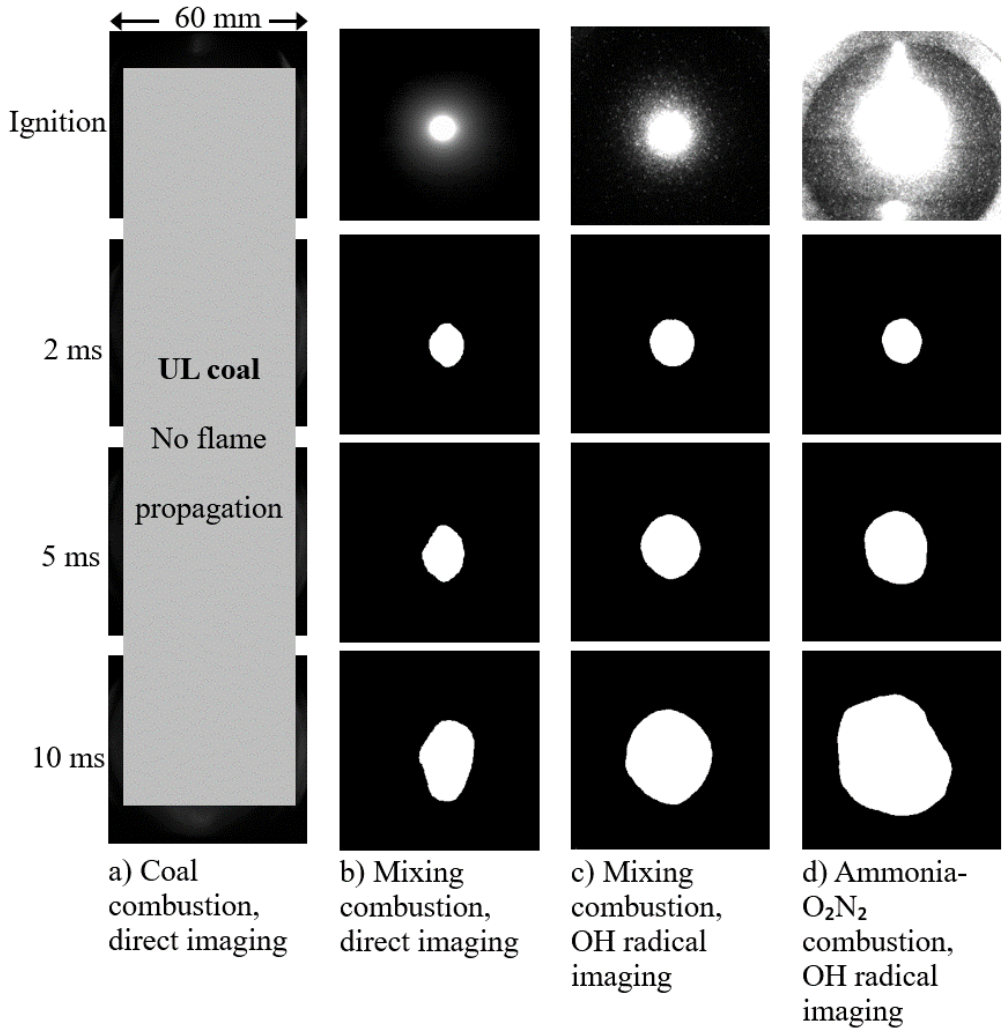

Figure 4. 23 The UL coal flame and ammonia flame for *u*' = 0.32 m/s.

UL coal did not sustain the flame propagation, however, UL coal sustained flame propagation in mixing combustion. At the same elapsed time, the relatively small scale of flame images can be observed for coal flame and ammonia flame in mixing combustion compared to ammonia flame in ammonia-O_2N_2 combustion. Expected that, ammonia addition in mixing combustion increased the ignition capability of the UL coal. Thus, UL coal sustains flame propagation in mixing combustion. However, the UL coal particle cloud may cause heat absorption to ammonia flame in lower turbulence intensity, thus decreased the flame propagation of the whole flame.

Figure 4.24, 4.25 and 4.26 shows the flame radius as a function of elapsed time for C5, TW, KK and UL coal in mixing combustion for *u*' = 0.32, 0.65 and 0.97 m/s, respectively. Flame radius is increasing as elapsed time increases in all cases. However, the gradient trends that represent flame radius increasing rate are different depending on the type of coal and *u*'. The flame radius as a function of elapsed time for ammonia-O_2N_2 combustion for the same *u*' also showed on the same figure as a reference to compare the flame radius increasing trends in mixing combustion. In general, by using the simultaneous measurement, the ammonia flame radius shows a bigger radius than coal flame at the initial period of flame propagation. The flame propagation velocity trends were obtained from the relationship of flame radius as a function of elapsed time.

Figure 4.24 shows the flame radius as a function of time for *u*' = 0.32 m/s. C5 and TW coal and ammonia have a higher gradient trend in mixing combustion than ammonia-O_2N_2 combustion. KK coal and ammonia flame in mixing combustion shows similar trends to ammonia-O_2N_2 combustion. However, UL coal and ammonia flame in mixing combustion show lower gradient trend than that in the ammonia-O_2N_2 combustion.

Figure 4.25 shows the flame radius as a function of time for *u*' = 0.65 m/s. C5 and TW coal and ammonia have a higher gradient trend in mixing combustion than ammonia-O_2N_2 combustion. KK coal and ammonia flame in mixing combustion shows similar trends to ammonia-O_2N_2 combustion. In mixing combustion, UL coal shows flame radius increase later than ammonia flame at the initial period, then the increasing rate was faster as elapsed time increases. As the elapsed time increase, the ammonia flame in mixing combustion have a bigger flame radius than UL coal flame but smaller than that in the ammonia-O_2N_2 combustion.

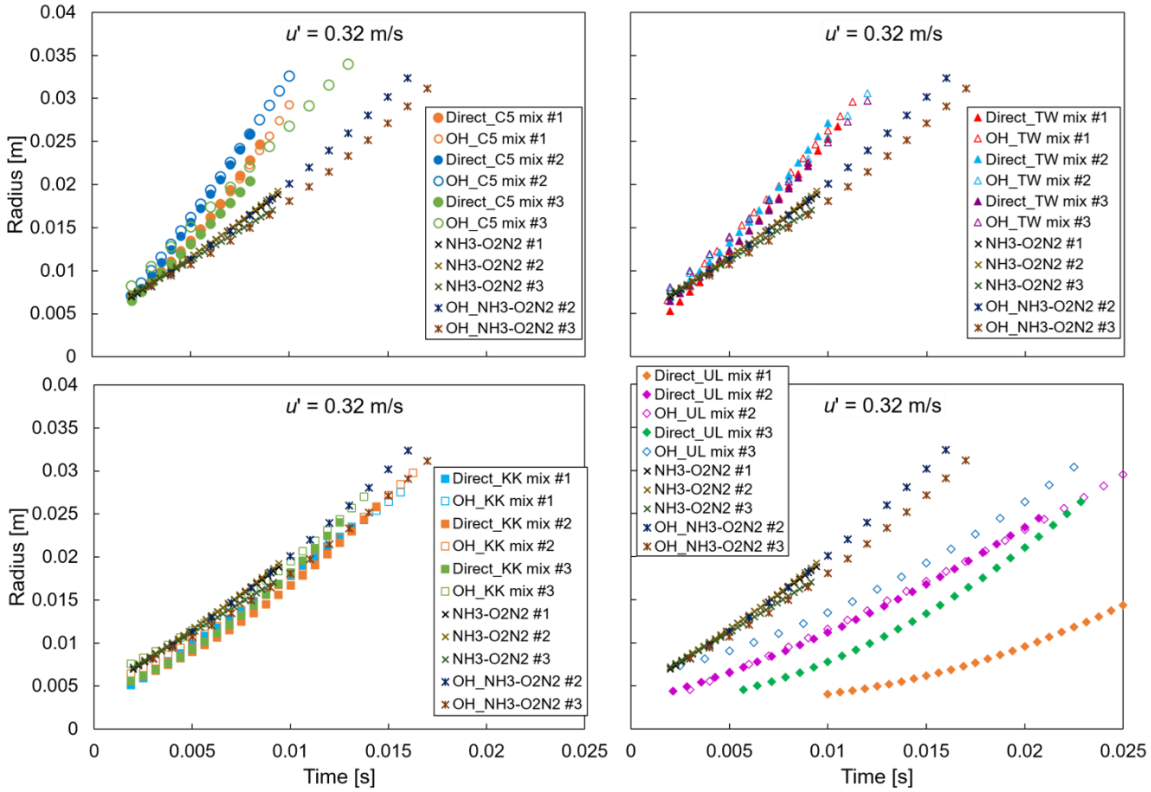

Figure 4. 24 Flame radius as a function of elapsed time for u' = 0.32 m/s.

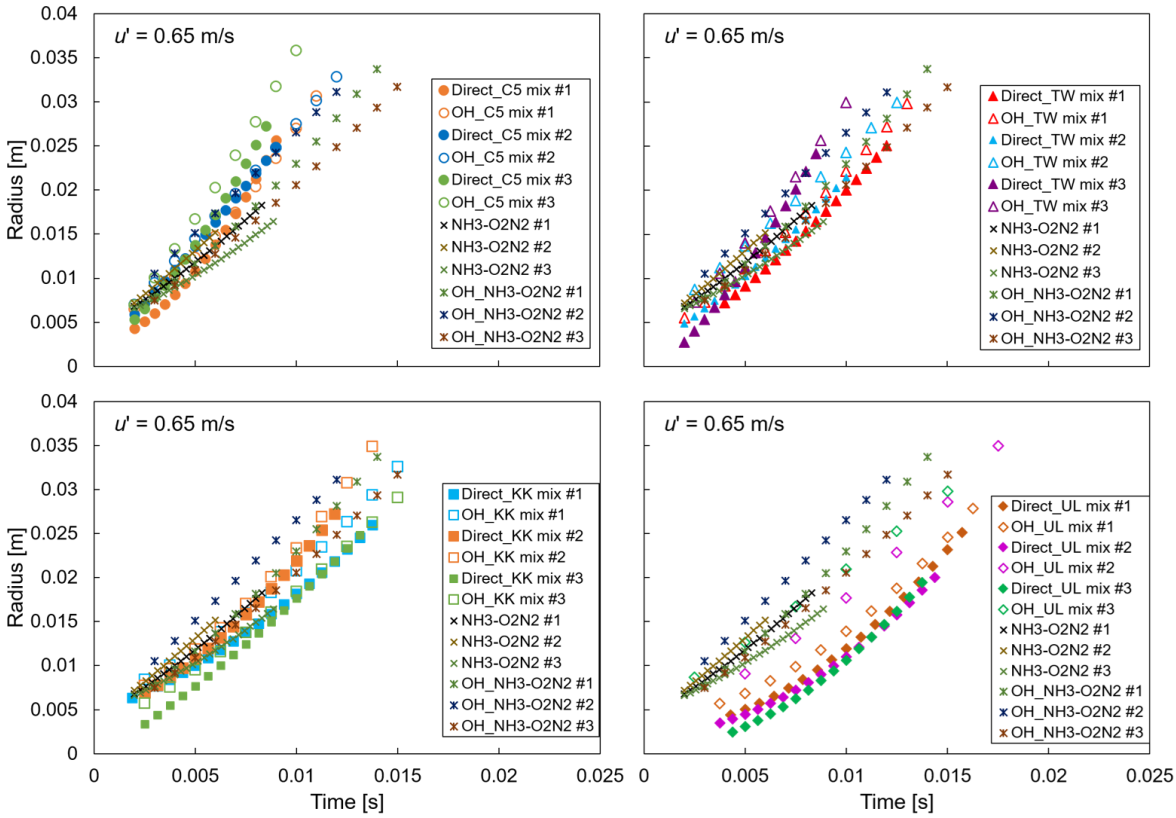

Figure 4. 25 Flame radius as a function of elapsed time for *u*' = 0.65 m/s.

Figure 4.26 shows the flame radius as a function of time for *u*' = 0.97 m/s. C5, TW and KK coal, and ammonia have a higher gradient trend in mixing combustion than ammonia-O_2N_2 combustion. In mixing combustion, UL coal shows flame radius increase later than ammonia flame at the initial period, then the increasing rate was faster as elapsed time increases. Furthermore, the ammonia flame in mixing combustion shows higher increasing trend than that in the ammonia-O_2N_2 combustion.

Figure 4.27, 4.28 and 4.29 shows the flame propagation velocity as a function of flame radius for various type of coal in mixing combustion for *u*' = 0.32, 0.65 and 0.97 m/s, respectively. Flame propagation velocity increases as the flame radius increases for all cases. The flame propagation velocity as a function of flame radius for ammonia-O_2N_2 combustion for the same *u*' also showed in the same figure as a reference to compare the flame propagation trends. In general, even the ammonia flame has a higher flame

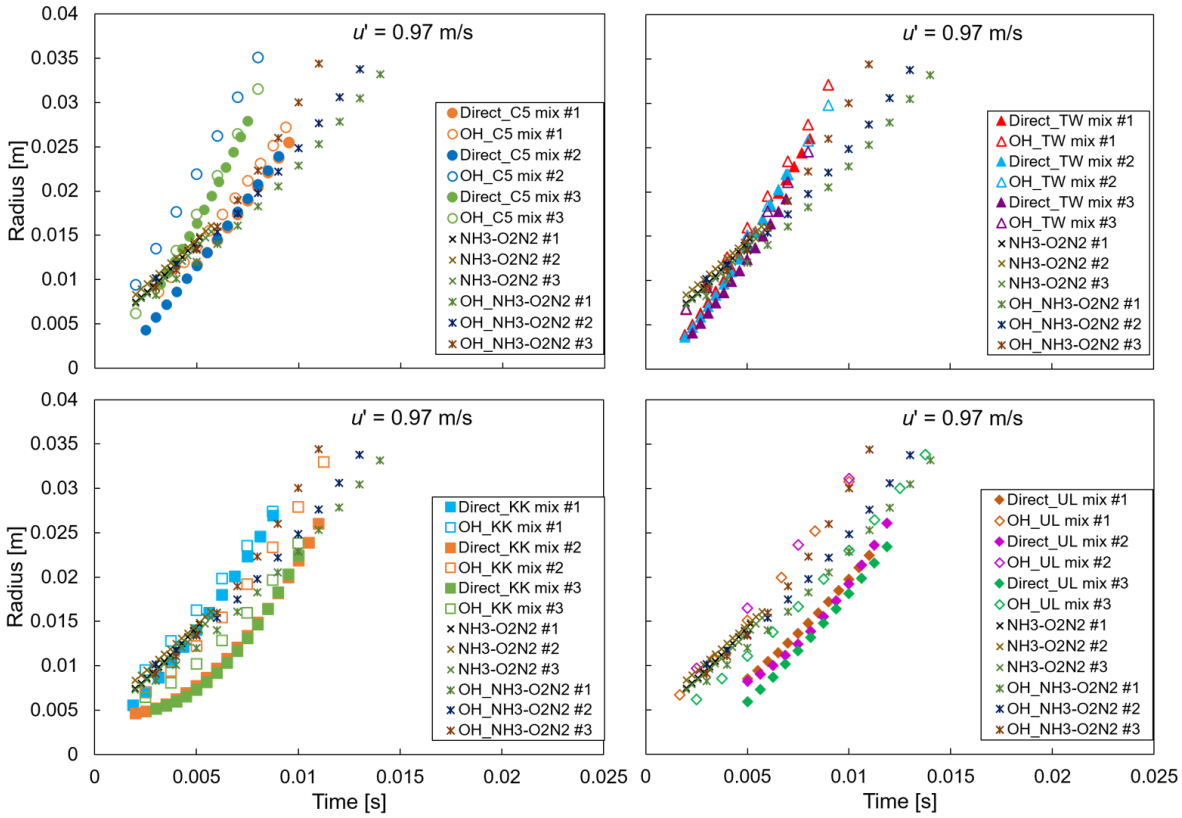

Figure 4. 26 Flame radius as a function of elapsed time for *u*' = 0.97 m/s.

propagation at the initial stage, the overall gradient is lower than coal flame in the same experiment. It showed the coal flame propagation velocity increased as the elapsed time increases, a similar trend as coal combustion of C5 coal. This is due to increasing of the flame front area caused by turbulent eddies that wrinkled the flame front. Thus, the increases of the volatile matter released increased the fuel in the gas phase near to the flame front. Consequently, the flame propagation velocity increase. Later on, in the final results, flame propagation velocity at r = 10.45 mm is shown in the relationship of flame propagation velocity and turbulence intensity.

Figure 4.27 shows the flame propagation velocity as a function of flame radius for u' = 0.32 m/s. C5 and TW coal, and ammonia have higher flame propagation velocity in mixing combustion than the ammonia-O_2N_2 combustion. KK coal which contains less volatile matter than C5 and TW coal has near flame propagation velocity to the ammonia-

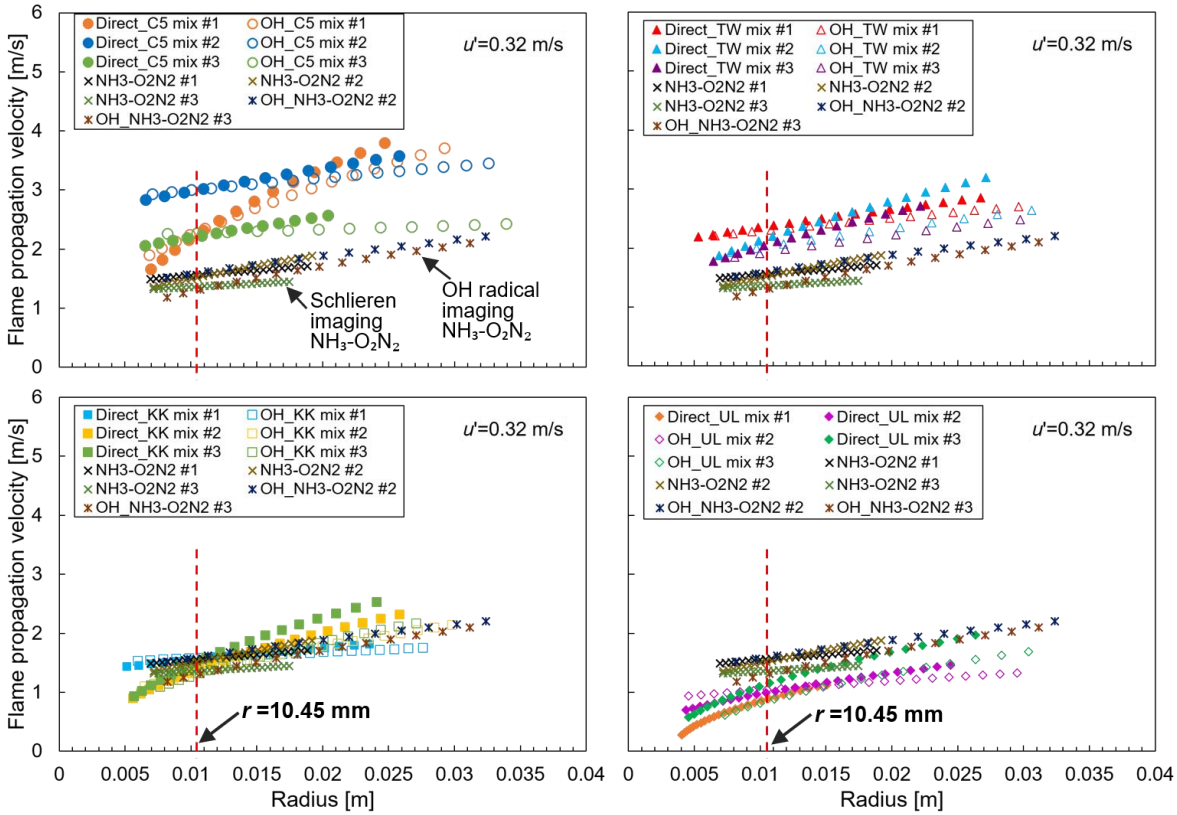

Figure 4. 27 Flame propagation velocity as a function of flame radius for u' = 0.32 m/s.

O_2N_2 combustion. UL coal and ammonia flame in mixing combustion showed lower flame propagation rate than that in the ammonia-O_2N_2 combustion.

Figure 4.28 shows the flame propagation velocity as a function of flame radius for u' = 0.65 m/s. C5 and TW coal and ammonia have higher flame propagation velocity in mixing combustion than that in the ammonia-O_2N_2 combustion. The flame propagation velocity of KK and UL coal and ammonia flame in mixing combustion show similar trends to ammonia-O_2N_2 combustion. Figure 4.29 shows the flame propagation velocity as a function of flame radius for u' = 0.97 m/s. Obviously the C5 and TW coal, and ammonia flame have higher flame propagation velocity in mixing combustion than that in the ammonia-O_2N_2 combustion. While KK and UL coal and ammonia flame shows slightly higher flame propagation velocity in mixing combustion than that in the ammonia-O_2N_2 combustion.

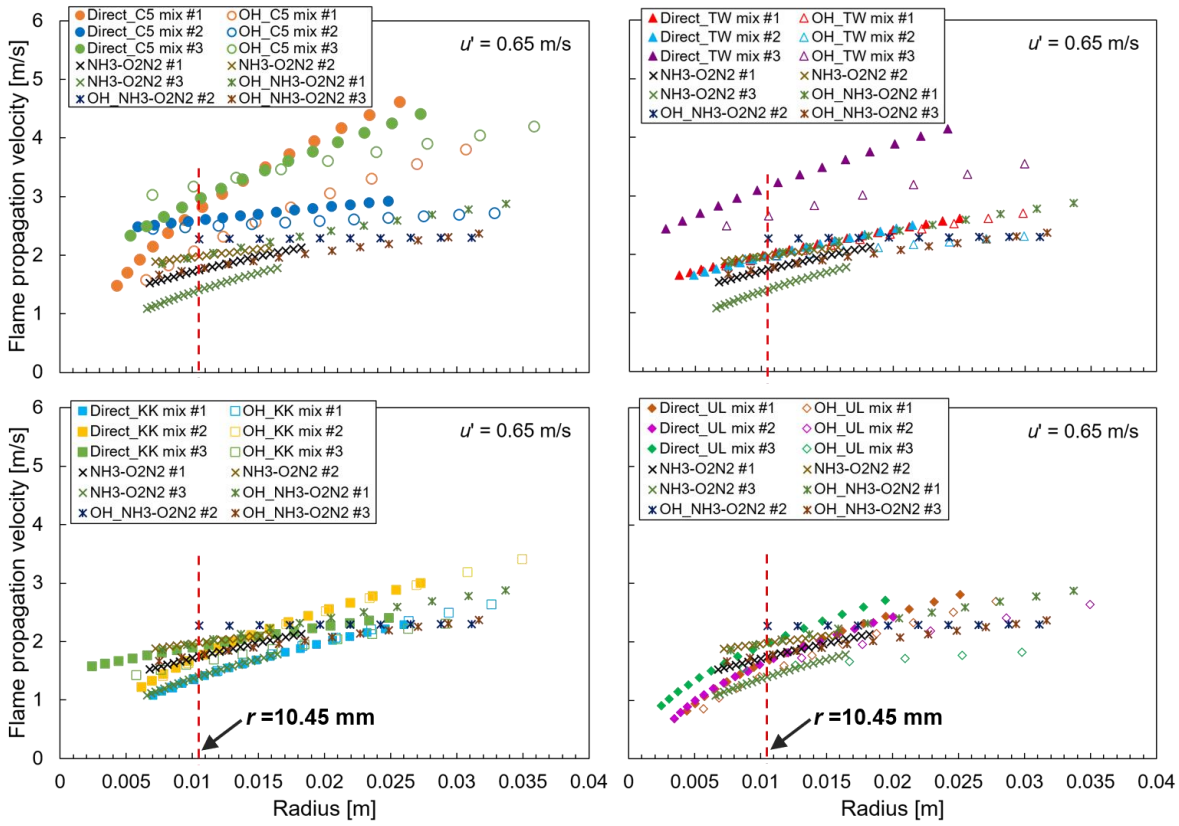

Figure 4. 28 Flame propagation velocity as a function of flame radius for u' = 0.65 m/s.

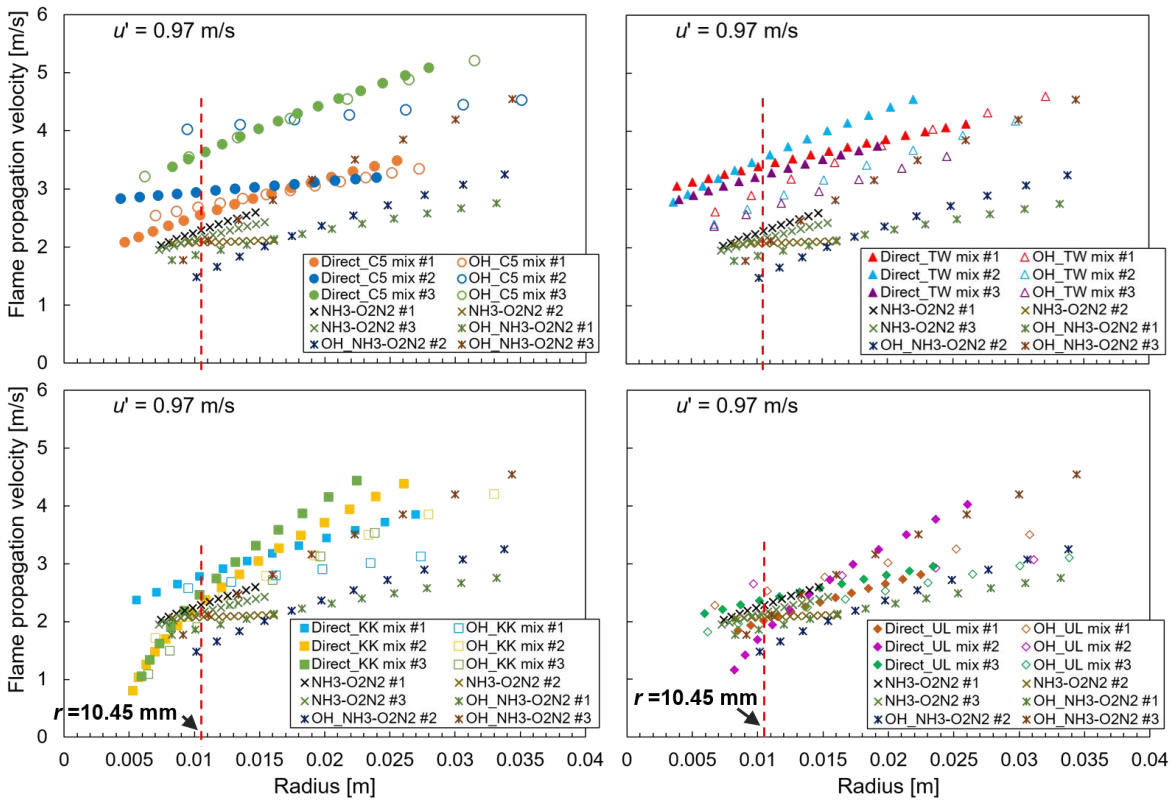

Figure 4. 29 Flame propagation velocity as a function of flame radius for u' = 0.97 m/s.

Figure 4.30 shows the flame propagation velocity at r =10.45 mm for NH_3-O_2N_2 (ammonia-O_2N_2) combustion with equivalence ratio of 0.6 for u'= 0.32, 0.65, 0.97 m/s. Both OH radical imaging and Schlieren flame imaging were plotted. Both imaging shows such error due to the different determination of the flame front. Schlieren imaging obtained from

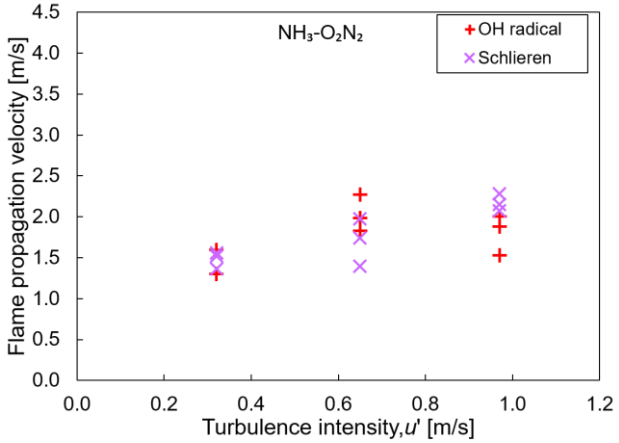

Figure 4. 30 Relationship between flame propagation velocity and turbulence intensity, u' for ammonia-O_2N_2.

different gas density, while OH radical imaging obtained from OH radical signal during the flame propagation. Also, both imaging is from a different window, thus may be different flame shape were captured. However, in the whole, both methods showed very close results, and the flame propagation velocity increases as *u*' increases. The flame propagation of ammonia-O_2N_2 combustion was compared to ammonia flame propagation in the mixing combustion. However, Schlieren photography was not able to be implemented for ammonia flame imaging in the mixing combustion due to the presence of the coal particle cloud. Therefore, for ammonia flame in the mixing combustion, only OH radical images data were plotted on the figures of mixing combustion results.

Figure 4.31 shows the flame propagation velocity as a function of turbulence intensity for mixing combustion of C5, TW, KK and UL coal . In general, for all turbulence

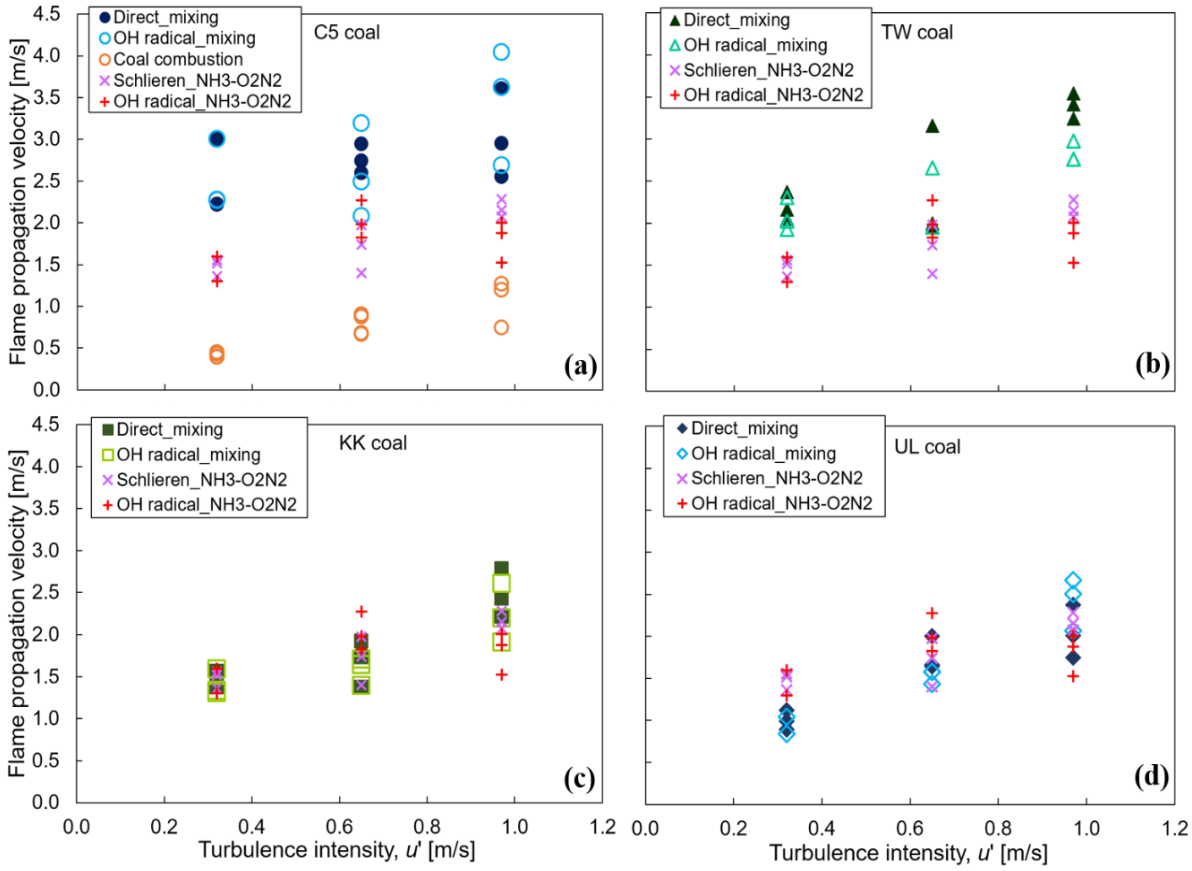

Figure 4. 31 Relationship between flame propagation velocity and turbulence intensity, *u*' for coal, ammonia-O_2N_2 and mixing combustion.

intensities, the flame propagation velocity of C5 coal flame in mixing combustion is about five times faster than that of C5 coal combustion. The flame propagation velocity of ammonia in mixing combustion is about two times faster than that of ammonia-O_2N_2 combustion without coal particle cloud.

The volatile matter release rate and the amount of volatile matter generated strongly affect flame stability [3]. Expected that, the volatile matter release rate and the amount of volatile matter generated determines the flame propagation behavior of coal and ammonia flame in the mixing combustion. In the mixing combustion, after spark ignition, in most of the cases the ammonia flame propagated first than coal flame. At the same time, the volatile matter released from coal particles after the heat transfer from spark ignition. Ammonia flame also preheats the coal particles, thus, the fuel in the gas phase was increased due to accumulated ammonia fuel and volatile matter gas from coal particles. This phenomenon increased the equivalence ratio of gaseous fuel near the ammonia flame front, in which the local equivalence ratio is increased. The global equivalence ratio of ammonia mixture is 0.6. The flame propagation velocity of ammonia is able to increase with increasing the equivalence ratio. Therefore, ammonia flame propagation velocity increases after the coal particles release the volatile matter. The initial release of the volatile matter was consumed during the ammonia flame propagation. Simultaneously, the coal particles continuously preheated during the ammonia flame propagation, thus the volatile matter released continuously. The coal flame front also preheated the unburned coal particles. The preheating of the unburned coal particles by ammonia flame propagation and coal flame front increased the volatile matter release rate. Consequently, coal flame propagation was faster. Therefore, the coal flame propagation velocity in mixing combustion is relatively higher than that in the coal combustion.

In the mixing combustion, the flame propagation velocity increases as the turbulence intensity increases, similar to coal combustion. This tendency is due to the increasing of the turbulent heat transfer rate at the flame front as the turbulence intensity increases, as described in [20]. A similar explanation can be adopted to the mixing combustion of TW coal which has nearly the same fuel ratio as C5 coal. Also, a similar explanation can be adopted for mixing combustion of the KK and UL coal in high turbulence intensity.

For KK and UL coal, the ammonia flame in mixing combustion increased the volatile matter release rate, thus increased the ignition capability of coal particles. In low turbulence intensity, UL coal and ammonia flame in mixing combustion shows lower flame propagation velocity than that in the ammonia combustion. This is due to the lowest volatile matter content of UL coal among the tested coal types. Ammonia flame increased the volatile matter release rate of the UL coal. Consequently, the UL coal sustained flame propagation in mixing combustion. However, at the same time, UL coal particle cloud may cause heat absorption which decreased the flame propagation velocity of ammonia in mixing combustion.

4.4.3 Concluding remarks

Flame propagation behavior for various coal types and ammonia in mixing combustion were clarified. Compared to coal combustion, the TW, KK and UL coal sustained a flame propagation in mixing combustion, for all the tested conditions. The flame propagation velocity of C5 coal flame in mixing combustion is about five times faster than that of C5 coal combustion. The flame propagation velocity of ammonia in mixing combustion is about two times faster than that of ammonia-O_2N_2 combustion. In the lower turbulence intensity; for low fuel ratio coal (C5), the flame propagation velocity increased,

and for high fuel ratio coal (TW, KK, UL), ammonia flame increased the ignition capability of coal particles. In the high turbulence intensities; ammonia flame increased the ignition capability of coal particles, and also increased the flame propagation velocity of coal clouds that higher than ammonia-O_2N_2 combustion. In mixing combustion, flame propagation velocity increases as turbulence intensity increases, similar to the coal combustion.

Chapter 5 Conclusions

In the present study of coal combustion, the effect of turbulence intensity and coal particle concentration on the flame propagation of pulverized coal particle clouds at atmospheric pressure were clarified. Common bituminous coal (C5) were examined in coal combustion. The flame propagation velocity of a pulverized coal particle cloud increases as the turbulence intensity increases. This is due to the increase in the turbulence heat transfer with the increase of the turbulence intensity. Compared to the turbulence intensity, the coal concentration has a weak effect on the flame propagation velocity, which is unique to pulverized coal combustions in a turbulent field. In quiescent coal clouds, flame propagation velocity has a maximum at the specific coal concentration. Therefore, this finding is one of the significant contributions of the present study and it is different from the results observed in previous pulverized coal combustion studies, as well as that of gaseous fuel combustion research.

Experiment in microgravity (μg) was performed to investigate the effects of gravity on flame propagation behavior of coal clouds. Common bituminous coal (C5) and low ignitable coal (TW) were examined. Due to a limited number of μg experiment, coal concentration, G was set to 2.0 kg/m^3 for u' of 0, 0.32, 0.65 and 0.97 m/s. Experiment under 1g and μg environments clarified the effects of gravity, turbulence intensity, and fuel ratio on the spherical turbulent flame propagation behavior of a pulverized coal particle cloud. In μg, the coal particle cloud is more flammable than in the 1g environment. Natural convection, which exists in the 1g environment, has a significant effect on the flame propagation behavior of common bituminous coal and low ignitable coal particle cloud at u' = 0 m/s. Turbulence intensity has a positive effect on flame propagation velocity for TW

coal, similar to C5 coal. In a turbulent, no significant different of the flame propagation velocity in μg and 1g environment.

Experiments on ammonia-air mixture performed by using the present experimental apparatus to investigate the turbulent effect on the flame propagation. Experimental data for ammonia-air flame propagation in the turbulent environment is not in the literature. In the present study, in a quiescent environment, flame propagation limit for equivalence ratio show good agreement to the previous study. In a turbulent environment, the flame propagation velocity increases as the turbulence intensity increases, similar to the other gaseous fuel. The flame propagation velocity of ammonia-air in a lean condition relatively higher in high turbulence intensity due to effects of turbulent eddies, Lewis number, *Le* and burned gas Markstein length, L_b. The maximum burning velocity, for laminar is in the rich mixture condition, but in turbulent is in lean mixture condition. Results also show the normalized turbulent flame propagation velocity, for $\emptyset \leq 1.0$, S_T/S_L increases as the equivalence ratio, $\emptyset$ decreases. The limit of flame propagation for various equivalence ratios in various turbulence intensities was also clarified in the present study.

Flame propagation behavior for various coal type and ammonia in mixing combustion were clarified by experimental study. In the coal-O_2N_2 combustion, the various type of coals sustained flame propagation only in certain conditions. However, the various type of coals sustained flame propagation in mixing combustion for all tested conditions. The flame propagation velocity of C5 coal flame in mixing combustion is about five times faster than that in C5 coal combustion without ammonia. Ammonia increased the flame propagation velocity of the coal particle cloud. The flame propagation velocity of ammonia in mixing combustion is about two times faster than that of ammonia-O_2N_2 combustion without coal particle cloud. This is because, the local equivalence ratio of gaseous fuel is increased. It showed that both fuels affect each other in the mixing combustion. In the lower

turbulence intensity; for low fuel ratio coal (C5), the flame propagation velocity increased, and for high fuel ratio coal (TW, KK, UL), ammonia flame increased the ignition capability of coal particles. In the high turbulence intensities; ammonia flame increased the ignition capability of coal particles, and also increased the flame propagation velocity of coal clouds that higher than ammonia-O_2N_2 combustion. In mixing combustion, flame propagation velocity increases as turbulence intensity increases, similar to the coal combustion. The effect of the addition of ammonia on the ignition characteristics and flame propagation velocity of common bituminous and low ignitable coal particle clouds was clarified.

Based on the thermal input, with ammonia addition (equivalence ratio = 0.6) and coal concentration of 0.6 kg/m³, coal particles can be saved around 20% (weight %), as described in Section 3.1.4. The findings of the present study can contribute to the fuel cost reduction and the improvement of energy security by being able to utilize the low ignitable pulverized coal particles. Moreover, in the coal-fired boiler, expected that the co-firing of coal-ammonia help to increase the burner stability, considering the flame propagation velocity is one of the important parameters for flame stability.

References

[1] K. Yamamoto, “微粉炭燃焼シミュレーションの現状と今後 Current Status and Future of Pulverized Coal Combustion Simulation,” *J. Combust. Soc. Japan*, vol. 58, no. 186, pp. 204–210, 2016.

[2] T. Suda, K. Masuko, J. Sato, A. Yamamoto, and K. Okazaki, “Effect of carbon dioxide on flame propagation of pulverized coal clouds in CO2/O2 combustion,” *Fuel*, vol. 86, no. 12–13, pp. 2008–2015, 2007.

[3] M. Taniguchi, H. Kobayashi, K. Kiyama, and Y. Shimogori, “Comparison of flame propagation properties of petroleum coke and coals of different rank,” *Fuel*, vol. 88, no. 8, pp. 1478–1484, 2009.

[4] R. Kurose, M. Ikeda, H. Makino, M. Kimoto, and T. Miyazaki, “Pulverized coal combustion characteristics of high-fuel-ratio coals,” *Fuel*, vol. 83, no. 13, pp. 1777–1785, 2004.

[5] O. Fujita, Kenichi Ito, Takaharu Tagashira, Jun’ichi Sato, “Measurement of flame propagation speed of coal dust cloud using a microgravity environment,” *Heat Transf. Microgravity*, vol. 269, 1993.

[6] L. D. Smoot, M. D. Horton, and G. A. Williams, “Propagation of laminar pulverized coal-air flames,” *Symp. Combust.*, vol. 16, no. 1, pp. 375–387, 1977.

[7] M. D. Horton, F. P. Goodson, and L. D. Smoot, “Characteristics of flat, laminar coal-dust flames,” *Combust. Flame*, vol. 28, no. C, pp. 187–195, 1977.

[8] M. Taniguchi, H. Kobayashi, and S. Auhata, “Laser ignition and flame propagation of pulverized coal dust clouds,” *Symp. Combust.*, vol. 26, no. 2, pp. 3189–3195, 1996.

[9] Y. Takano, O. Fujita, N. Shigeta, Y. Nakamura, and H. Ito, “Ignition limits of short-term overloaded electric wires in microgravity,” *Proc. Combust. Inst.*, vol. 34, no. 2, pp. 2665–2673, Jan. 2013.

[10] T. Kiga, S. Takano, N. Kimura, K. Omata, M. Okawa, T. Mori, and M. Kato, "Characteristics of pulverized-coal combustion in the system of oxygen/recycled flue gas combustion," *Energy Convers. Manag.*, vol. 38, pp. S129–S134, 1997.

[11] A. Hayakawa, T. Goto, R. Mimoto, Y. Arakawa, T. Kudo, and H. Kobayashi, "Laminar burning velocity and Markstein length of ammonia/air premixed flames at various pressures," *Fuel*, vol. 159, no. 0, pp. 98–106, 2015.

[12] C. K. Law, *Combustion physics*, 1st ed. New York: Cambridge University Press;2006.

[13] J. Goulier, N. Chaumeix, F. Halter, N. Meynet, and A. Bentaïb, "Experimental study of laminar and turbulent flame speed of a spherical flame in a fan-stirred closed vessel for hydrogen safety application," *Nucl. Eng. Des.*, vol. 312, pp. 214–227, 2017.

[14] D. Bradley, M. Z. Haq, R. A. Hicks, T. Kitagawa, M. Lawes, C. G. W. Sheppard, and R. Woolley, "Turbulent burning velocity, burned gas distribution, and associated flame surface definition," *Combust. Flame*, vol. 133, no. 4, pp. 415–430, Jun. 2003.

[15] A. Smallbone, K. Tsuneyoshi, and T. Kitagawa, "Turbulent and Stable/Unstable Laminar Burning Velocity Measurements from Outwardly Propagating Spherical Hydrogen-Air Flames at Elevated Pressures *," *J. Therm. Sci. Technol.*, vol. 1, no. 1, 2006.

[16] S. S. Shy, Y. W. Shiu, L. J. Jiang, C. C. Liu, and S. Minaev, "Measurement and scaling of minimum ignition energy transition for spark ignition in intense isotropic turbulence from 1 to 5 atm," *Proc. Combust. Inst.*, vol. 36, no. 2, pp. 1785–1791, 2017.

[17] K. Hadi, R. Ichimura, N. Hashimoto, A. Hayakawa, H. Kobayashi, and O. Fujita, "Experimental Study of Spherical Turbulent Flame Propagation of Ammonia-air in a Closed Vessel," in *56th Symposium (Japanese) on Combustion*, 2018.

[18] D. Dandy, "Bioanalytical Microfluidics Program," *Colorado State University*, 2018. [Online]. Available: http://navier.engr.colostate.edu/index.html.

[19] A. Hayakawa, Y. Miki, Y. Nagano, and T. Kitagawa, "Analysis of Turbulent Burning Velocity of Spherically Propagating Premixed Flame with Effective Turbulence

Intensity," *J. Therm. Sci. Technol.*, vol. 7, no. 4, pp. 507–521, 2012.

[20] K. Hadi, R. Ichimura, N. Hashimoto, and O. Fujita, "Spherical turbulent flame propagation of pulverized coal particle cloud in O_2/N_2 atmosphere," *Proc. Combust. Inst.*, vol. 37, pp. 2935–2942, 2019.

[21] C. Mandilas, M. P. Ormsby, C. G. W. Sheppard, and R. Woolley, "Effects of hydrogen addition on laminar and turbulent premixed methane and iso-octane-air flames," *Proc. Combust. Inst.*, vol. 31 I, pp. 1443–1450, 2007.

[22] T. Kitagawa, T. Nakahara, K. Maruyama, K. Kado, A. Hayakawa, and S. Kobayashi, "Turbulent burning velocity of hydrogen–air premixed propagating flames at elevated pressures," *Int. J. Hydrogen Energy*, vol. 33, no. 20, pp. 5842–5849, Oct. 2008.

[23] K. Xu, Y. Wu, Z. Wang, Y. Yang, and H. Zhang, "Experimental study on ignition behavior of pulverized coal particle clouds in a turbulent jet," *Fuel*, vol. 167, pp. 218–225, 2016.

[24] A. Hayakawa, Y. Miki, S. Kobayashi, Y. Nagano, and T. Kitagawa, "Effects of CO 2 and N 2 Dilutions on Laminar and Turbulent Flame Propagation," *SAE Pap.*, no. 2011-01-1878, pp. 1718–1727, 2011.

[25] R. Ichimura, K. Hadi, N. Hashimoto, A. Hayakawa, H. Kobayashi, and O. Fujita, "Extinction limits of an ammonia/air flame propagating in a turbulent field," *Fuel*, (under review) 2019.

WORK SCHEDULE

Research Activities	2015	2016		2017		2018		2019
	Oct.-Dec	H28 1st half	H28 2nd half	H29 1sthalf	H29 2nd half	H30 1st half	H30 2ndhalf	Jan.-March
Design and manufacture of experimental set-up	→							
Experimental apparatus testing and improvements in laboratory		→	→	→				
Experiment and data collection Coal combustion in normal gravity.(series 1, 2, 3) Coal combustion in microgravity. Ammonia-air combustion Ammonia-O_2N_2 combustion Coal-Ammonia combustion.				→	→	→	→	
Thesis Submission Final defense (expected date)							Dec. 2018	Jan. 2019

Appendices

Appendix 1 Combustion chamber and the fan

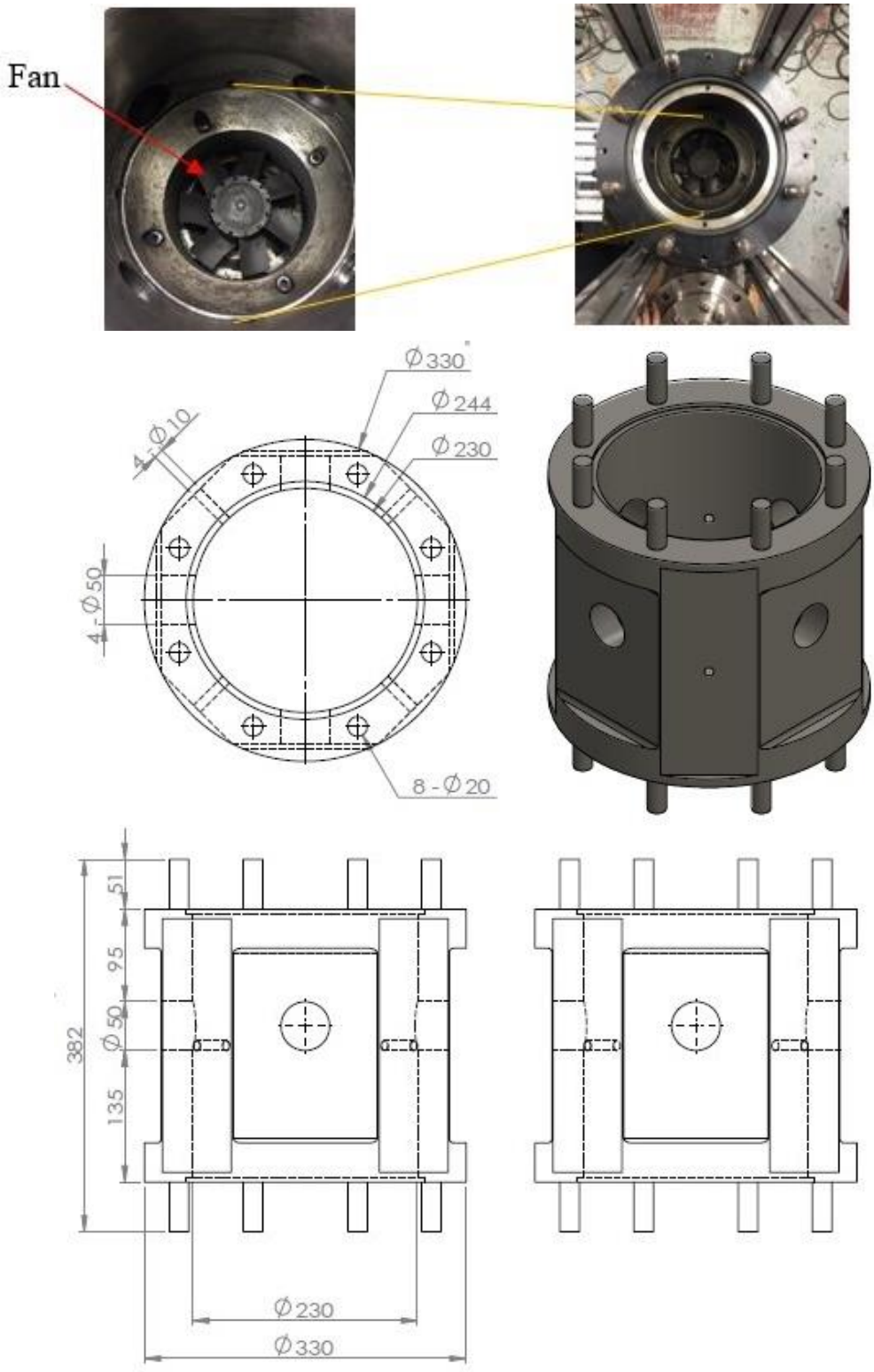

Appendix 2 Experimental apparatus

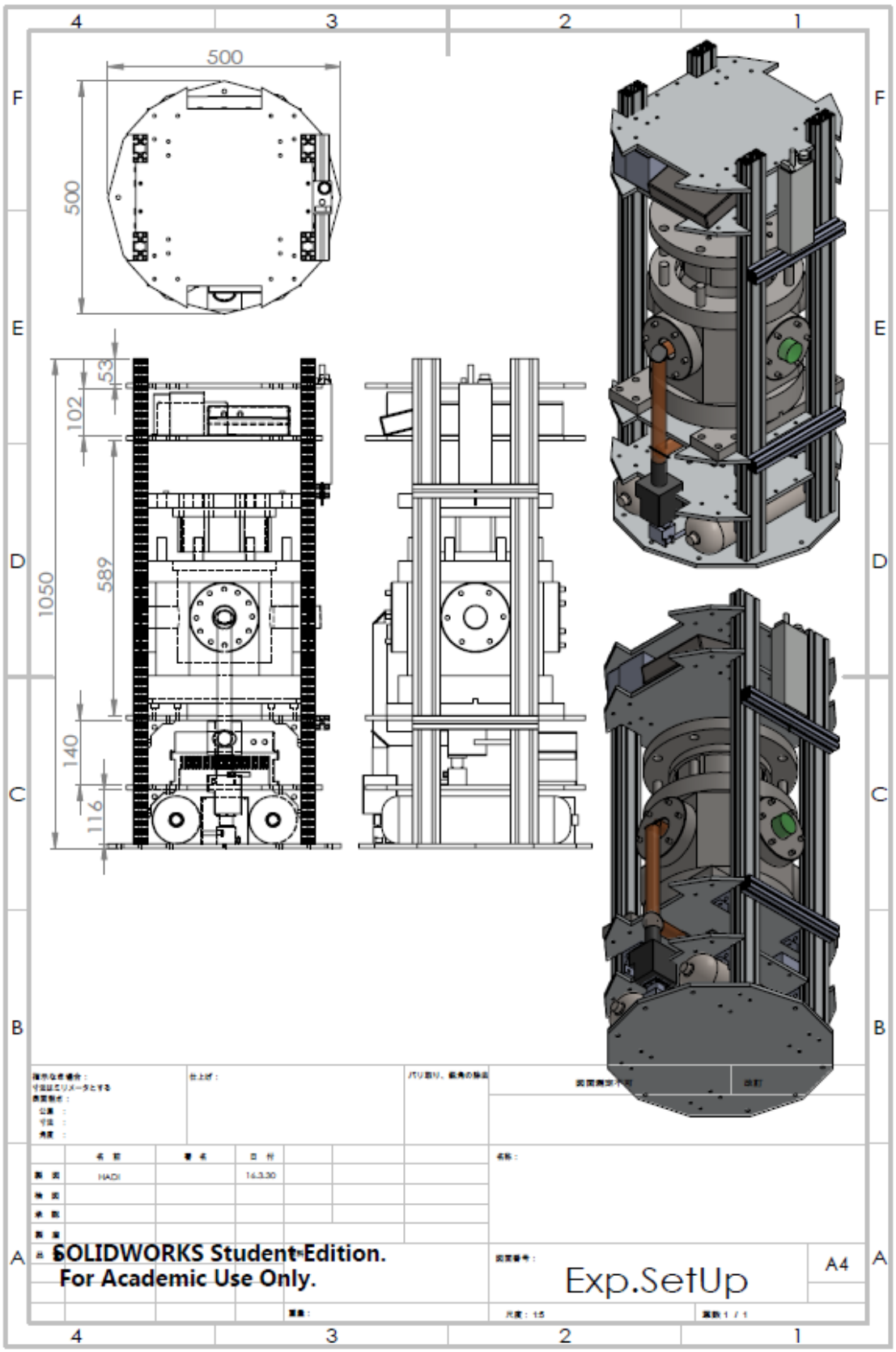

Appendix 3 Chamber – Top cover

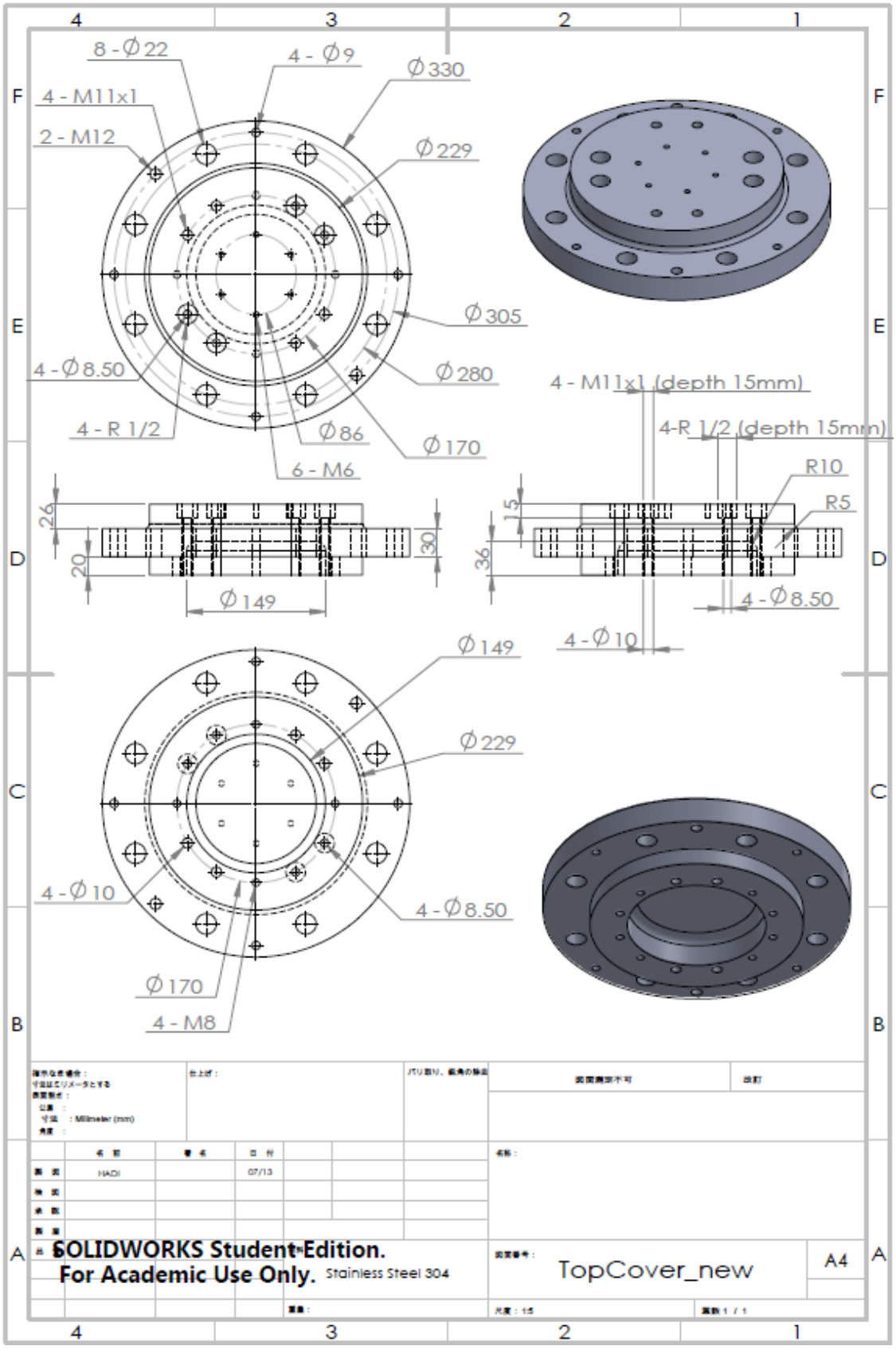

Appendix 4 Chamber – Top sphere

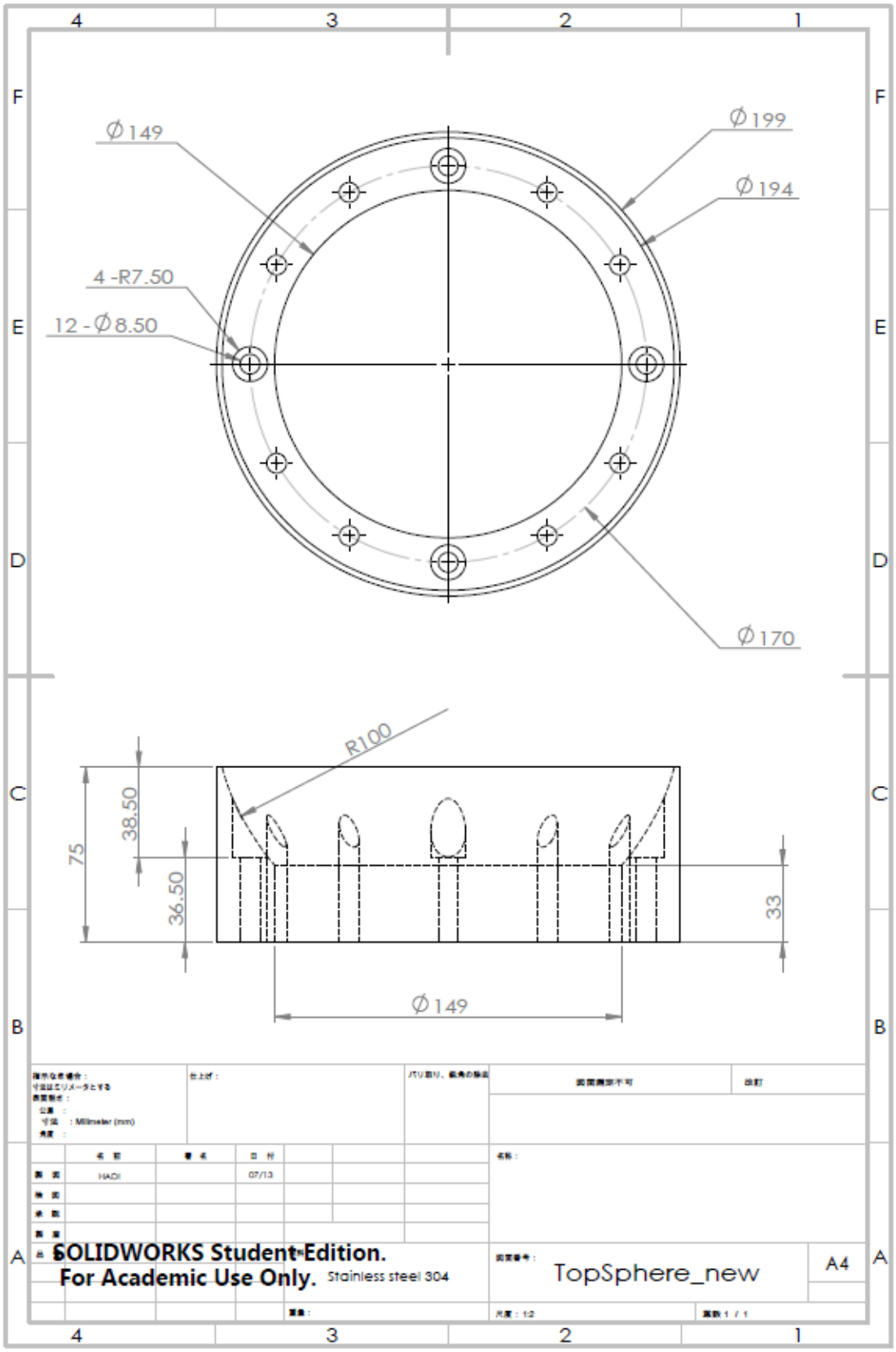

Appendix 5 Chamber – Bottom cover

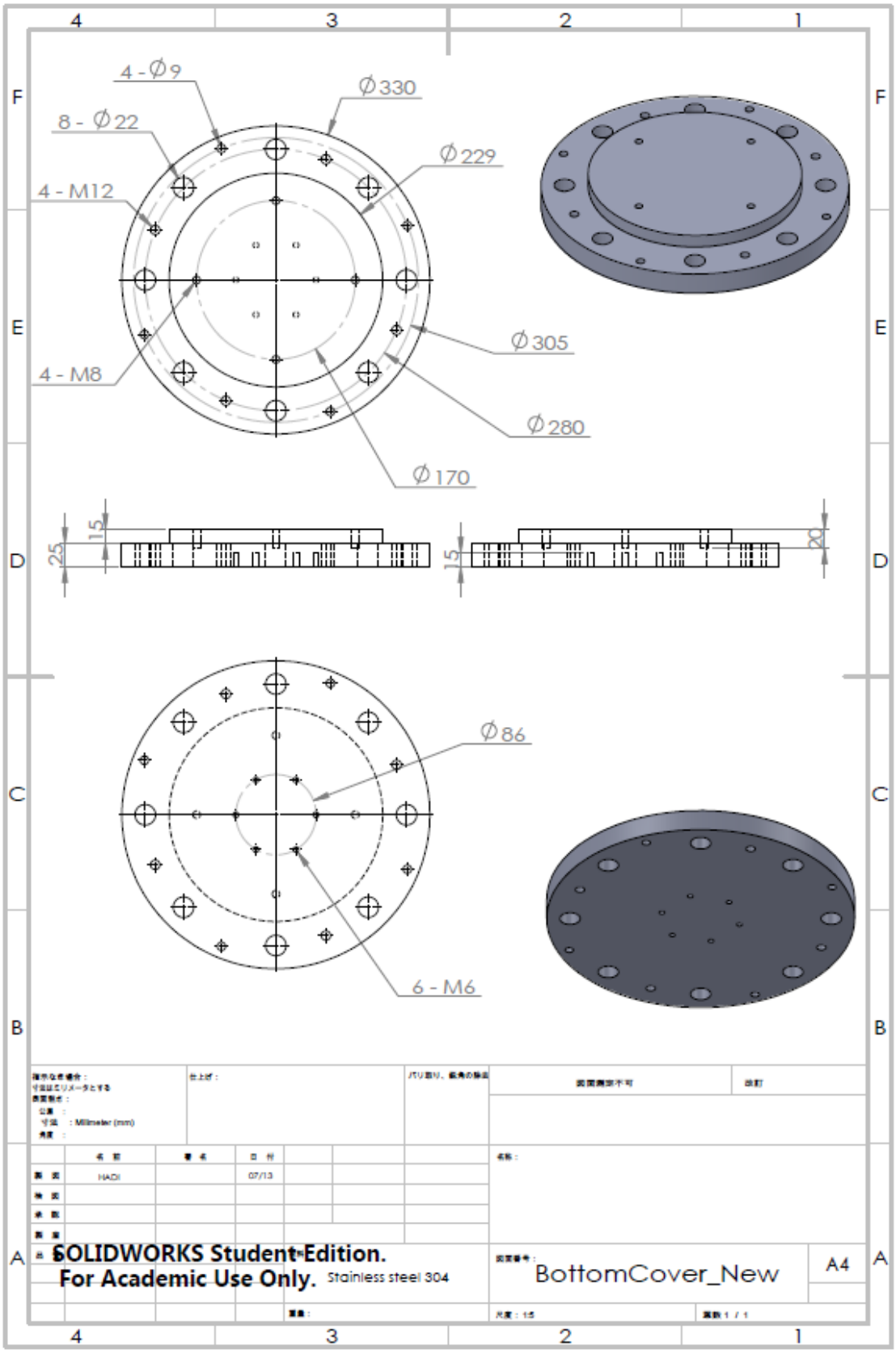

Appendix 6 Chamber – Bottom sphere

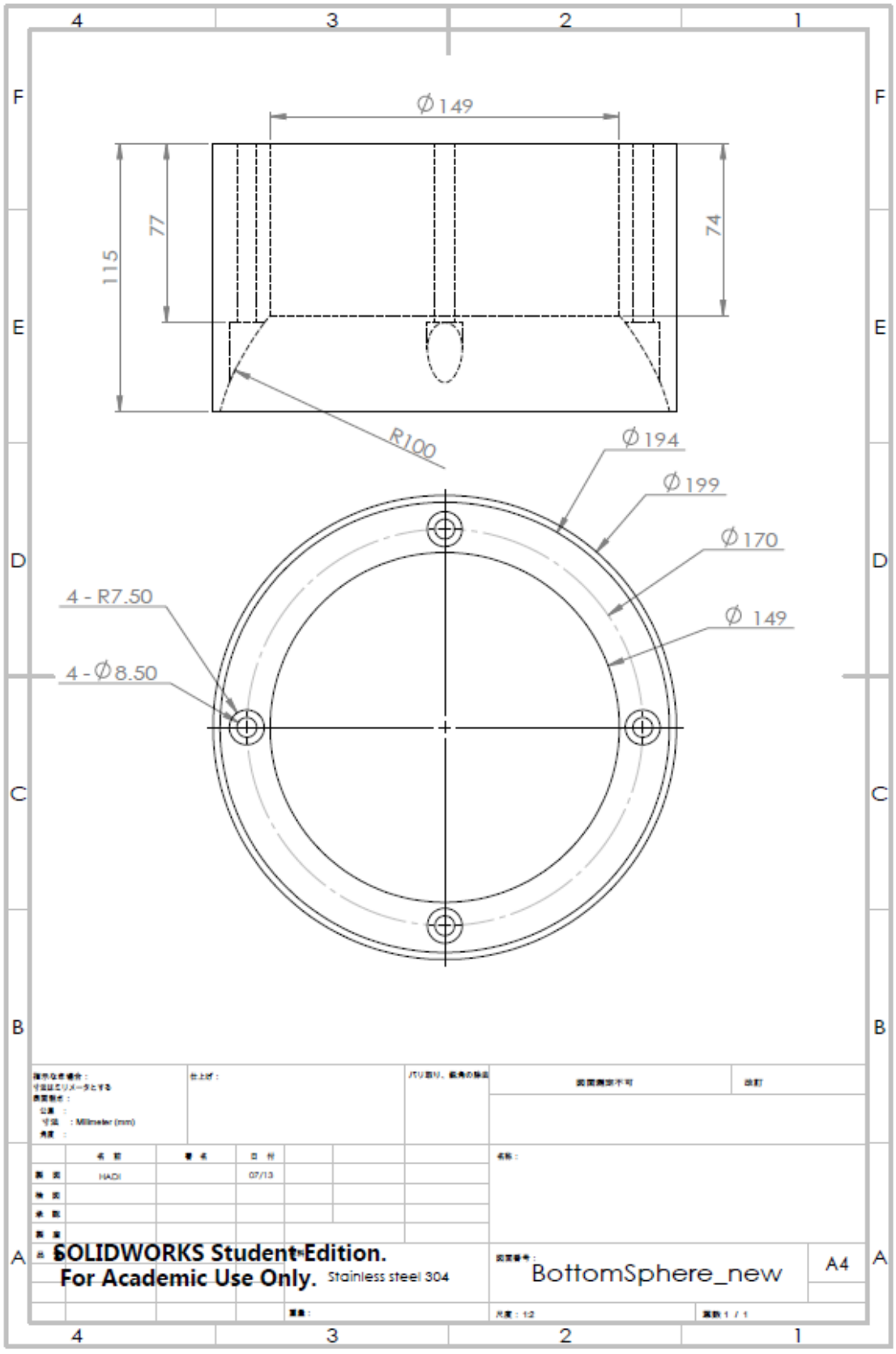

Appendix 7 Mechanical sealing slots on Top Cover

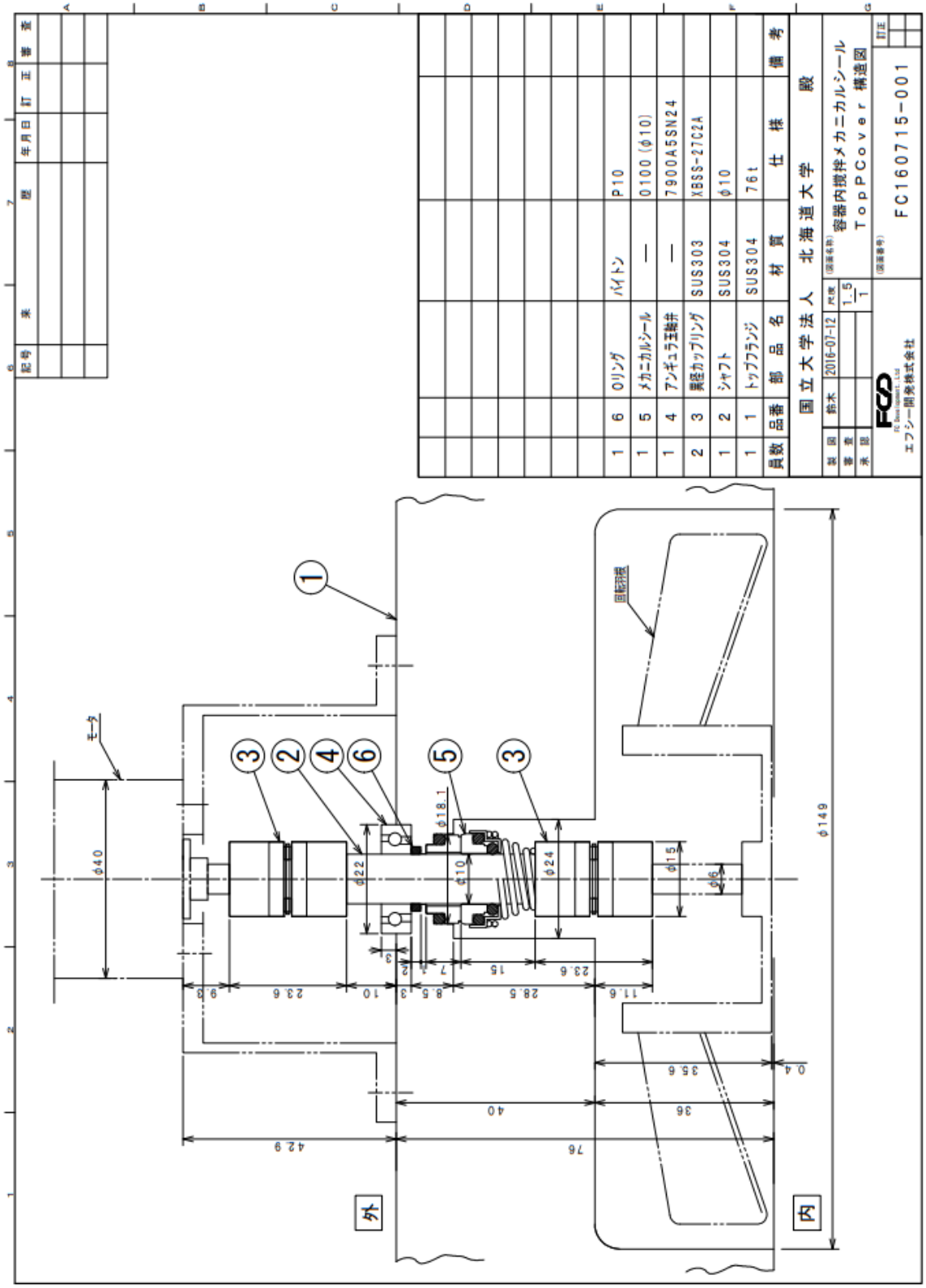

Steel spring of mechanical sealing (Top and bottom cover) were changed to rubber spring to provide more consistent compression of mechanical sealing.

Appendix 8 Mechanical sealing slots on Bottom Cover

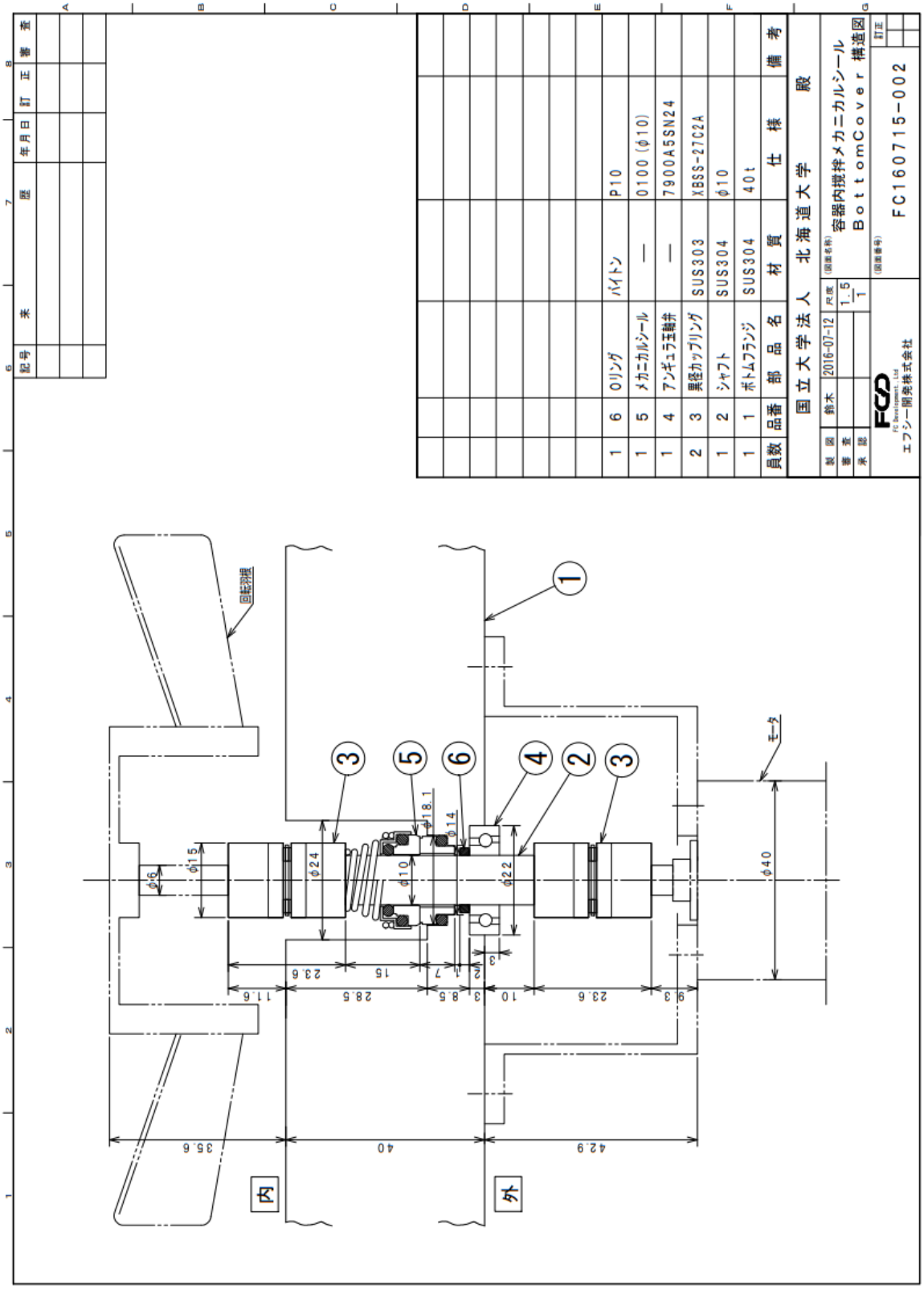

Appendix 9 Sequence KV studio ladder diagram

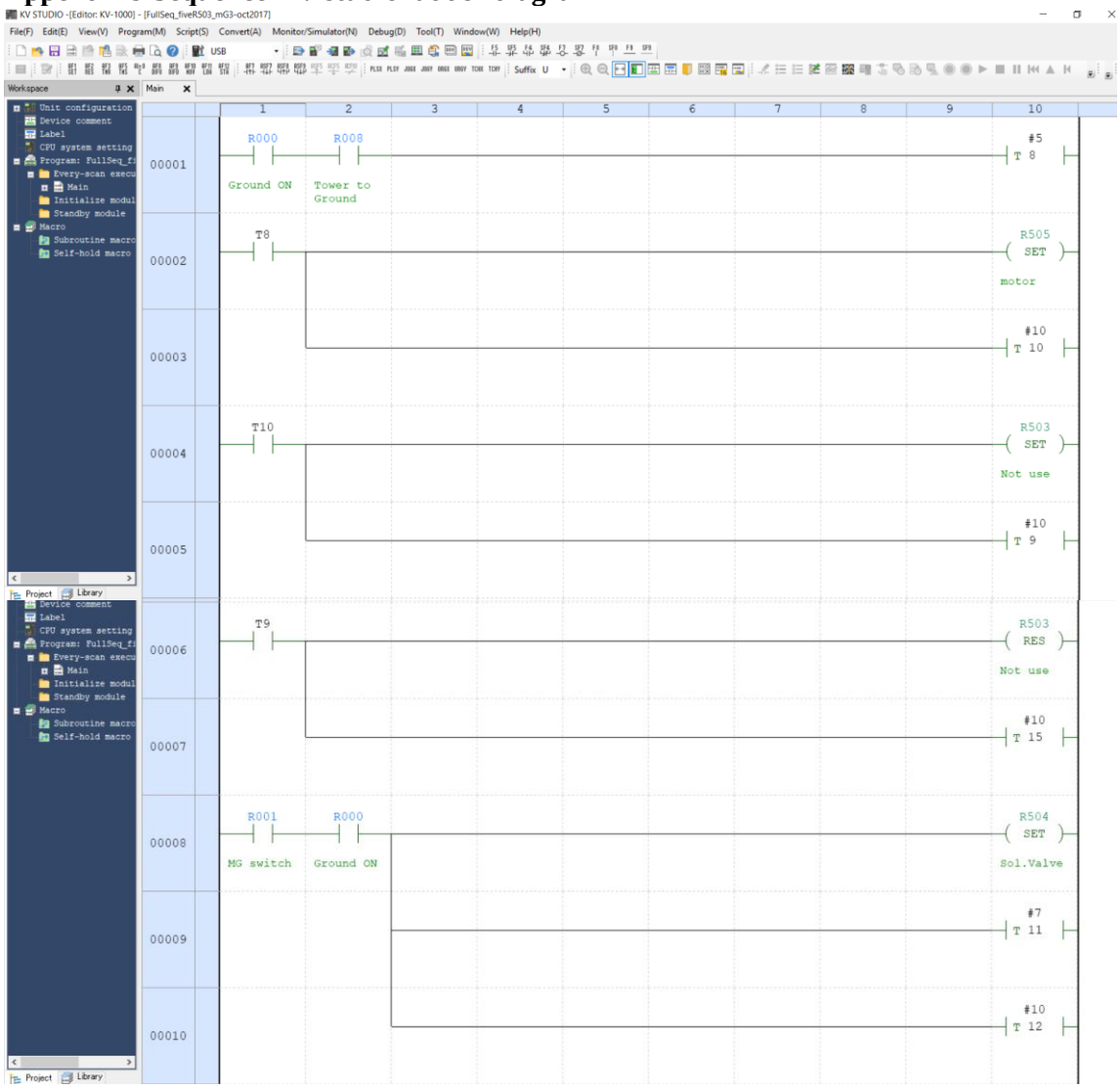

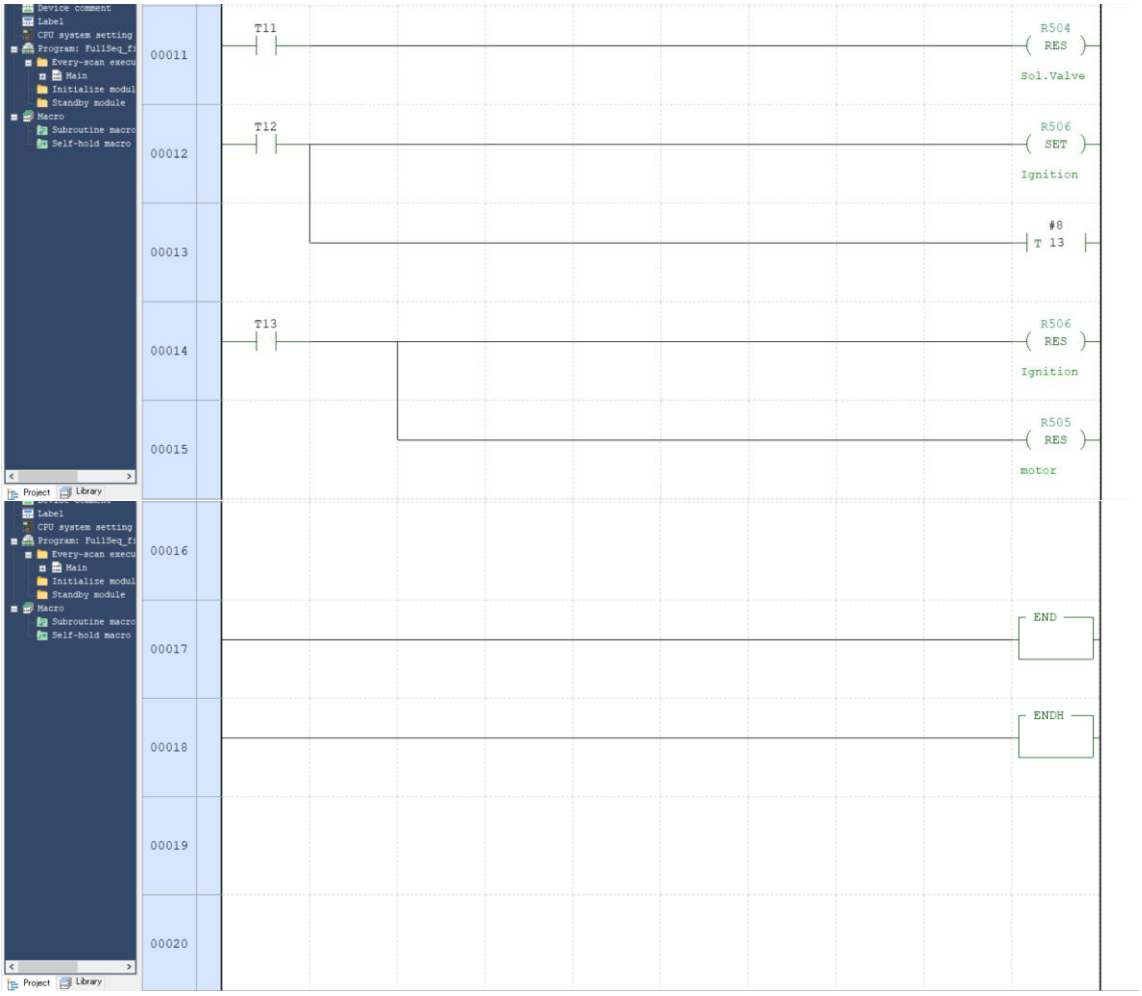

The data logger and camera triggered by the same trigger point as the “Ignition”.

This means the data logger and camera trigger connected to the same relay at the “Ignition” relay.

Achievements

Journal publications:

1. **Khalid Hadi**, Ryo Ichimura, Nozomu Hashimoto, Osamu Fujita, "Spherical turbulent flame propagation of pulverized coal particle clouds in an O_2/N_2 atmosphere", ***Proceedings of the Combustion Institute*** (I.F.2017 = 5.336) Vol. 37 (2018). DOI: 10.1016/j.proci.2018.09.021
2. **Khalid Hadi**, Ryo Ichimura, Nozomu Hashimoto, Osamu Fujita, "Development of an Experimental Apparatus for Spherical Turbulent Flame Propagation of Pulverized Coal Particle Clouds in a Microgravity Environment", ***International Journal of Microgravity Science and Application,*** (under review).
3. Ryo Ichimura, **Khalid Hadi**, Nozomu Hashimoto, Akihiro Hayakawa, Hideaki Kobayashi, Osamu Fujita, "Extinction limits of an ammonia/air flame propagating in a turbulent field", ***Fuel,*** (under review).

Conference publications:

1. **Khalid Hadi**, Ryo Ichimura, Nozomu Hashimoto, Osamu Fujita, "Experimental Study of Spherical Turbulent Flame Propagation of Pulverized Coal Particle Cloud in O_2/N_2 Atmosphere", **11th Asia-Pacific Conference on Combustion**, Sydney, Australia, (2017.12, Oral presentation). p. 259.
2. Ryo Ichimura, **Khalid Hadi,** Nozomu Hashimoto, Akihiro Hayakawa, Hideaki Kobayashi, Osamu Fujita, "Experimental Study of Turbulent Flame Propagation of Ammonia/Air Mixture in a Fan-Stirred Closed Vessel", **14th International**

Conference on Combustion and Energy Utilization, Sendai, Japan, (2018.11, Oral presentation).

3. Nozomu Hashimoto, **Khalid Hadi**, Ryo Ichimura, Osamu Fujita, Experimental study on turbulent flame propagation of coal particle cloud in a fan-stirred closed vessel, The 14th Japan-China Symposium on Coal and C1 Chemistry, C212, Hokkaido University, Sapporo, 2018/9/27.
4. **Khalid Hadi**, Ryo Ichimura, Nozomu Hashimoto, Akihiro Hayakawa, Hideaki Kobayashi, Osamu Fujita, "Experimental Study of Spherical Turbulent Flame Propagation of Ammonia-air in a Closed Vessel", **56th Symposium (Japanese) on Combustion,** Osaka, Japan, (2018.11, Oral presentation).
5. **Khalid Hadi**, Ryo Ichimura, Nozomu Hashimoto, Osamu Fujita, "Experimental Study of Spherical Turbulent Flame Propagation of Pulverized Coal Particle Cloud at Atmospheric Pressure in Microgravity Environment", **Journal of the Japan Society of Microgravity Application (JASMAC Proceedings)**, (2017.11, Oral presentation), p27A03.
6. Ryo Ichimura, **Khalid Hadi,** Nozomu Hashimoto, Osamu Fujita, "Flame propagation characteristics of pulverized coal particles in turbulent flow field", **46th Student Lecture of Graduation Research presented by Japan Society of Mechanical Engineers Hokkaido Branch**, Muroran, Hokkaido, Japan, (2017.3, Oral presentation).
7. Ryo Ichimura, **Khalid Hadi,** Nozomu Hashimoto, Osamu Fujita, "Effect of Turbulence Intensity and Coal Concentration on Spherically Propagating Flame of Pulverized Coal Particles", **49th Autumn Meeting presented by the Society of**

Chemical Engineers, Japan (SCEJ), Nagoya, Japan, (2017.9, Oral presentation).

8. Ryo Ichimura, **Khalid Hadi,** Nozomu Hashimoto, Akihiro Hayakawa, Hideaki Kobayashi, Osamu Fujita, "Experimental Study of Turbulent Flame Propagation of Ammonia/Air Mixture in a Fan-Stirred Closed Vessel", **14th International Conference on Combustion and Energy Utilization**, Sendai, Japan, (2018.11, Oral presentation).